AD-A102 121 ROCKWELL INTERNATIONAL THOUSAND OAKS CA SCIENCE CENTER F/G 11/2
HIGH TEMPERATURE MECHANICAL PROPERTIES OF POLYPHASE CERAMICS BA--ETC(U)
APR 81 F F LANGE, D R CLARKE, B I DAVIS F49620-77-C-0072
UNCLASSIFIED SC5099.4FR AFOSR-TR-81-0555 NL

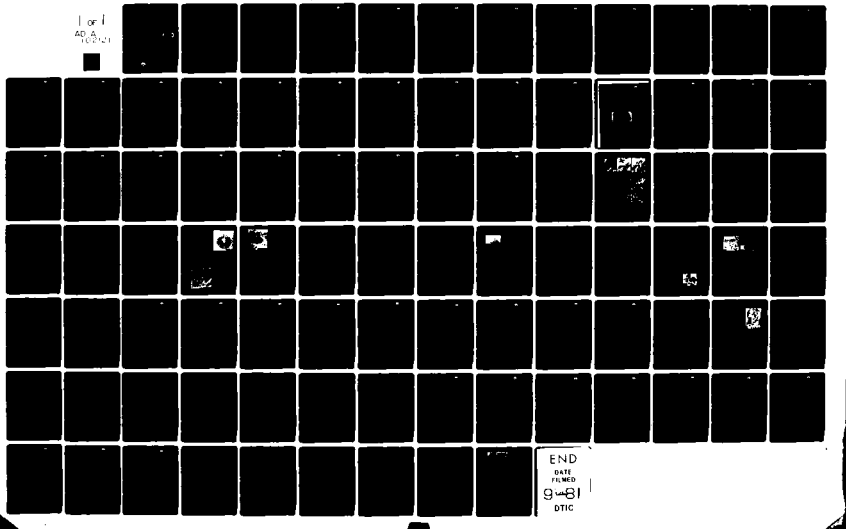

12

SC5099.4FR

LEVEL II

SC5099.4FR

Copy No. _____

HIGH TEMPERATURE MECHANICAL PROPERTIES OF POLYPHASE CERAMICS BASED ON SILICON NITRIDE

FINAL REPORT FOR THE PERIOD
February 1, 1977 through January 31, 1981

CONTRACT NO. F49620-77-C-0072

Prepared for

Air Force Office of Scientific Research
Bolling Air Force Base
Washington, D.C. 20332

F.F. Lange, D.R. Clarke, B.I. Davis

APRIL 1981

Approved for public release; distribution unlimited

"Research sponsored by the Air Force Office of Scientific Research (AFSC) United States Air Force, under Contract No. F49620-77-C-0072. The United States Government is authorized to reproduce and distribute reprints for governmental purposes notwithstanding any copyright notation hereon."

Rockwell International
Science Center

UNCLASSIFIED

SECURITY CLASSIFICATION OF THIS PAGE (When Data Entered)

REPORT DOCUMENTATION PAGE	READ INSTRUCTIONS BEFORE COMPLETING FORM
1. REPORT NUMBER (19) AFOSR-TR-81-0555	2. GOVT ACCESSION NO. AD-A102 727	3. RECIPIENT'S CATALOG NUMBER
4. TITLE (and Subtitle) High Temperature Mechanical Properties of Polyphase Ceramics Based on Silicon Nitride,	5. TYPE OF REPORT & PERIOD COVERED Final Report 02/01/77 through 01/31/81
	6. PERFORMING ORG. REPORT NUMBER SC5099.4FR
7. AUTHOR(s) F.F. Lange, D.R. Clarke and B.I. Davis	8. CONTRACT OR GRANT NUMBER(s) F49620-77-C-0072
9. PERFORMING ORGANIZATION NAME AND ADDRESS Rockwell International Science Center 1049 Camino dos Rios Thousand Oaks, CA 91360	10. PROGRAM ELEMENT, PROJECT, TASK AREA & WORK UNIT NUMBERS 61102F 2306/A2
11. CONTROLLING OFFICE NAME AND ADDRESS Air Force Office of Scientific Research Electronic & Solid State Sciences Bolling AFB, DC 20332	12. REPORT DATE April 1981
	13. NUMBER OF PAGES 96
14. MONITORING AGENCY NAME & ADDRESS(if different from Controlling Office) (9) Final rept. 1 Feb 77-31 Jan 81.	15. SECURITY CLASS. (of this report) Unclassified
	15a. DECLASSIFICATION/DOWNGRADING SCHEDULE

16. DISTRIBUTION STATEMENT (of this Report)

Approved for public release; distribution unlimited

17. DISTRIBUTION STATEMENT (of the abstract entered in Block 20, if different from Report)

18. SUPPLEMENTARY NOTES

19. KEY WORDS (Continue on reverse side if necessary and identify by block number)

Silicon nitride, fabrication, phase equilibrium, strength oxidation

20. ABSTRACT (Continue on reverse side if necessary and identify by block number)

Results for the four year effort concerning the high temperature mechanical properties of polyphase ceramics based on Si_3N_4 are described. Initial work showed that subcritical crack growth at high temperature was caused by cavitation. Phase equilibria work identified the lowest melting eutectic in the Si_3N_4-Mg_2SiO_4-MgO portion of the Si-Mg-O-N system and linked the volume fraction of the residual glassy phase to material composition. Subsequent creep studies related creep mechanism to composition through the

DD FORM 1 JAN 73 1473 EDITION OF 1 NOV 65 IS OBSOLETE

UNCLASSIFIED 389949

SECURITY CLASSIFICATION OF THIS PAGE (When Data Entered)

volume fraction of the glassy phase. Creep resistance was observed to increase after a pre-oxidation treatment. Other work at Rockwell International Science Center showed that oxidation produced compositional changes and that the detrimental glassy phase was a fugitive of oxidation. Recent work culminated this study to show that the high temperature strength of polyphase Si_3N_4 could be at least doubled through compositional changes induced by oxidation.

PROGRAM SUMMARY

The last year effort has culminated this program by demonstrating that the high temperature strength of polyphase Si_3N_4 could be at least doubled by post-fabrication oxidation treatment. Specimens of various polyphase Si_3N_4 materials fabricated in the Si-Mg-O-N system and commercial NC-132 were subjected to oxidation treatments prior to flexural strength determinations at 1400°C. The strength increase for three series of experimental materials was dependent on their initial composition, which also governed their oxidation kinetics. The flexural strength of NC-132 measured at 1400°C increased from 40,000 psi to 84,000 psi after an oxidation treatment at 1500°C/300 hrs. Compositional changes as determined by x-ray analysis showed that the composition shifted towards the Si_3N_4-Si_2N_2O tie line, strongly suggesting that the volume fraction of the glassy phase decreased during oxidation. This is consistent with a previous study of the oxidation behavior of these materials (D. R. Clarke and F. F. Lange, J. Am. Ceram. Soc. 63, 586 (1981). Details of this work are found in Appendix 1.

Another approach to decrease the glassy phase content was also attempted. This approach was to promote compositional changes by heat-treatment in argon. Predictable compositional changes did occur, and high resolution electron microscopy revealed that the glass phase did decrease. Although this study did result in a greater understanding of environmental interactions, the depleted layer was highly porous and this approach resulted in a weaker material. Details are reported in Appendix 2.

The culmination of this work resulting in a significant method to strengthen poor polyphase Si_3N_4 materials was a result of a directed effort relating fabrication, phase equilibria, microstructure and properties. Work was started by illustrating that sub-critical crack growth, which is responsible for high temperature strength degradation, was caused by the cavitation of the viscous phase adjacent to the slowly propagating crack (see Appendix 3). Work proceeded by determining the lowest temperature eutectic

composition in the Si_3N_4-Mg_2SiO_4-MgO portion of the Si-Mg-O-N system (see Appendix 4). This work showed that the volume fraction of the residual glass phase, which was assumed to have a composition close to the eutectic composition, could be related to the bulk composition. That is, using the level rule for phase diagrams, bulk compositions closer to the eutectic composition will contain a greater proportion of the eutectic melt and therefore, a greater proportion of the residual glassy phase. This result explained why compositions in this system with an MgO/SiO_2 molar ratio of ~2 exhibited lowest strength at 1400°C (F. F. Lange, J. am. Ceram. Soc. 61, 53 (1978)). Namely, the join between Si_3N_4 and the lowest eutectic occurs at a MgO/SiO_2 molar ratio of 1.6.

During this same period, it was shown that the surface pits developed during the oxidation of Si_3N_4 materials fabricated in the Si-Mg-O-N system was due to iron-type inclusions. These surface pits introduce a new and unwanted flaw distribution. Details are presented in Appendix 5.

Since high temperature strength degradation was linked to cavitational creep, and the volume content of the glassy phase was linked to composition through phase equilibria, effort was then directed to understand the creep behavior as a function of composition. Results of this effort showed that two different and concurrent creep mechanisms exist, viz. diffisuional creep and cavitational creep. The dominance of one mechanism over the other was governed by the volume fraction of the liquid phase. Cavitational creep would dominate for compositions closer to the eutectic, i.e., compositions containing a greater proportion of the glassy phase. Diffusional creep would dominate for composition furthest from the eutectic (see Appendix 6). It was also observed that the cavitational creep would also dominate at higher stresses, whereas, at lower stresses, diffusional creep would predominate (Appendix 7).

Viscoelastic effects in these materials were also characterized with high resolution electron microscopy (Appendix 8).

During this same period, the high temperature creep and oxidation resistance of a new material fabricated in the Si-Sc-N-O system was also characterized. Although this material was difficult to fabricate, its high temperature properties were superior to other known polyphase Si_3N_4 materials (Appendix 9).

Creep work was terminated after two further studies. The first was the determination of the temperature dependence of materials that either exhibit cavitational creep or diffusional creep (Appendix 10). The second study resulted in the significant observation that the creep resistance could be greatly improved by a pre-oxidation treatment (Appendix 11). This observation led to the significant method of strengthening polyphase Si_3N_4 materials which culminated this program during the last year.

In addition to the above directed work, one other study was performed to illustrate the development of compressive surface stresses due to molar volume changes induced by oxidation. This work was carried out with several materials fabricated in the Si-Ce^{+3}-O-N system. The Ce-apatite crystalline phase oxidizes to CeO_2 and SiO_2 to produce a molar volume change of ~15%. Oxidation of this secondary phase at temperatures between 400-600°C results in surface compressive stresses which can aid in strengthening. Another significant observation was that these surface stresses could be relieved at the higher temperatures by the extrusion of the oxidation products to the surface (Appendix 12).

Further details for each of these studies are given in the Appendices.

LIST OF PUBLICATIONS RESULTING FROM AFOSR PROGRAM

1. "Eutectic Studies in the Si_3N_4-Si_2N_2O-Mg_2SiO_4-MgO system," J. Am. Ceramic Soc. 62, 617 (1979).

2. "Evidence for Cavitation Crack Growth in Polyphase Si_3N_4," J. Am. Ceram. Soc. 62, 222 (1979).

3. Reaction of Iron with Si_3N_4 Materials to Produce Surface Pitting," J. Am. Ceramic Soc. 61, 270 (1978).

4. "Dense Silicon Nitride Ceramics: Fabrication and Interrelations with Properties," Processing of Crystalline Ceramics, p. 597, Ed by H. Palmour II, R. F. Davis and T. M. Hare, Plenum, 1977.

5. "Development of Surface Stresses During the Oxidation of Several Si_3N_4/CeO_2 Materials," J. Am. Ceram. Soc. 62, 629 (1979).

6. "Compressive Creep of Si_3N_4/MgO Alloys, Part 1: Effect of Composition, J. Mat. Sci. 15, 601 (1980).

7. "Ibid: Part 2: Source of Viscoelastic Effect," J. Matr. Sci. 15, 611 (1980).

8. "Ibid: Part 3: Effects of Oxidation Induced Compositional Change," J. Mat. Sci. 15, 616 (1980).

9. "Ibid: Part 4: Activation Energies," sent to J. Mat. Sci.

10. "A New Si_3N_4 Material: Phase Relations in the System Si-Sc-O-N and Preliminary Property Studies," J. Am. Ceram. Soc. (in press).

11. "Compressive Creep and Oxidation Resistance of a $Si_3N_4/Y_2Si_2O_7$ Material," sent to J. Am. Ceram. Soc.

12. "Strengthening of Polyphase Si_3N_4 Materials Through Oxidation," to be published.

13. "Comparison of Argon and Air Heat Treatments of Hot-Pressed Si_3N_4," to be published.

PERSONNEL INVOLVED

F. F. Lange
D. R. Clarke
P. E. D. Morgan
B. I. Davis

APPENDIX 1

STRENGTHENING OF POLYPHASE Si_3N_4 MATERIALS THROUGH OXIDATION

F. F. Lange, B. I. Davis and M. G. Metcalf
Structural Ceramics Group
Rockwell International Science Center
Thousand Oaks, California 91360

ABSTRACT

Specimens of various polyphase Si_3N_4 materials fabricated in the Si-Mg-O-N system and commercial NC-132 were subjected to oxidation treatments prior to flexural strength determinations at 1400°C. It was demonstrated that a pre-oxidation treatment could significantly improve the high temperature strength. The compositional change induced by oxidation which can decrease the volume fraction of the viscous phase present in these materials at high temperatures is believed to be responsible for the observed strengthening.

1.0 INTRODUCTION

The continuous glassy intergranular phase that exists in most (if not all) polycrystalline Si_3N_4 materials plays an important role in both oxidation and mechanical property phenomena.[1] At high temperatures, this intergranular phase becomes viscous and both a path for fast diffusion[2] and a source for stress-induced cavitation.[3] Oxidation phenomena takes advantage of this continuous viscous phase for inward and outward diffusion of oxidation reactants and products.[2] The viscous phase is responsible for mechanical property degradation at high temperature. Under stress, it is a path for material rearrangement (diffusional creep).[3] The propensity of the viscous phase to cavitate under stress is responsible for the slow-crack growth phenomena by polyphase Si_3N_4 at high temperatures[4] and thus, its strength degradation.

Previous investigations have shown that oxidation resistance,[2,5] creep resistance[3] and high temperature strength[5] of polyphase Si_3N_4 fabricated in the Si-Mg-O-N system depends on its composition. All three of these properties decrease as the material's composition moves closer to the eutectic composition in the Si_3N_4-Si_2N_2O-Mg_2SiO_3 compatibility triangle.[6] These observations strongly suggest that the volume fraction of the glassy intergranular phase, which governs diffusional flux and cavitational propensity, is determined by the lever rule developed for determining phase content from phase diagrams. That is, the composition of the glassy phase is similar to the eutectic composition (i.e., the last liquid to solidify after fabrication) and its volume content depends on the bulk composition relative to the eutectic composition. Thus, within the limits of the compositions studied, the volume fraction of the glassy intergranular phase appears to increase as the bulk composition moves closer to the eutectic composition.

Discovery that the creep resistance of several different polyphase Si_3N_4 materials could be improved by a pre-oxidation treatment[7,8] was our first indication that the high temperature strength may also be improved by the same treatment.

During this same period, results of oxidation studies[2] had shown that compositional change is not only exhibited by the formation of a silicate surface scale, but also by a gradient of both the additive cation and the crystalline phases from the surface to the interior. As detailed elsewhere,[2] the additive cation and cation impurities that reside in the glassy intergranular phase diffuse to the surface in an attempt to equilibrate the glass composition with the SiO_2 formed by the oxidation of Si_3N_4. This outward diffusion forms a gradient of depleted additive (and impurity) cation(s). Oxygen, in the glassy phase originally associated with the outward diffusing cation(s), is left behind to react with Si_3N_4 to form Si_2N_2O. The volume fraction of the glassy phase is thus reduced by its loss of both the outward moving cation(s) and the oxygen which reacts to form Si_2N_2O.* Thus depending on the initial bulk composition, the glassy intergranular phase can be a fugitive of the oxidation process.

The compositional gradient produced by oxidation can best be visualized by the following demonstration. Oxidize a polyphase Si_3N_4 specimen for a period sufficient to form a relatively thick surface scale. Section the specimen and re-expose the freshly cut surface to a much shorter oxidation period. Upon examination, the sectioned surface will reveal the compositional gradient due to the greater oxidation resistance (and thus thinner scale) of the cation depleted zone. An example is shown in Fig. 1 (initial composition: 0.755 Si_3N_4, 0.120 SiO_2, 0.125 MgO; oxidized 300 hrs at 1400°C in air, sectioned and reoxidized for 0.5 hrs 1400°C). Quantitative microchemical and x-ray analysis of this same cross section as presented elsewhere[2] also shows that the compositional change produced by oxidation extends to the center of this specimen.

*Equilibrium considerations may also require that the viscous phase maintain its original composition. If this is the case, a portion of the SiO_2 in the viscous phase can react with the Si_3N_4 to produce Si_2N_2O which further reduces the volume fraction of the viscous phase.

It was therefore concluded that since detrimental glass phase can be a fugitive of the oxidation process, oxidation could improve the high temperature mechanical properties as first discovered during creep experiments and as it will now be demonstrated through strength measurements.

2.0 EXPERIMENTAL

The object of this study was to determine the effect of a pre-oxidation treatment on the high temperature strength of polyphase Si_3N_4. Materials fabricated in the Si-Mg-O-N system were chosen for this study. Since prolonged oxidation is known to produce surface pits in these materials[9,10] which introduce a detrimental, new flaw population, pre-oxidized specimens were reground to remove the surface pits prior to strength determinations.

The first group of bar specimens examined were diamond cut and ground from 19 different materials which form three series of compositions previously investigated at high temperatures in studies concerning strength,[5] creep[3] and oxidation resistance.[2] Materials in each series contained a fixed mole fraction of Si_3N_4 (either 0.91, 0.833 or 0.755) and a given MgO/SiO_2 molar ratio that could range between 0.1 and 11. Fabrication details have been presented elsewhere.[5] All 19 specimens were placed on a reaction-bonded Si_3N_4 setter with raised knife-edge contracts and oxidized together in air at 1400°C for 300 hrs. The specimens were weighed before and after oxidation. After oxidation, each specimen was separately surface ground until surface pits, formed to various depths on the different materials, were no longer observed by visual inspection with a binocular microscope.

The second group of specimens were cut from a large billet of NC-132 hot-pressed Si_3N_4 obtained recently from the Norton Company. This group was separated into different sets. Flexural strength measurements were made at room temperature and 1400°C without a preoxidation treatment. The other sets were subjected to oxidation in air at either 1400°C or 1500°C for various

periods prior to regrinding and strength determinations at either room temperature or 1400°C. The amount of material removed by regrinding was dependent on the depth of the surface pits formed during oxidation as discussed above.

All flexural testing was performed on bar specimens (approximate dimensions of 0.3 × 0.6 × 3.2 cm) using a 4-point loading device with inner and outer spans of 1.27 cm and 2.54 cm, respectively, and a cross-head speed of 0.05 cm/min. X-ray diffraction analysis was used to determine the crystalline phase content of the surfaces of the unoxidized and oxidized, reground specimen; intensity ratio of the (111) Si_2N_2O and (200) Si_3N_4 diffraction peaks determined by an area analysis was used to report compositional changes.

3.0 RESULTS

3.1 Compositions with Various MgO/SiO_2 Ratios

Table 1 lists the specimens, their initial compositions, their weight gain during oxidation per unit area, and their flexural strengths (1400°C in air) after the 1400°C/300 hr oxidation treatment. The second from last column lists the average flexural strengths previously measured at 1400°C with specimens cut from the same billet. The last column lists the percent change in strength due to the pre-oxidation treatment. Figure 2 illustrates, for comparative purposes, the strength data (room temperature, 1400°C, and pre-oxidized, 1400°C) for the series containing 0.91 mole fraction Si_3N_4.

Both Table 1 and Fig. 2 illustrate that a pre-oxidation treatment can significantly improve the high temperature strength of polyphase Si_3N_4 materials. Within each series, the largest increase occurs for compositions with an MgO/SiO_2 molar ratio between 1 to 3. Also, compositions with $MgO/SiO_2 > 4$ exhibit a strength decrease after oxidation.

Flexural strength calculations assumed an elastic stress-strain behavior. Data obtained previously for unoxidized specimens tested at 1400°C with an MgO/SiO_2 ratio ranging between 1 to 3 exhibited a non-elastic behavior

upon stressing to failure, indicative of lower strengths than reported in Table 1 and Fig. 2. On the other hand, all pre-oxidized specimens did exhibit an elastic stress-strain response to failure. Thus, the strength difference for compositions within this range of MgO/SiO_2 ratios is even greater than that reported in Table 1.

Figure 2 reports the Si_2N_2O/Si_3N_4 ratio determined on ground surfaces of both unoxidized and oxidized (1400°C/300 hr) specimens. This ratio is plotted as a function of the initial MgO/SiO_2 molar ratio. Data for the unoxidized specimens are representative of the material's bulk. But because oxidation produces a gradient in the Si_2N_2O/Si_3N_4 ratio,[2] data for specimens subjected to oxidation are only representative of the depth for which material was removed by grinding to eliminate surface pits. Although data for the oxidized specimens are not representative of its bulk, it does show that compositional changes as outlined in the introduction did take place, i.e., the average bulk composition decreases its MgO/SiO_2 ratio and shifts toward the Si_3N_4-Si_2N_2O tie line. Note that the larger changes occur for materials with an initial MgO/SiO_2 molar ratio between 0.5 and 3.0.

3.2 Commercial Si_3N_4 Material

Table 2 lists the oxidation treatments for which the specimens of NC 132 were subjected. As shown, most of the specimens were subjected to various periods of oxidation at 1400°C prior to regrinding and strength testing. After it was discovered that excessive periods (>500 hrs) at 1400°C were required to achieve modest strength gains at high temperatures, the remaining specimens were oxidized at 1500°C. As indicated in Table 2, significant strengthening can be achieved by a pre-oxidation treatment at 1500°C. It was also demonstrated that such a treatment did not impair the room temperature strength. A detailed description of these results now follows.

Flexural strength measurements of unoxidized specimens at 25°C and 1400°C resulted in an average strength of 878 MPa and 282 MPa, respectivity. The load-deflection response of these specimens at 1400°C was nonlinear

Table 1. Oxidation and Strength Data for Si-Mg-O-N Compositions Oxidized at 1400°C/300 Hr

Initial Composition (mole fraction) Si_3N_4	MgO	SiO_2	MgO/SiO_2 Molar Ratio	Weight Change (mg/cm^2)	Flexural Strength (MPa)	Prior Flexural Strength (MPa)	% Change
0.910	0.020	0.070	.29	0.93	482	343	+40
0.910	0.030	0.060	.50	1.36	534	339	+57
0.910	0.040	0.050	.80	1.74	445	307	+45
0.910	0.055	0.035	1.57	1.78	327	183	+79
0.910	0.065	0.025	2.60	2.39	500	269	+86
0.833	0.015	0.152	0.10	0.21	452	287	+58
0.833	0.030	0.137	0.22	1.40	420	352	+19
0.833	0.040	0.127	0.31	2.09	319	341	-7
0.833	0.052	0.110	0.47	2.02	452	334	+35
0.833	0.085	0.082	1.04	3.34	377	211	+79
0.833	0.120	0.047	2.55	5.31	350	280	+25
0.833	0.144	0.023	6.26	4.72	411	476	-14
0.755	0.020	0.225	0.09	0.93	405	225	+80
0.755	0.055	0.190	0.29	1.92	455	269	+69
0.755	0.085	0.160	0.53	3.18	449	279	+61
0.755	0.125	0.120	1.04	4.30	338	199	+70
0.755	0.155	0.090	1.72	4.41	510	193	+164
0.755	0.190	0.055	3.45	4.47	500	414	+21
0.755	0.225	0.020	11.25	5.94	324	408	-26

Table 2. Flexural Strength Results for Commercial Si_3N_4

Oxidation Treatment Temp (°C)	Oxidation Treatment Time (hr)	Test Temp (°C)	Number	Wt. Gain/ Area (mg/cm^2)	Depth Removed (cm)	Average Strength (MPa)	Weight Parameters m	Weight Parameters σ_0 (MPa)
None		25	7	-	-	878	8	924
None		1400	8	-	-	282	(±4%)**	
1400	50	1400	3	1.61	0.015	254	(±4%)	
1400	100	1400	3	2.13	0.020	256	(±7%)	
1400	256	1400	4	-	-	288	(±8%)	
1400	332	25	8	2.39	0.020	982	15	1014
1400	332	1400	8	2.39	0.020	280	24	286
1400	548	1400	3	-*	0.020	376	(±6%)	
1500	206	25	7	-*	0.050	805	11	834
1500	206	1400	7	-*	0.050	482	17	496
1500	306	1400	5	-*	0.050	571	(±3%)	

* Scale flaked off during oxidation.

** Numbers in brackets denote percent difference of either maximum or minimum strength values from average.

indicating extensive creep during strength testing. Although the strength of these specimens at 1400°C is listed as 282 MPa, the author recognizes that the material's true strength could be significantly lower due to the extensive creep and the use of an elastic solution to calculate strength.[11] In addition, the area of subcritical crack growth could easily be distinguished as previously reported,[12] i.e., the fracture area traversed by the slowly moving crack can be distinguished by a rougher topography caused by extensive cavitation.

Short periods of oxidation (50 hr) prior to strength testing resulted in a nearly linear load-deflection response. After a pre-oxidation period of 100 hrs the load-deflection response was linear to fracture. Judging the first results obtained on the materials fabricated by the author (see Section 3.1), high temperature strengthening was expected for oxidation periods of ~300 hrs at 1400°C. But contrary to this expectation, modest strengthening was not observed until the oxidation period at 1400°C was increased to 548 hrs. It then became obvious that significant strengthening could be achieved within a more reasonable period by increasing the oxidation kinetics by increasing the oxidation temperature. It was thus demonstrated that a pre-oxidation treatment of 300 hrs at 1500°C could raise the 1400°C strength of NC 132 from <30% to 70% of its room temperature value. It is expected that longer periods at 1500°C or higher temperatures will result in further strengthening.

Another objective was to determine if the pre-oxidation treatment might influence the lower temperature strengths. As indicated in Table 2, room temperature strength measurements were obtained with reground specimens after oxidation treatments of 1400°C/332 hr and 1500°C/206 hrs. Data obtained after the 1400°C/332 hr treatment indicates a modest strengthening (~12%), and as shown in Fig. 3, a narrower strength distribution. As shown in Fig. 3, the 1500°C/206 hr treatment resulted in a strength distribution similar to that obtained at room temperature for specimens that were not subjected to a pre-oxidation treatment.

Figure 3 also reports the Weibull strength statistics of the high temperature data where linear load-deflection response was observed. Table 2 reports the two Weibull parameters for these data. As indicated, minimal strength scatter is observed for all high temperature results. This is indicative of slow-crack growth as first pointed out by Charles.[13] It should be noted that although slow-crack growth was prevalent at high temperatures, the fracture surface did not reveal any topographical difference between the slow and fast crack growth regions.

Attempts were made to obtain oxidation kinetics through weight change measurements. As shown in Table 2, data was limited to the shorter periods at 1400°C. The oxide scale flaked off at longer periods and during the 1500°C treatments. Table 2 also shows that the surface pits were deeper for longer oxidation periods or higher temperature. One oxidized specimen (1400°C/332 hrs) tested at 1400°C without regrinding resulted in a strength of 165 MPa. This much lower strength was due to fracture initiating at a deep surface pit.

The x-ray diffraction analysis results obtained from the ground surfaces of specimens subjected to various oxidizing treatments are shown in Fig. 4. Conversion of the Si_2N_2O/Si_3N_4 intensity ratio to weight percent Si_2N_2O was carried out according to the calibrated method described by Mencik and Short.[14] This analysis, as used here, assumed no other phase present other than either Si_2N_2O or Si_3N_4. As shown in Fig. 4, the Si_2N_2O content increases rapidly for short periods of oxidation at 1400°C and then levels off at longer periods. Oxidation at 1500°C promotes a greater compositional change.

4.0 DISCUSSION

As detailed above, the high temperature strength of polyphase Si_3N_4 materials can be significantly improved by an oxidation treatment. For the system chosen for examination here, which develops surface pits during oxidation due to localized surface reactions with Fe-type inclusions,[10] surface

regrinding is necessary to realize these strength improvements. It is expected that for other material systems that do not exhibit surface pitting (e.g., materials in the Si_3N_4-Si_2N_2O-$Y_2Si_2O_7$ system), regrinding may not be necessary.

The strength improvements can be related to the compositional changes induced by oxidation. Oxidation shifts the average bulk composition towards Si_2N_2O. This compositional shift changes the volume content of the liquid in equilibrium with the crystalline phases. Most of the materials studied here had initial compositions within the Si_3N_4-Si_2N_2O-Mg_2SiO_4 compatibility triangle, which contains the lowest melting eutectic of the two compatibility triangles in which Si_3N_4 is an equilibrium phase.[6] For these materials any compositional shift towards the Si_3N_4-Si_2N_2O tie line will decrease the volume content of the eutectic melt and thus result in a strengthening. On the other hand, for compositions in the Si_3N_4-Mg_2SiO_4-MgO compatibility triangle ($MgO/SiO_2 > 2$), a small compositional shift toward the Si_3N_4-Si_2N_2O tie line would move the composition into the Si_3N_4-Si_2N_2O-Mg_2SiO_4 compatibility triangle to increase the volume fraction of the eutectic melt (and therefore the residual glass phase) and thus result in a strength decrease. This is observed for the two materials in series 2 and 3 (Table 1) with the highest initial MgO/SiO_2 ratios. Further oxidation resulting in a greater compositional shift should again produce a strengthening for these two materials.

The extent of the oxidation required to produce a desired strengthening will depend on the material's initial composition, which controls its initial oxidation kinetics,[5] and on temperature, which also controls oxidation kinetics. Impurities must also be included in considering the material's composition. Impurities not only help govern the eutectic composition, its melting temperature and its volume fraction, but they can also diffuse to the surface during oxidation.[2] Thus a specific oxidation treatment scheduled cannot be presently recommended for an arbitrary composition without analitical relations between oxidation kinetics, compositional change and residual glass phase contents.

The question of to what depth from the surface an oxidation treatment can produce the compositional change required for significant strengthening has not been answered here. Previous experiments involving quantitative compositional measurements show that for specimens of the size used here (~0.3 cm thick), a significant compositional change does occur at the center of the specimen after ~300 hr at 1400°C. For the specimens treated here, the thickness was reduced by 15% to 35% by surface grinding. Judging from the compositional profiles obtained from the previous studies, it appears that much of the steep portion of the compositional gradient was removed. This suggests that the compositional changes reported in Figs. 3 and 5 are nearly representative of the specimen's center.

Another interesting result was the slight strengthening obtained at room temperature after the 1400°C/332 hr treatment. Oxidation reactions produce both molar volume changes and compositional gradients. Either one or both of these phenomena will produce residual surface stresses. The reaction $2Si_3N_4 + 1.5\ O_2 \rightarrow 3Si_2N_2O + N_2$ results in a molar volume increase of ~20%. Although most of the compressive stresses produced by this volume increase are expected to relax during oxidation, some may remain to produce the apparent room temperature strengthening observed after the 1400°C/332 hr treatment.

In conclusion, it has been shown that a pre-oxidation treatment can significantly increase the high temperature mechanical properties of dense, polyphase Si_3N_4 without affecting their low temperature strength. Oxidation resistance is also significantly improved by this treatment. This observation suggests that Si_3N_4 compositions that can easily be sintered because of a large amount of a liquid phase, but have poor high temperature properties can be improved by a post-fabrication oxidation treatment.

ACKNOWLEDGEMENTS

This work was supported by the Air Force Office of Scientific Research, Contract No. F49620-77-C-0072. We would like to thank D. R. Clarke for many useful discussions.

5.0 REFERENCES

1. F. F. Lange, "Silicon Nitride Polyphase Systems: Fabrication, Microstructure, and Properties," International Metals Reviews, 25[1] (1980).

2. D. R. Clarke and F. F. Lange, "Oxidation of Si_3N_4 Alloys: Relation to Phase Equilibria in the System Si_3N_4-SiO_2-MgO," J. Am. Ceram. 63[9-10], 586 (1980).

3. F. F. Lange, B. I. Davis, D. R. Clarke, "Compressive Creep of Si_3N_4/MgO Alloys: Part 1: Effect of Composition," J. Mat. Sci. 15, 601 (1980).

4. F. F. Lange, "Evidence for Cavitation Crack Growth in Si_3N_4," J. Am. Ceram. soc. 62[3-4], 222 (1979).

5. F. F. Lange, "Phase Relations in the System Si_3N_4-SiO-MgO and Their Interrelation with Strength and Oxidation," J. Am. Ceram. Soc. 61, 53 (1978).

6. F. F. Lange, "Eutectic Studies in the System Si_3N_4-Si_2N_2O-MgO," J. Am. Ceram. Soc. 62[11-12], 617 (1979).

7. F. F. Lange, B. I. Davis, D. R. Clarke, "Compressive Creep of Si_3N_4/MgO Alloys: Part 3: Effects of Oxidation Induced Compositional Change," J. Mat. Sci. 15, 616 (1980).

8. F. F. Lange, B. I. Davis and H. C. Graham, "Compressive Creep and Oxidation Resistance of a Si_3N_4 Material Fabricated in the Si_3N_4-Si_2N_2O-$Y_2Si_2O_7$ system," to be published.

9. S. C. Signhal, "Strength Degradation of Si_3N_4 due to Oxidation," Brittle Materials Design, High Temperature Gas Turbin Materials Technology, AMMRC CTR 76-32, Vol. IV, p. 197, Dec. 1976.

10. F. F. Lange, "Reaction of Iron with Si_3N_4 Materials to Produce Surface Pitting," J. Am. Ceram. Soc. 61[5-6], 170 (1978).

11. C. A. Anderson, D. P. Wei and R. Kossowsky, "Analysis of the Time-Dependent Flexural Test," Deformation of Ceramics, Ed by R. C. Bradt and R. E. Tressler, pp. 383-398 (1975) Plenum Press.

12. F. F. Lange, "High-Temperature Strength Behavior of Hot-Pressed Si_3N_4: Evidence for Sub-critical Crack Growth," J. Am. Ceram. Soc. 57[2], 84 (1974).

13. R. J. Charles, "Dynamic Fatigue of Glass," J. Appl. Phys. 29[12], 1967 (1958).

14. Z. Mencik and M. A. Short, "Quantitative Phase Analysis of Synthetic Silicon Nitride by X-ray Diffraction: An Improved Procedure," Tech. Rept. No. SR-72-98 ford Motor Company, Sept. 5, 1972.

Fig. 1 Oxidized cross section of a specimen previously oxidized at 1400°C/300 hrs. White film on parameter is the initial oxide scale. White center is produced by thin oxide scale formed on the less resistant composition. Darker zone illustrates the depth of compositional change which is more resistant to oxidation.

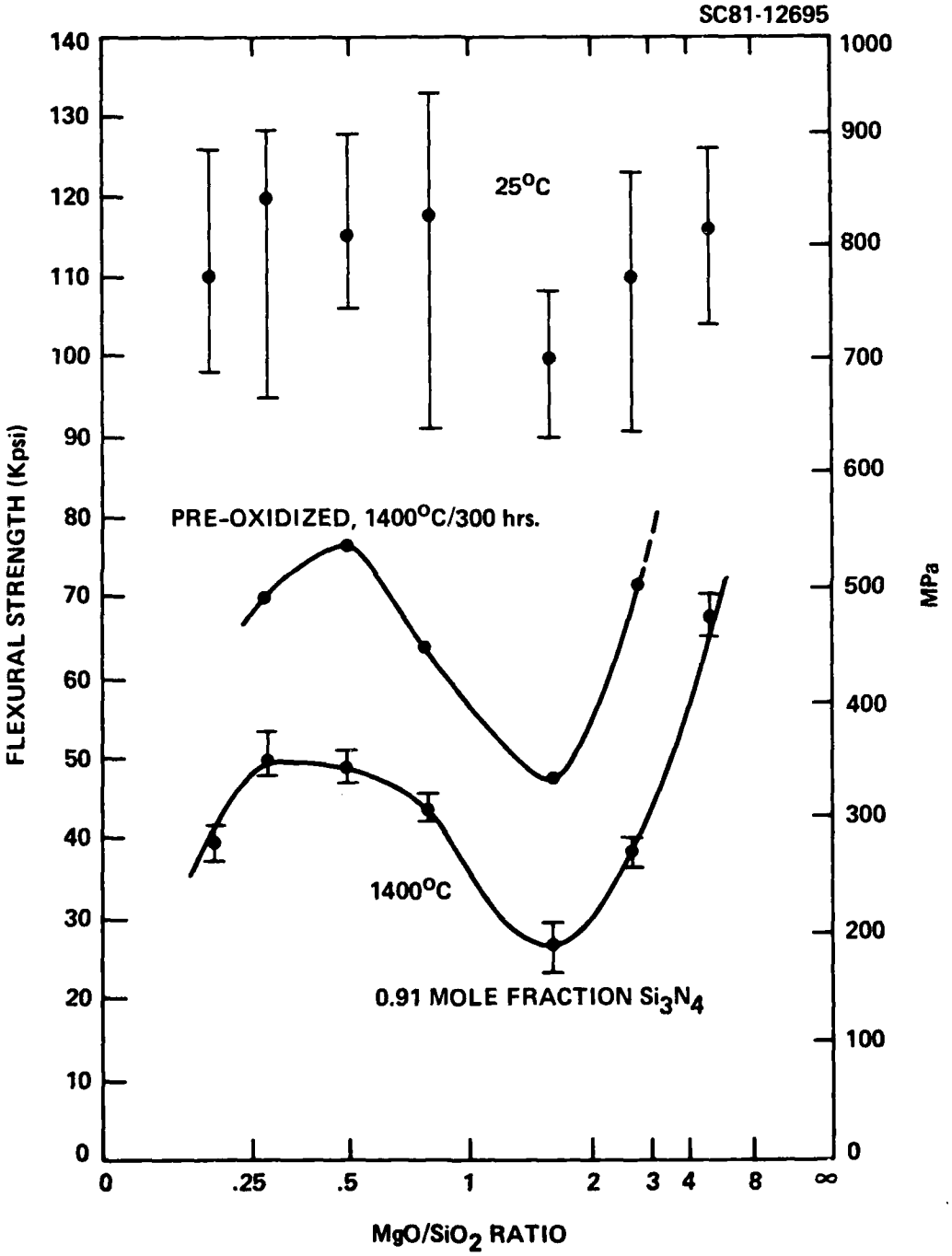

Fig. 2 Flexural strength data for the series containing 0.91 mole fraction Si_3N_4. Data include the 5 specimens subjected to a 1400°C/300 hr pre-oxidation treatment.

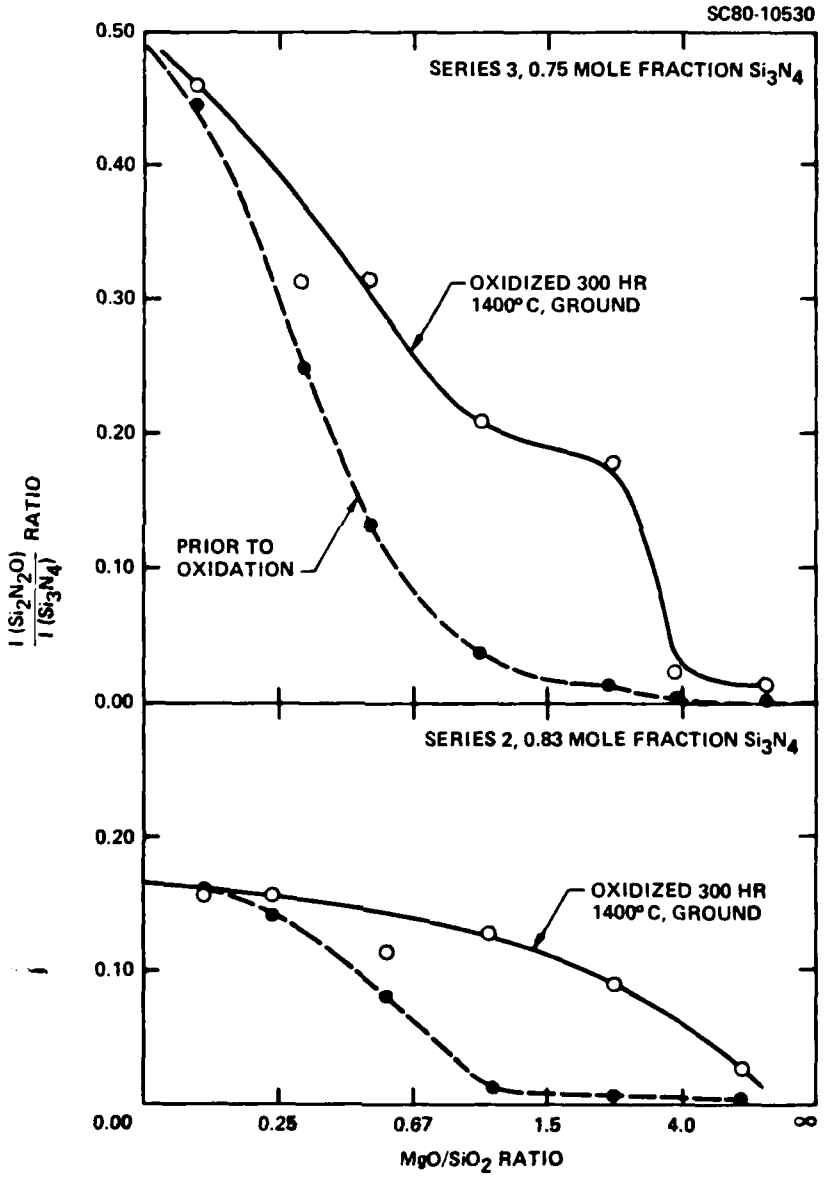

Fig. 3 Ratio of X-ray diffraction intensities of Si_2N_2O and Si_3N_4 prior to and after the 1400°C/300 hr pre-oxidation treatment as plotted against the initial Mg o/SiO_2 molar ratio.

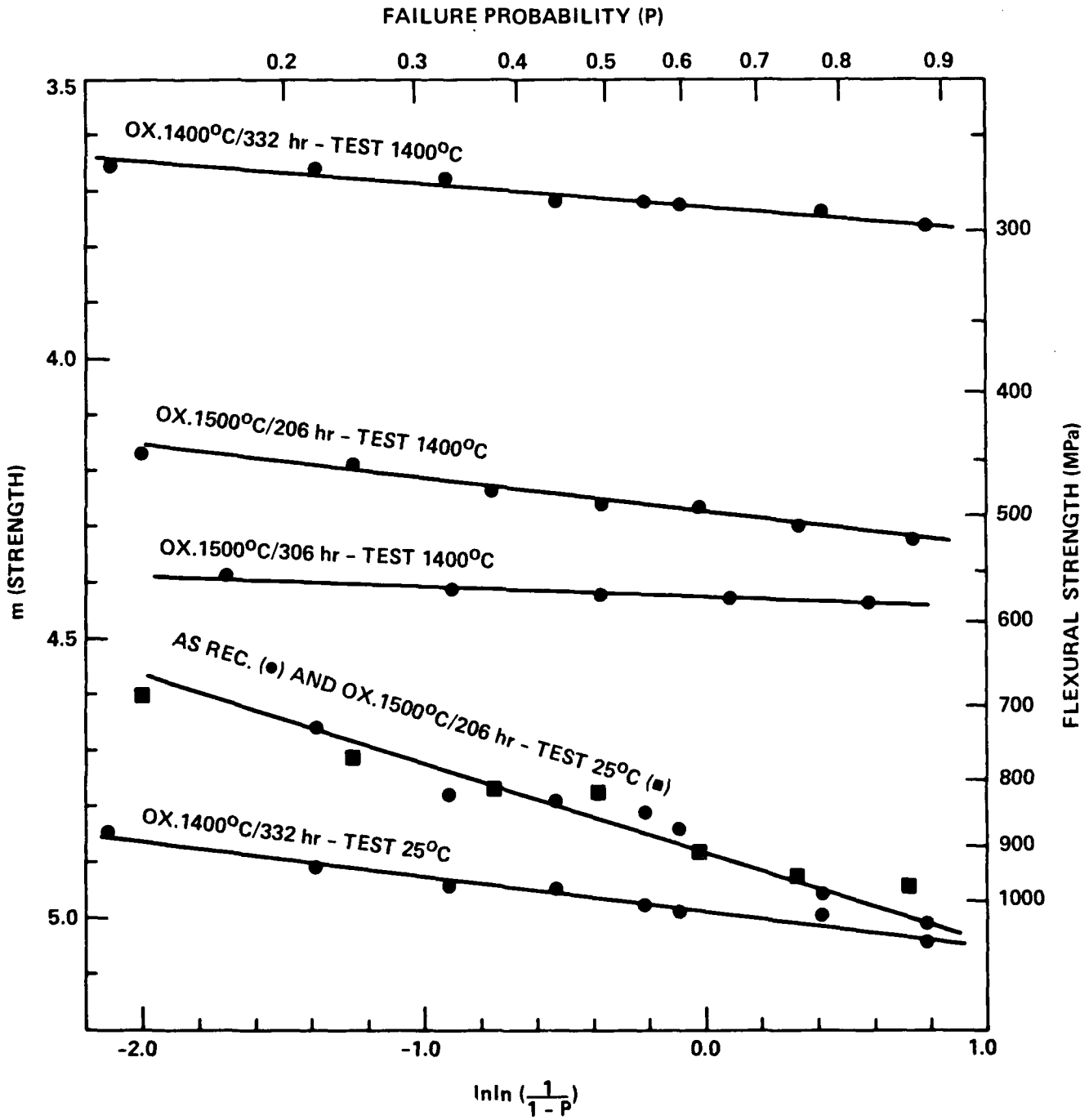

Fig. 4 Statistics for the flexural strength data of NC-132 Si_3N_4 material subjected to different pre-oxidation treatments.

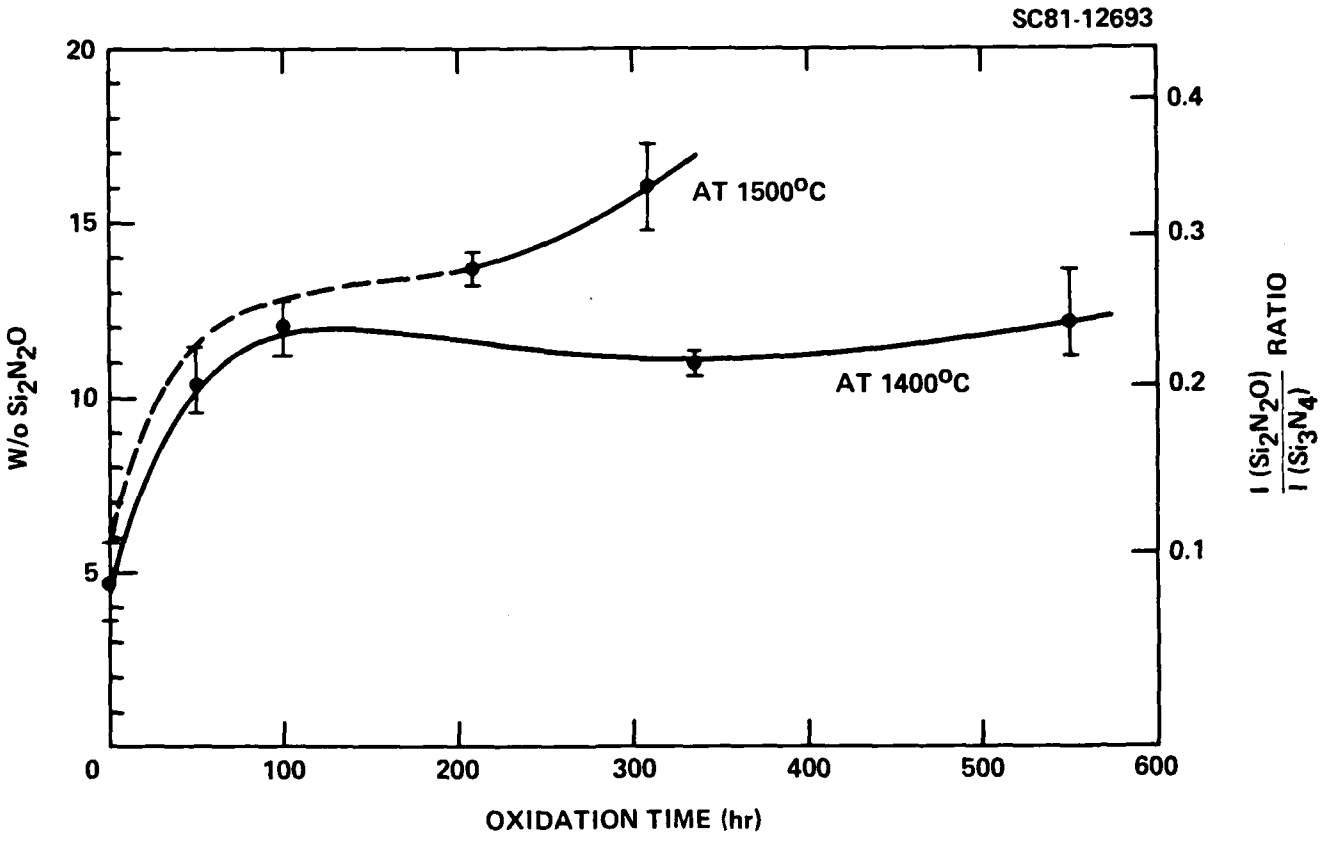

Fig. 5 Si_2N_2O content of NC-132 reground surfaces subjected to pre-oxidation treatments at 1400° and 1500°C as a function of treatment period.

APPENDIX 2

COMPARISON OF ARGON AND AIR HEAT TREATMENTS OF HOT PRESSED SILICON NITRIDE

D. R. Clarke
Rockwell International Science Center
Thousand Oaks, California 91360

INTRODUCTION

The majority of silicon nitride alloys densified with an additive contain a continuous intergranular glass phase.[1-3] This may act as a fast, or short circuit, diffusion path enabling rapid transport of ions from the interior of the material to the surface or vice versa. Such an effect has been demonstrated[4,5] during a study of the oxidation of hot-pressed silicon nitride materials. On oxidation it has been found that an oxide scale, rich in impurity and additive cations (e.g., Mg, Ca, Fe, Na), is formed on the surface[4,6-8] and a concentration gradient of the additive cation (Mg or Y for instance) is established below the scale[4,9] together with a concentration gradient of Si_2N_2O into the interior of the material.[4,5] These observations have been rationalized[4] on the basis of an effective diffusion couple formed between the surface SiO_2, created by the oxidation intergranular phase with migration occurring through the intergranular phase in an attempt to equilibrate the diffusion couple. Thus the effect of the oxidation is to draw both impurity and additive cations to the surface from the intergranular phase reducing the volume fraction of the phase and decreasing its impurity concentration.[4] As a result there is a consequential improvement in the high temperature strength[10] and creep resistance[11] of the materials.

An alternative approach to modifying the intergranular phase has been suggested by Morgan et al,[12] who have shown that heat treating silicon nitride materials in an argon gas atmosphere chemically reduces the crystalline oxide

phases present. As the intergranular phase is also an oxide containing phase[13] it might be expected that it too may be reduced. This suggestion is tested in the present work together with the possibility of combining heat treatments in air and in argon gas to both decrease the cation impurities and reduce the intergranular glass phase.

EXPERIMENTAL DETAILS

A MgO hot-pressed silicon nitride, having a composition 0.755 mol Si_3N_4, 0.90 mol SiO_2, 0.155 mol MgO, was chosen to compare the effects of differing heat treatments. The material was prepared by ball milling composite powders in methanol, drying and subsequently hot-pressing at 1750°C in graphite dies for two hours. Five rectangular bar samples were cut from the hot pressed billet. Two of the samples were oxidized by heating in air at 1400°C for 300 hrs. One of these two was then heated together with two of the remaining samples in flowing, high purity argon gas at 1400°C for 300 hrs. Then, one of the samples heat treated in argon was oxidized for 300 hrs at 1400°C in air. The fifth sample was not heat treated and was used as a control. In this manner the effects of heating for a prolonged period in air, argon, air followed by argon, and argon followed by air could be compared.

RESULTS

After the heat treatment, both the sample heated in air and the one in argon followed by air exhibited a visible, white scale. The other two materials were free of any scale and appeared greenish in color. These were also rather soft, resembling chalk in leaving a mark on sliding along a piece of wood. In addition, the sample heated first in argon, then in air contained large cracks along the length of the sample (Fig. 1).

X-ray diffraction patterns were recorded from both the surface and from a region, just below (~0.1 mm) the surface, exposed by grinding away any surface scale. The crystalline phases detected on the surface and below the

surface are listed in Tables I and II, respectively. The most notable finding is that on oxidation Si_2N_2O is formed in the interior of the sample whereas on heating in argon any Si_2N_2O below the surface is removed. Also on oxidation, either of the as-fabricated material or of an argon heat-treated sample, a scale consisting of $MgSiO_3$ and SiO_2 is formed. In the case of the sample first heated in argon SiO_2 is detectable below the surface as well as in the scale.

The surface scales produced by heating in air were indistinguishable from those previously reported for the oxidation scales on hot-pressed Si_3N_4. The morphology is illustrated by the scanning electron micrograph of Fig. 2. X-ray microanalysis indicated the scale to be rich in Mg, Ca, Al and Fe. The surfaces produced by exposure to argon at 1400°C were quite distinct (Fig. 3) being porous and having whisker-like growths. Only Si, Fe and W were detected on the surface by x-ray microanalysis. The surface of the sample first heated in air and then in argon was similar.

With the exception of the material heated in air the depth of the alterations produced by the various heat treatments could be readily seen in polished cross sections of the samples. These are reproduced in the optical micrographs of Fig. 4. The mottled appearance is attributable to regions of porosity. The interface between the unaffected core region and the altered sheath region is quite abrupt as is illustrated by the SEM of the polished cross section of the material heated first in air then in argon (Fig. 5). The depth of alteration is appreciable; 1.5 mm for the sample heated in argon.

The microstructure of the sample heated in argon was investigated by transmission electron microscopy. In the core region the microstructure was similar to that previously reported[1,3] for the hot-pressed material consisting of silicon nitride grains with the glass phase principally located at three and four-grain pockets and also along the two-grain junctions. Samples from just below the surface were difficult to prepare on account of the friability of the material. Nevertheless, the material in the sheath region was similar to that of the core region with the significant exception that instead of the

intergranular phase at the three- and four-grain junctions there were cavities. This is illustrated by the transmission electron micrograph of Fig. 6 where cavities have formed at the largest grain-junctions but not at the smallest. The intergranular phase at the two-grain junctions has remained intact in this region as is indicated by the characteristic[14] bright lines in the dark field image of the figure. The micrograph also indicates that in this region the glass phase in the three-grain junction pockets has not been entirely reduced but some remains coating the grains.

DISCUSSION

The experimental results described above demonstrate that substantial internal compositional changes, with consequential microstructural alteration, can be produced by heat treatments in reducing and oxidizing environments. No such changes are found in CVD silicon nitride. The depth of the changes below the surface and the modification of the intergranular phase indicate that rapid diffusion along the continuous intergranular phase is responsible for the magnitude of the effects observed.

The observation that the intergranular glass phase can be removed by heating in an argon atmosphere is consistent with the findings of Morgan et al that crystalline oxide phases, notably Si_2N_2O, in silicon nitride disappear under the same conditions (see Table II also). The porosity noted at three- and four-grain junction pockets by transmission electron microscopy indicate that continuous, interconnected open channels into the interior of the silicon nitride are produced by prolonged exposure to argon at 1400°C. It seems likely that the intergranular phase is also removed from the two-grain junctions, albeit at a slower rate due to their narrower (~1 mm) width, but difficulties in transmission electron microscope sample preparation due to the fragility of the material near the surface, precluded the necessary observations. The development of a network of continuous channels into the material is consistent with the observation that on subsequent heating in air for 300 hrs at 1400°C SiO_2 (as cristobalite), the oxidation product of Si_3N_4, was

detectable by x-ray diffraction in the interior of the material; SiO_2 is not normally found below the oxide scale on oxidation of fully dense silicon nitride as reported elsewhere and in Table II. The formation of SiO_2 (cristobalite) within the silicon nitride material and the subsequent volume increase on cooling is thought to be responsible for the observed cracking of the material (Fig. 1). One question that remains unanswered is the form and microstructural location of the additive and impurity cations, normally present in solution in the intergranular phase, after the argon gas heat-treatment. However, it is clear that they remain within the material because on subsequent oxidation of the material they are detectable in the surface oxide scale, by x-ray microanalysis and by the formation of clino-enstatite ($MgSiO_3$), just as is the material subjected to only an oxidation treatment.

Together the results suggest that a post-fabrication heat treatment for hot-pressed silicon nitride consisting of an oxidation step, to draw out the impurity and cation impurities, followed by controlled a reduction step to decrease further the volume fraction of the intergranular phase may lead to materials having improved high temperature properties.

REFERENCES

1. D. R. Clarke and G. Thomas, "Grain Boundary Phases in a Hot-Pressed MgO Fluxed Silicon Nitride," J. Am. Ceram. Soc. 60[11-12], 491-97 (1975).

2. L. K. V. Lou, T. E. Mitchell and A. H. Heuer, "Impurity Phases in Hot-Pressed Si_3N_4," J. Am. Ceram. Soc. 61[9-10], 392-96 (1978).

3. D. R. Clarke and G. Thomas, "Microstructure of Y_2O_3 Fluxed Hot-Pressed Silicon Nitride," J. Amer. Ceram. Soc. 61[3,4], 114-118 (1978).

4. D. R. Clarke and F. F. Lange, "Oxidation of Si_3N_4 Alloys: Relation to Phase Equilibria in the System Si_3N_4-SiO_2-MgO," J. Am. Ceram. Soc. 63[9,10], 586-593 (1980).

5. D. R. Clarke and F. F. Lange, "Oxidation of Silicon Nitride Alloys: An Experimental Test of Cation Diffusion," submitted J. Am. Ceram. Soc.

6. W. C. Tripp and H. C. Graham, "Oxidation of Si_3N_4 in the Range 1300°C-1500°C," J. Am. Ceram. Soc. 59[9,10], 399-403 (1976).

7. A. J. Kiehle, L. K. Heung, P. J. Gielisse and T. J. Rockett, "Oxidation Behavior of Hot-Pressed Si_3N_4," J. Am. Ceram. Soc. 58[1-2], 17-20 (1975).

8. S. C. Singhal, "Thermodynamics and Kinetics of Oxidation of Hot-Pressed Si_3N_4," J. Mater. Sci. 11[3] 500-509 (1976).

9. D. Cubicciotti, K. H. Lau, and R. L. Jones, "Rate-Controlling Process in the Oxidation of Hot-Pressed Silicon Nitride," J. Electrochem. Soc. 119[6], 791-93 (1972).

10. F. F. Lange, G. Schnittgrind and D. R. Clarke, to be published

11. F. F. Lange, B. I. Davis and D. R. Clarke, "Compressive Creep of Si_3N_4/MgO Alloys," J. Mater Sci. 15, 616-618 (1980).

12. P. E. D. Morgan, C. Wu and W. J. McDonough, "Internal Phase Changes in Dense Si_3N_4 Associated with High Temperature Oxidation," in press.

13. D. R. Clarke, N. J. Zaluzec and R. W. Carpenter, "The Intergranular Phase in Hot-Pressed Silicon Nitride Alloys: I. Elemental Composition," submitted.

14. D. R. Clarke, "On the Detection of Thin Intergranular Films by Electron Microscopy," Ultramicroscopy 4[1], 33-44 (1979).

Table I

Crystalline Phases on Surface After Heat Treatment at 1400°C

Heat Treatment	Phases
Air, 300 hr	$MgSiO_3$, SiO_2
Argon, 300 hr	β-Si_3N_4, WC, WSi_2
Air, 300 hr + Argon, 300 hr	β-Si_3N_4, WC, WSi_2
Argon, 300 hr + Air, 300 hr	$MgSiO_3$, SiO_2, β-Si_3N_4

Table II

Crystalline Phases ~0.1 mm Below Surface After Heat Treatment at 1400°C

Heat Treatment	Phases
Air, 300 hr	β-Si_3N_4, Si_2N_2O, WC
Argon, 300 hr	β-Si_3N_4, WSi_2, WC
Air, 300 hr + Argon, 300 hr	β-Si_3N_4, WSi_2, WC
Argon, 300 hr + Air, 300 hr	β-Si_3N_4, Si_2N_2O, SiO_2, WC

APPENDIX 3

Reprinted from the Journal of The American Ceramic Society Vol. 62 No. 3-4 March-April 1979

Evidence for Cavitation Crack Growth in Si_3N_4

F. F. LANGE*

ABOVE a given temperature (which appears to depend on gross composition[1] and impurities[2,3]) polyphase Si_3N_4 materials show subcritical crack growth.[4-6] Since some Si_3N_4 materials contain an amorphous phase,[7-8] and since certain compositions fabricated in the system Si_3N_4-SiO_2-MgO containing CaO impurities can have eutectics < 1400 C,[10] the formation and linking of cavities in the liquid phase ahead of a crack has been suggested as a mechanism for slow crack growth.[4,11-13] Observations in the present work confirmed this mechanism.

Specimens used for a previous study,[1] fabricated with composite powders containing a fixed molar content of Si_3N_4 and varying MgO/SiO_2 molar ratios were fractured in 4-point bending at 1400 C in air, cooled to room temperature, and refractured with a chisel to reveal the microstructure underlying the high-temperature fracture surface. Fracture surfaces were examined with an SEM.

The high-temperature fracture surface appeared oxidized (to different degrees depending on composition (Ref. 1)). Areas of slow crack growth similar to those previously reported could be easily identified for compositions with an MgO/SiO_2 ratio < 2. Typically, these areas contained thin wedges of material of different sizes and shapes which were torn away from the main fracture surface but still firmly attached at one end (see Figs. 3 and 4, Ref. 11), i.e. the wedges were formed by a large secondary crack which undercut a volume of material. The large crack-opening displacement indicated that extensive nonelastic deformation was associated with

Received June 9, 1978, revised copy received September 27, 1978.
Supported by the Air Force Office of Scientific Research under Contract No. F49620-77-C-0072.
The writer is with the Structural Ceramics Group, Rockwell International Science Center, Thousand Oaks, California 91360.
*Member, the American Ceramic Society.

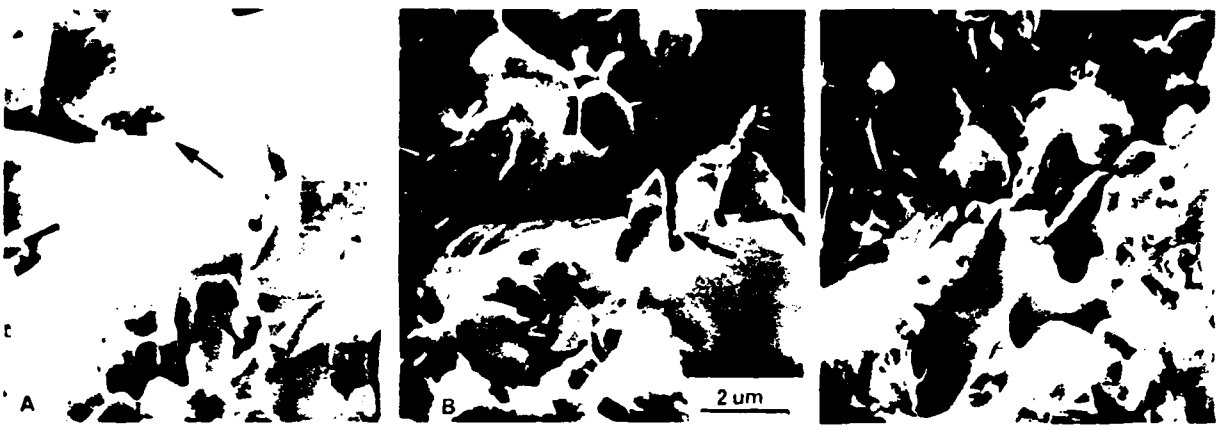

Fig. 1. Apparent viscous phase between separating grains of Si_3N_4, showing (*A*) large void, (*B*) "stringers," and (*C*) complete separation of grains. Observations made on room-temperature fracture surface within highly cavitated zone underlying 1400 C fracture surface.

both the material within the wedge and the secondary crack. Areas of fast crack growth appeared relatively smooth at low magnifications. At higher magnifications, the topographies of both the slow- and fast-crack-growth areas were indistinguishable. The topography was formed by the long prismatic Si_3N_4 grains (which appeared to undergo extensive separation from one another) coated with a fluid-like material which could represent the oxidation product.

Observations of the room-temperature fracture surfaces adjacent the high-temperature fracture surfaces showed that the microstructure beneath the latter contained many voids and large separations between adjacent grains. Qualitative observations indicated that the thickness of material containing the large void content increased for materials with compositions closer to the ternary eutectic within the Si_3N_4-Si_2N_2O-Mg_2SiO_4 compatibility triangle[10] (e.g. either by decreasing the Si_3N_4 content or by shifting toward an MgO/SiO_2 ratio of 1.6). Within a given material, maximum void contents were observed beneath the area of slow crack growth. By observing areas at higher magnifications, evidence was obtained for what appeared to have been a viscous phase between grains which had separated during fracture at 1400 C. Figure 1(*A*) shows the room-temperature fracture surface of an apparent viscous-phase "pocket" containing a large void. Fig. 1(*B*) shows "stringers" between two separating grains analogous to the stringers produced by printers ink between two separating plates, and Fig. 1(*C*) shows the complete separation of two grains with the remnants of the viscous phase adhering to the separated surfaces. Of the three, the latter was observed most frequently.

Occasionally the room-temperature fracture surface would cut through one of the torn wedges to reveal the microstructure of the material ahead of the secondary crack. For example, in Fig. 2 the secondary crack had propagated by the formation and linking of voids ahead of the crack.

The present evidence shows that slow crack growth in polyphase Si_3N_4 occurs by cavitation and that a liquid can be part of the high-temperature microstructure of these polyphase materials. These observations are consistent with those reported by Tighe.[14]

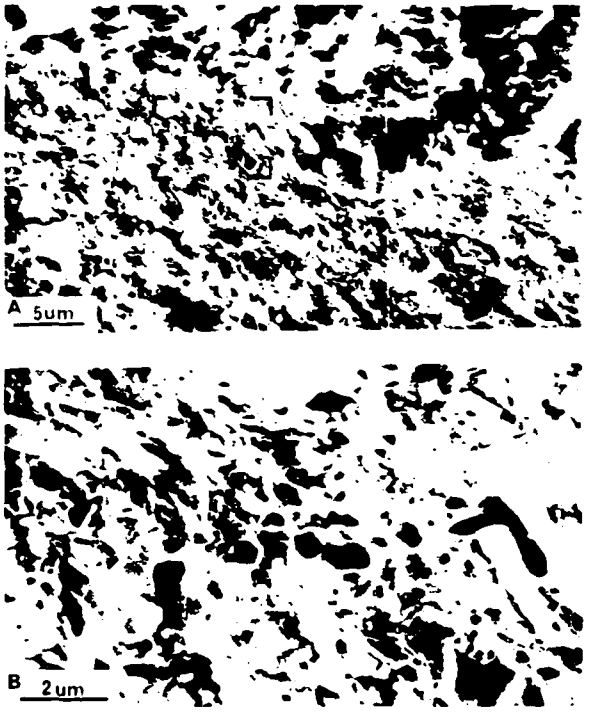

Fig. 2. Example of cavitation crack growth in polyphase Si_3N_4. (*A*) Intersection of room-temperature and 1400 C fracture surfaces, showing wedge separating from high-temperature fracture surface. (*B*) higher-magnification view of secondary crack which produced wedge of material.

[1] F. F. Lange, "Phase Relations in the System Si_3N_4-SiO_2-MgO and Their Interrelation with Strength and Oxidation," *J. Am. Ceram. Soc.* **61** [1–2] 53–56 (1978).
[2] J. L. Iskoe, F. F. Lange, and F. S. Diaz, "Effect of Selected Impurities on the High Temperature Mechanical Properties of Hot-Pressed Si_3N_4," *J. Mater. Sci.* **11** [5] 908–12 (1976).
[3] D. W. Richerson, "Effect of Impurities on the High Temperature Properties of Hot Pressed Silicon Nitride," *Am. Ceram. Soc. Bull.* **52** [7] 560–62 (1973).
[4] F. F. Lange, "High Temperature Strength Behavior of Hot-Pressed Si_3N_4: Evidence for Subcritical Crack Growth," *J. Am. Ceram. Soc.* **57** [2] 84–87 (1974).
[5] A. G. Evans and S. M. Wiederhorn, "Crack Propagation and Failure Prediction in Silicon Nitride at Elevated Temperatures," *J. Mater. Sci.* **9** [2] 270–78 (1974).
[6] A. G. Evans, L. R. Russell, and D. W. Richerson, "Slow Crack Growth in Ceramic Materials at Elevated Temperatures," *Metall. Trans. A* **6** [4] 707–16 (1975).
[7] A. G. Evans and J. V. Sharp, "Microstructural Studies on Silicon Nitride," *J. Mater. Sci.* **6** [10] 1292–1302 (1971).
[8] R. Kossowsky, "Microstructure of Hot-Pressed Silicon Nitride," *ibid.* **8** [11] 1603–15 (1973).
[9] D. R. Clarke and G. Thomas, "Grain Boundary Phases in a Hot Pressed MgO Fluxed Silicon Nitride," *J. Am. Ceram. Soc.* **60** [11–12] 491–95 (1977).
[10] F. F. Lange, "Eutectic Studies in the Si_3N_4-Si_2N_2O-Mg_2SiO_4-MgO System", submitted to the *Journal of the American Ceramic Society*.
[11] F. F. Lange, pp. 223–38 in Ceramics for High Performance Applications. Edited by J. J. Burke, A. E. Gorum, and R. N. Katz. Brook Hill, Chestnut Hill, Mass., 1974.
[12] F. F. Lange, pp. 361–81 in Deformation of Ceramic Materials. Edited by R. C. Bradt and R. E. Tressler. Plenum, New York, 1975.
[13] R. Raj, unpublished work.
[14] N. J. Tighe, "Structure of Slow Crack Interfaces in Silicon Nitride," *J. Mater. Sci.* **13** [7] 1455–63 (1978).

APPENDIX 4

Reprinted from the Journal of The American Ceramic Society, Vol. 62, No. 11-12 November-December 1979

Eutectic Studies in the System Si_3N_4-Si_2N_2O-Mg_2SiO_4

F. F. LANGE*

Rockwell International Science Center, Thousand Oaks, California 91360

Melting experiments have established three important eutectics in this system: (1) the Si_3N_4-Mg_2SiO_4 binary eutectic composition, $0.07Si_3N_4 + 0.93Mg_2SiO_4$, at 1566 C, (2) the Si_2N_2O-Mg_2SiO_4 binary eutectic composition, $0.17Si_2N_2O + 0.83Mg_2SiO_4$, at 1525 C, and (3) the Si_3N_4-Si_2N_2O-Mg_2SiO_4 ternary eutectic composition, $0.04Si_3N_4 + 0.14Si_2N_2O + 0.82Mg_2SiO_4$, at 1515 C. Systematic replacement of MgO with CaO in the ternary eutectic reduced its melting temperature to 1325 C for a CaO/MgO molar ratio of 0.67. The results of this study are discussed in relation to fabrication, microstructure, and high-temperature strengths.

I. Introduction

In a recent paper,[1] it was shown that the high-temperature strength of Si_3N_4 hot-pressed with the aid of MgO is strongly dependent on the MgO/SiO_2 molar ratio. At 1400 C, strength minima were observed in three compositional series when the MgO/SiO_2 molar ratio approached 2. Since the high-temperature strength behavior of polyphase Si_3N_4 alloys is believed to be governed by a liquid phase, these new strength-compositional observations suggested that the content of the liquid phase, and thus the strength, should be related to the eutectics within the system. Work was therefore initiated to determine eutectic compositions and temperatures within the portion of the system Si_3N_4-SiO_2-MgO where Si_3N_4 is known to be an equilibrium phase.[1] Since the impurity, CaO, is known to degrade the high-temperature strength of Si_3N_4/MgO alloys,[2] the effect of CaO on the melting temperature of one of the ternary eutectics was also investigated. The results of this work will be discussed in terms of the expected equilibrium and nonequilibrium microstructures of these polyphase materials and the effect of these microstructures on the high-temperature mechanical properties.

II. Experimental Procedure

Previous work established that Si_3N_4 is an equilibrium phase in two compatibility triangles of the system Si_3N_4-SiO_2-MgO: Si_3N_4-MgO-Mg_2SiO_4 and Si_3N_4-Si_2N_2O-Mg_2SiO_4.[1] This work also indicated that the eutectics associated with these two compatibility triangles might be close to the Mg_2SiO_4 end-member. Thus, the investigation to determine eutectic compositions and temperatures was concentrated in the Mg_2SiO_4-rich region of the system Si_3N_4-Si_2N_2O-Mg_2SiO_4.

A carbon heating system was chosen for this investigation to duplicate the atmospheric conditions used during the hot-pressing of Si_3N_4 materials. Melting experiments were chosen to determine the eutectics of interest. Seven master compositions of composite powders containing Si_3N_4, SiO_2, and MgO were prepared by liquid milling in plastic bottles containing tungsten carbide milling media. Compositions within the compositional area defined by the seven master batches (Fig. 1) were prepared by mixing proper proportions of two or more of the master compositions with a mortar and pestle. Each composition was pressed into one of an array of blind holes drilled into a graphite disk (5 cm in diam. by 1.25 cm thick). The disk was covered with graphite paper,* placed with a cylindrical graphite die with end-plungers, and heated in a hot-press containing a nitrogen atmosphere to the desired temperature for 30 min under a uniaxial stress of 7 MPa. Temperature was measured with a Pt-Pt10Rh thermocouple placed in a hole drilled in the graphite die to the depth of the specimens. The thermocouple was rebeaded after each experiment; it could not be used above 1600 C in the carbonaceous environment.

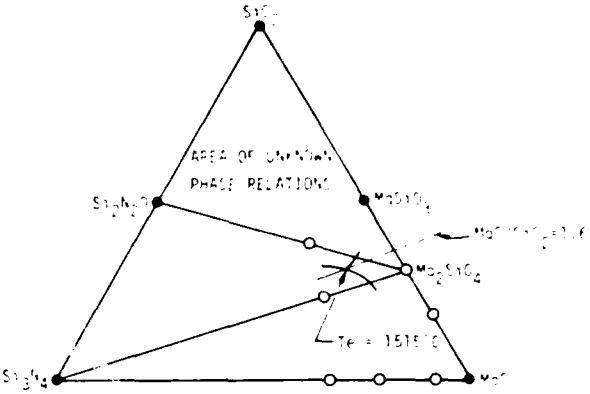

Fig. 1. Phase diagram of the system Si_3N_4-SiO_2-MgO illustrating the eutectics and the extent of boundary curves determined in the present work. Subsolidus tie lines were determined previously (Ref. 1). The seven master compositions are represented by filled circles.

After cooling, each composition was examined for the characteristics of melting. Below 1500 C, molten compositions formed spherical beads and above 1500 C the molten compositions appeared to wet the graphite surface. Compositions which exhibited incomplete melting and/or densification retained the shape of the container. Specimens and graphite disks were not reused; new powder and containers were used for subsequent experiments.

When a composition was observed to melt, adjacent, new compositions were mixed to replace those that did not melt for subsequent experiments at lower temperatures. This procedure was iterated until the lowest melting composition, viz. the eutectic composition, was determined. Using two stacked graphite disks, up to 46 compositions could be investigated in a single experiment.

Once the lowest ternary eutectic was determined, the effect of CaO on the melting temperature of this composition was determined by forming a series of compositions in which CaO systematically replaced the MgO. Experiments were conducted on this series to determine the composition with the lowest melting temperature.

III. Results

The melting experiments described above established three eutectics in the system Si_3N_4-Si_2N_2O-Mg_2SiO_4: (1) the Si_3N_4-Mg_2SiO_4 binary eutectic composition, $0.07Si_3N_4 + 0.93Mg_2SiO_4$ at 1560 C, (2) the Si_2N_2O-Mg_2SiO_4 binary eutectic composition, $0.17Si_2N_2O + 0.85Mg_2SiO_4$ at 1525°C, and (3) the Si_3N_4-Si_2N_2O-Mg_2SiO_4 ternary eutectic composition, $0.04Si_3N_4 + 0.14Si_2N_2O + 0.82Mg_2SiO_2$ at 1515°C. These eutectics and the extent of the observed boundary curves are illustrated on the phase diagram shown in Fig. 1. The ternary eutectic in the Si_3N_4-MgO-Mg_2SiO_4 compatibility triangle was not determined because experiments were not conducted above 1600°C.

Received June 9, 1978; revised copy received May 29, 1979.
Supported by the Air Force Office of Scientific Research under Contract No. F49620-77-C-0072.
*Member, the American Ceramic Society.
*Grafoil, Union Carbide Corp., New York, N.Y.

†Expressed as mole fractions.

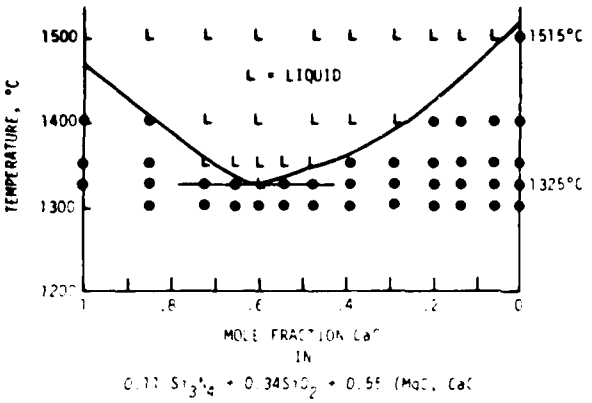

Fig. 2. The join between the ternary eutectic $0.11Si_3N_4 + 0.34SiO_2 + 0.55MgO$ and its CaO counterpart, illustrating the results of melting experiments

The effect of substituting CaO for MgO on melting temperature of the known ternary eutectic is shown in Fig. 2. The lowest melting composition in this series occurs for the composition $0.04Si_3N_4 + 0.14SiO_2 + 0.82$ $(0.4MgO + 0.6CaO)$ at 1325°C.

IV. Discussion

(1) Eutectics, Densification, and Microstructure

As expected, Si_3N_4 takes part in a generalized reaction with SiO_2 and MgO to form eutectic melts. The ternary eutectic temperature observed in this work is ≈50°C lower than the lowest eutectic in the binary system $MgO\text{-}SiO_2$.[3,4] Lower eutectics might be expected in the $Si_2N_2O\text{-}Mg_2SiO_4\text{-}SiO_2$ portion of the system, which was not explored in the present work. Since Si_3N_4 alloys are fabricated at >1650°C, liquid phase sintering phenomena appear, as expected, to be responsible for densification.

Neglecting the effects of impurities for the moment, composite powder (Si_3N_4, MgO, SiO_2) compositions in the $Si_3N_4\text{-}Si_2N_2O\text{-}Mg_2SiO_4$ compatibility triangle may form transient, nonequilibrium liquids during heating due to lower-temperature eutectics outside of the system studied here, but once equilibrium is obtained, a liquid will exist only above the system's ternary eutectic of 1515°C. The volume fraction of the liquid can be increased by either increasing the temperature or shifting the composition toward that of the eutectic. When impurities such as CaO are included, the composition no longer rests within the system $Si_3N_4\text{-}SiO_2\text{-}Mg_3N_2\text{-}MgO$, viz. reactions including CaO must be considered as depicted by the hypothetical equivalence diagram shown in Fig. 3. The shaded compositional element in this hypothetical phase diagram could represent the compatibility element for the compositions previously discussed, including CaO as an impurity. Although the element's eutectic is presently unknown, the results of melting experiments shown in Fig. 2 for compositions along the dashed line in Fig. 3 illustrate that the eutectic temperature could be <1325°C. Thus, the effect of CaO would be to lower the temperature where the composite powders would react to form a liquid. At temperatures exceeding the element's eutectic temperature, the content of the liquid would depend on the CaO content, viz. compositions with larger CaO impurity would be closer to the eutectic. Other impurities commonly associated with Si_3N_4 powder, e.g. oxides of Al and Fe, could have similar effects. Thus, in general, impurities will lower the temperature where the first equilibrium liquid would be observed and the liquid content would depend on the impurity content. Densification kinetics should therefore depend not only on gross composition (e.g. $Si_3N_4\text{-}SiO_2$ and MgO contents), but also on impurities.

When densification is achieved at the fabrication temperature, the liquid will begin to solidify as the temperature is lowered. The last bit of liquid will solidify at the eutectic temperature defined by the

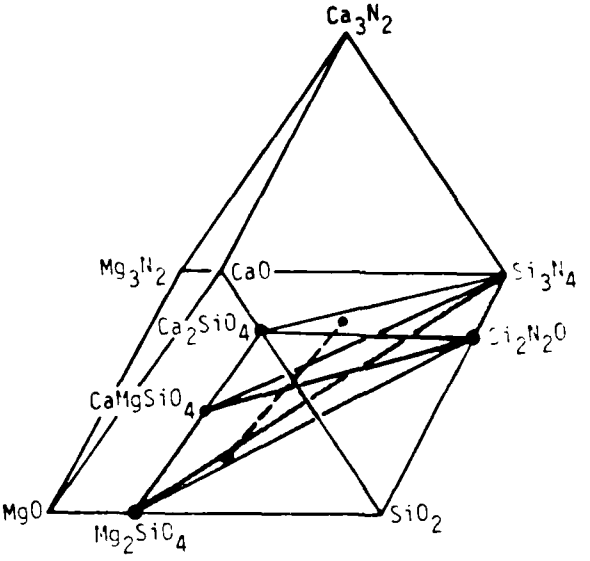

Fig. 3. Phase diagram of the system $Si_3N_4\text{-}SiO_2\text{-}Mg_3N_2\text{-}MgO\text{-}Ca_3N_2\text{-}CaO$, illustrating the shaded hypothetical compatibility element $Si_3N_4\text{-}Si_2N_2O\text{-}CaMgSiO_4\text{-}MgSiO_4$. The dashed line illustrates the join shown in Fig. 2

composition's compatibility element. The subsolidus microstructure of these polyphase materials will depend on several factors, e.g. if crystalline phases solidify during cooling, the amount and type of secondary crystalline phases will depend on the composition of the starting powders and the subsolidus phase relations. The configuration of the secondary phases will depend on interfacial energy considerations and their volume fraction as defined by rules of phase equilibria. If the liquid solidifies as a glass, it is not unreasonable to suggest that its composition and melting temperature may approximate that of the eutectic, since it would be the last to solidify. For this case, the subsolidus microstructure would represent the frozen, supersolidus microstructure.

(2) Eutectics and Mechanical Properties

Since a liquid phase will alter all subsolidus mechanical properties, relations between the high-temperature mechanical properties of polyphase Si_3N_4 alloys and their eutectics should be expected. If the secondary phases are crystalline, a liquid will not reappear on heating until the eutectic temperature is reached. At this temperature, strength should fall precipitously as observed for SiC-Si composites.[5] On the other hand, if the secondary phases are amorphous, the mechanical properties might be expected to gradually decrease as the eutectic temperature is approached, viz. the viscosity of silicate glasses can begin to decrease several hundred degrees prior to reaching the eutectic temperature. In this case, degradation of subsolidus mechanical properties might be expected to begin 100 to 300°C below the eutectic temperature, as observed for Si_3N_4 alloys.[6]

The effects of composition and impurities on the high-temperature strength of Si_3N_4/MgO alloys can be explained in terms of observed eutectics. The line drawn between Si_3N_4 and the ternary eutectic (Fig. 1) describes compositions containing an MgO/SiO_2 molar ratio of 1.6. The liquid content above the eutectic (or the subsolidus glass content) for a series of compositions with a fixed amount of Si_3N_4 but variable MgO/SiO_2 will be a maximum where the MgO/SiO = 1.6. Previous studies[1] with three series of materials resulted in high-temperature strength minima at an MgO/SiO_2 molar ratio between ≈1.5 and 2.0. These results are consistent with the argument that all materials within each series contained a viscous phase at the test temperature and that the volume content of the viscous phase was maximized at an MgO/SiO_2 molar ratio of ≈1.6.

Studies have also shown that the high-temperature strength of an

Si_3N_4/MgO alloy decreased in proportion to the amount of the CaO intentionally added to the starting composition to simulate and study the effect of impurities.[2] Previous explanations for this effect have been that CaO will decrease the viscosity of the amorphous phase at high temperatures.[2,6,7] But, as pointed out by Powell and Drew[8] and observed by Turkdogan and Bills,[9] CaO and MgO have very similar effects on the viscosity of silicate glasses. In light of the current work, a more consistent explanation is that the CaO will increase the volume content of the amorphous phase according to the phase equilibria considerations discussed. Strength at high temperatures will depend not only on the presence of the viscous phase but also on its volume content, as shown by Williams and Singer.[10]

The discussion resulting from the present work concerning the effect of composition, impurities, and eutectics on fabrication, microstructure, and mechanical properties should generally apply to all Si_3N_4/metal oxide polyphase alloy systems and to all polyphase systems in general. When an impurity in a single-phase material exceeds its solid-solubility limit, the material must be considered polyphase, which immediately invokes phase equilibria considerations to explain fabrication, microstructure development, and properties.

Acknowledgments: The writer thanks L. J. Gauckler for helpful discussions in choosing a method for determining eutectics and M. G. Metcalf for technical assistance.

References

[1] F. F. Lange, "Phase Relations in the System Si_3N_4-SiO_2-MgO and Their Interrelation with Strength and Oxidation," *J. Am. Ceram. Soc.*, **61** [1–2] 53–56 (1978).

[2] J. L. Iskoe, F. F. Lange, and F. S. Diaz, "Effect of Selected Impurities on the High Temperature Mechanical Properties of Hot-Pressed Si_3N_4," *J. Mater. Sci.*, **11** [5] 908–12 (1976).

[3] E. M. Levin, C. R. Robbins, and H. F. McMurdie, *Phase Diagrams for Ceramists*, 1964. Edited by M. K. Reser. American Ceramic Society, Columbus, OH, 1964.

[4] F. R. Boyd, J. L. England, and B. T. C. Davis, "Effects of Pressure on the Melting and Polymorphism of Enstatite, $MgSiO_3$," *J. Geophys. Res.*, **69** [12] 2101–09 (1964).

[5] C. W. Forrest, P. Kennedy, and J. V. Shennan, pp. 99–123 in *Special Ceramics 5*. Edited by P. Popper. British Ceramic Research Association, Stoke-on-Trent, 1972.

[6] F. F. Lange, "Hot Temperature Strength Behavior of Hot-Pressed Si_3N_4 Evidence for Subcritical Crack Growth," *J. Am. Ceram. Soc.*, **57** [2] 84–87 (1974).

[7] R. Kossowsky, "The Microstructure of Hot-Pressed Si_3N_4," *J. Mater. Sci.*, **8** [10] 1603–15 (1973).

[8] B. D. Powell and P. Drew, "The Identification of a Grain Boundary Phase in Hot-Pressed Si_3N_4 by Auger Electron Spectroscopy," *J. Mater. Sci.*, **9** [5] 1867–72 (1974).

[9] E. T. Turkdogan and P. M. Bills, "A Critical Review of Viscosities of Calcia-Magnesia-Alumina-Silica Melts," *Am. Ceram. Soc. Bull.*, **39** [7] 362–67 (1960).

[10] J. A. Williams and A. R. E. Singer, "Deformation, Strength and Fracture Above the Solidus Temperature," *J. Inst. Met.*, **96** [1] 5–12 (1968).

Reprinted from the Journal of The American Ceramic Society Vol 63, No 3-4 March-April 1980

CORRECTION

Eutectic Studies in the System Si_3N_4-Si_2N_2O-Mg_2SiO_4

F. F. Lange

J. Am. Ceram. Soc., **62** [11-12] 617-19 (1979)

The eutectic compositions should read: (1) The Si_3N_4-Mg_2SiO_4 binary eutectic composition, $0.19Si_3N_4 + 0.81\ Mg_2SiO_4$ at 1560°C, (2) the Si_2N_2O-Mg_2SiO_4 binary eutectic composition, $0.39Si_2N_2O + 0.61Mg_2SiO_4$ at 1525°C, and (3) the ternary eutectic composition, $0.10Si_3N_4 + 0.30Si_2N_2O + 0.60Mg_2SiO_4$ at 1515°C. Figure 2 correctly reports the ternary eutectic in terms of Si_3N_4, SiO_2, and MgO.

APPENDIX 5

Reprinted from the Journal of The American Ceramic Society, Vol. 61, No. 5-6 May-June, 1978

Reaction of Iron with Si_3N_4 Materials to Produce Surface Pitting

F. F. LANGE*

THE purpose of this note is to show that surface pits result from the reaction of Fe with most Si_3N_4 alloys fabricated with MgO, whereas pitting does not result for certain Si_3N_4 alloys fabricated with Y_2O_3.

Singhal[1] has shown that the long term oxidation of commercial Si_3N_4 fabricated with MgO leads to degradation of flexural strength ranging from 30% for periods ≥ 300 h at 1100 C to 60% for ≥ 100 h at 1375 C. Large surface pits formed during oxidation appear to be responsible for the degradation, e.g. pits are common fracture origins and strength can be regained after removing the pits by surface grinding.[1] Similar, but less extensive oxidation/strength testing of Si_3N_4 fabricated within the system Si_3N_4-Si_2N_2O-$Y_2Si_2O_7$ leads to $\approx 15\%$ strength reduction for oxidation periods up to 400 h at 1375 C[2]; surface pitting was not observed for this material.

The formation of surface pits during oxidation suggests the presence of heterogeneously distributed reactive sites. Sources for such sites could include aggregated second phases, large contaminant particles introduced during fabrication, and furnace debris. Although aggregated second-phase particles are likely sources for Si_3N_4 hot-pressed with MgO,* the effect of large contaminant particles was sought in the present work.

Several large, metallic-appearing particles were located on the surface of commercial NC-132 Si_3N_4 with light microscopy. The particles were typically aggregated, aggregated subsurface particles could be observed with crossed polars (Fig. 1). Each group of particles was relocated in an SEM and identified with the aid of EDAX. All particles consisted of Si, W, and Fe, a few also contained Ni, Cr, and/or Co. Other workers[4,5] have reported similar contaminants in hot-pressed Si_3N_4. One common contaminant is WSi_2 due to the WC media used to mill the powder before hot-pressing; another is Fe, which is added by some workers[6] to increase the nitriding rate in producing Si_3N_4 powder.

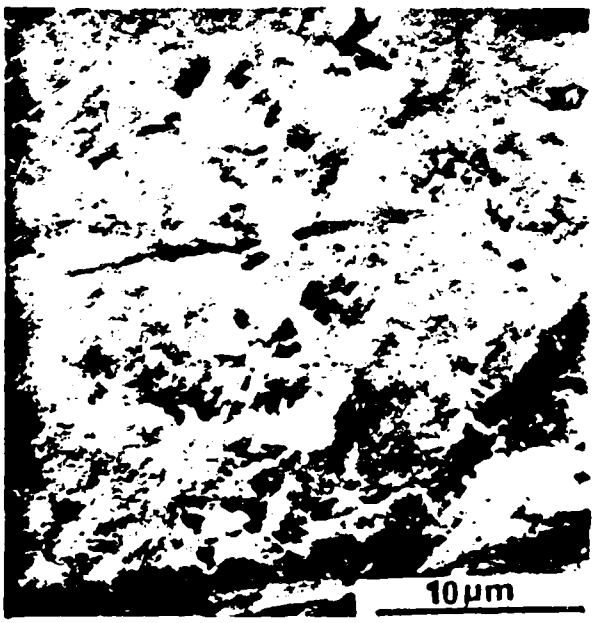

Fig. 1. Scanning electron micrograph of ground and partially polished surface of NC-132 Si_3N_4, showing aggregated inclusions consisting of Si, W, and Fe.

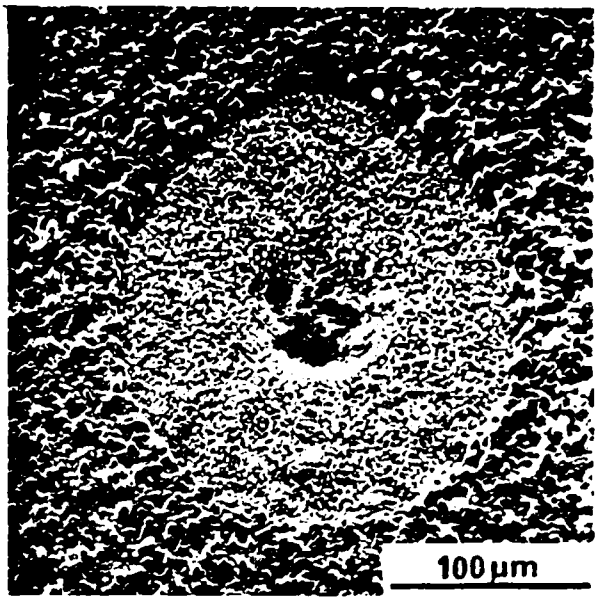

Fig. 2. Scanning electron micrograph of surface pit and reactive zone formed during oxidation (1400°C/0.5 h) of Fe particle on hot-pressed specimen containing 0.83 mol fraction Si_3N_4, with an MgO/SiO_2 molar ratio of 5.

Short-period oxidation tests at 1300° and 1400 C indicated greater reactivity at the impurity sites which could be relocated, but due to the ambiguity of relocating most of the sites beneath the oxide scale, a second group of experiments was conducted in which small particles (≈ 200 μm) of Fe were placed on the surfaces of different Si_3N_4 materials. Emphasis was placed on Fe due to the volatile nature of tungsten oxides. The Si_3N_4 materials investigated included NC-132 Si_3N_4,† a series of materials containing 0.83 mol fraction Si_3N_4 with different MgO/SiO_2 molar ratios,[3] and Si_3N_4 fabricated with 0.840, 0.055, and 0.105 mol fraction of Si_3N_4, Y_2O_3, and SiO_2, respectively.[2] Each specimen was oxidized at 1400 C for up to 4 h.

For the materials with different MgO/SiO_2 molar ratios, the surface reaction at the site of the Fe particle ranged from no apparent reaction for the material with $MgO/SiO_2 = 0.1$ to a glassy reactive zone containing a shallow pit for $0.1 < MgO/SiO_2 < 0.5$ to a highly reactive, deeply pitted area for $MgO/SiO_2 < 0.5$ (Fig. 2). The reactive area for NC-132 Si_3N_4 was similar to the material within the series with $MgO/SiO_2 = 0.5$. Surface cracks, presumed to form during cooling, were observed within all reactive zones. No apparent reaction occurred for the $Si_3N_4/Y_2O_3/SiO_2$ material (Fig. 3).

These results show that surface pitting produced during the oxidation of Si_3N_4-MgO alloys can be caused by heterogeneously distributed Fe contaminants and that the reactivity/pitting increases as the MgO/SiO_2 molar ratio is increased. Previous studies[3] showed that, when $MgO/SiO_2 < 2$, the equilibrium secondary phases are Si_2N_2O and Mg_2SiO_4 and, when $MgO/SiO_2 > 2$, the secondary phases are Mg_2SiO_4 and MgO. Nonequilibrium magnesium silicate-nitrogen glasses are presumed to be present also. The reaction in oxidizing environments between Fe and the secondary phases is presumed to involve FeO and SiO_2, the oxidation products of Fe and Si_3N_4, respectively, and the equilibrium/nonequilibrium magnesium phases present in Si_3N_4-MgO alloys. Such reactions can produce relatively low temperature eutectics.[8] The absence of significant

Received January 23, 1978
Supported by the Air Force Office of Scientific Research under Contract No. F49620-77-C-0072.
The writer is with the Structural Ceramics Group, Rockwell International Science Center, Thousand Oaks, California 91360.
*Member, the American Ceramic Society.
*The magnesium compounds present in the Si_3N_4-MgO alloys are not compatible with SiO_2, the oxidation product of Si_3N_4 (Ref. 3).

†Norton Co., Worcester, Mass.

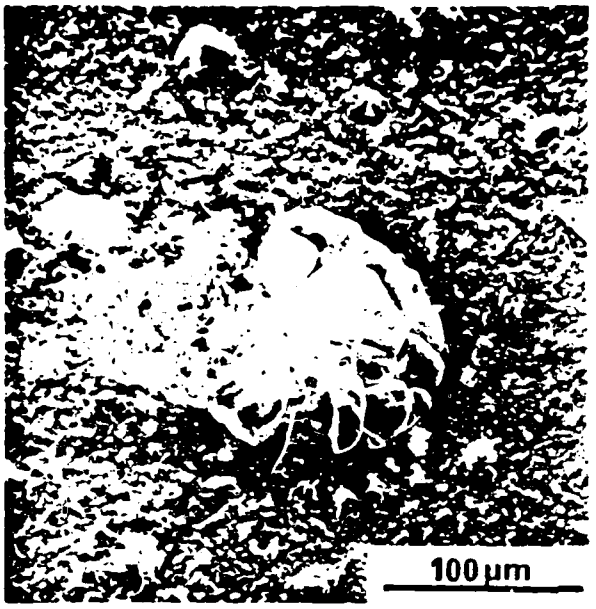

Fig. 3. Scanning electron micrograph showing relatively little reaction between Fe particle and $Si_3N_4/Y_2O_3/SiO_2$ material after oxidation at 1400°C for 4 h. Part of Fe oxide particle has been removed to illustrate reactive surface.

reactivity in the $Si_3N_4/Y_2O_3/SiO_2$ material indicates a tolerance for Fe contamination in this system without severe oxidation/strength degradation.

---

[1] (a) S. C. Singhal, "Strength Degradation of Si_3N_4 Due to Oxidation", unpublished work.

(b) A. F. McLean, E. A. Fisher, R. J. Bratton, and R. J. Miller, "Brittle Materials Design, High Temperature Gas Turbine," Interim Tech. Repts. AMMRC-CTR-75-28, Sept. 1975 and AMMRC CTR-76-12, April 1976.

[2] F. F. Lange and S. C. Singhal, unpublished work.

[3] F. F. Lange, "Phase Relations in the Si_3N_4-SiO_2-MgO Systems and Their Interrelation with Strength and Oxidation," *J. Am. Ceram. Soc.*, **61** [1–2] 53–56 (1978).

[4] R. Kossowsky, "Microstructure of Hot-Pressed Si_3N_4," *J. Mater. Sci.*, **8** [11] 1603–15 (1973).

[5] H. R. Baumgartner and D. W. Richerson, pp. 367–86 in Fracture Mechanics of Ceramics, Vol. 1. Edited by R. C. Bradt, D. P. H. Hasselman, and F. F. Lange. Plenum, New York, 1974.

[6] P. Popper and S. N. Ruddlesden, "Preparation, Properties and Structure of Silicon Nitride," *Trans. Br. Ceram. Soc.*, **60** [9] 603–26 (1961).

[7] F. F. Lange, S. C. Singhal, and R. C. Kuznicki, "Phase Relations and Stability Studies in the Si_3N_4-SiO_2-Y_2O_3 Pseudoternary System," *J. Am. Ceram. Soc.*, **60** [5–6] 249–52 (1977).

[8] E. M. Levin, C. R. Robbins, and H. F. McMurdie, Phase Diagrams for Ceramists. Edited by M. K. Reser. American Ceramic Society, Columbus, Ohio, 1964, Figs. 682, 687.

APPENDIX 6

JOURNAL OF MATERIALS SCIENCE 15 (1980) 601–610

Compressive creep of Si_3N_4/MgO alloys

Part 1 *Effect of composition*

F. F. LANGE, B. I. DAVIS, D. R. CLARKE
Rockwell International Science Center, Thousand Oaks, California 91360, USA

The compressive creep behaviour of four compositions within the Si_3N_4–Mg_2SiO_4–Si_2N_2O compatibility triangle were studied in air at 1400° C. Strain rate ($\dot{\epsilon}$) versus stress (σ) was analysed to determine the stress exponent, n ($\dot{\epsilon} = A\sigma^n$). Cavitation during creep was determined by precise (sink–float) density measurements. Compositions close to the Si_3N_4–Si_2N_2O tie line exhibited no cavitation and had $n \simeq 1$, whereas compositions close to the Si_3N_4–Mg_2SiO_4 tie line exhibited extensive cavitation and had $n \simeq 2$. Test results are interpreted in terms of the volume fraction of the viscous phase present.

1. Introduction

Composition strongly affects the creep resistance of polyphase Si_3N_4 alloys fabricated with a densification aid [1–8]. Investigators who have examined the creep resistances of a variety of Si_3N_4 alloys have shown that the creep rate at a specific temperature and stress can vary by orders of magnitude depending on composition [1, 2]. The effects of some impurities [8] (e.g. CaO) and gross composition [1, 2, 5, 7] (type and amount of the densification aid) have been qualitatively documented.

Earlier investigators suggested that the general degradation of mechanical properties at high temperatures was due to the presence of viscous phase between the Si_3N_4 grains. High-resolution electron microscopy work has since confirmed that a continuous glassy phase does exist in most Si_3N_4 alloys [9, 10]. Assuming that the composition of the glassy phase is similar to the eutectic composition (i.e. the last liquid to solidify during cooling) of the compatibility triangle in which the composition was fabricated, Lange [11] pointed out that the content of the glass will depend on composition in the manner described by rules of phase equilibria; the volume fraction of the glassy "grain-boundary phase" will increase as the composition of the alloy is shifted toward the eutectic composition. Likewise, the temperature where degradation is first apparent should be related to the eutectic temperature. Since impurities must be included in phase equilibrium considerations, they will influence the eutectic composition and temperature. In this manner, the effects of impurities and gross composition can be combined, shifting the alloy composition either toward or away from the eutectic composition to either decrease or increase the high temperature properties, respectively [11]. The observed change in strength with composition for three series of materials in the Si–Mg–O–N system is consistent with this idea [12]. It is expected that creep resistance should follow suit.

Most investigators have directed the analysis of creep behaviour in terms of phenomena which produce cavities. This direction resulted from both TEM studies which reveal cavities at triple points in crept specimens [3, 4] and stress exponents for creep rate that do not correspond to conventional (e.g. diffusion and/or dislocation) models. One notable exception to this general trend was Seltzer's [2] observation of a linear stress dependence for several compositions in the Si–Al–O–N system fabricated with $\leqslant 30$ wt % Al_2O_3.* Other materials in this same system containing $\geqslant 40$ wt % Al_2O_3 had larger stress exponents, consistent with those reported for all other Si_3N_4 materials [2]. Thus, Seltzer's measurements suggest that at least two different mechanisms can dominate the creep

* This complete series of alloys, fabricated by the present author, were hot-pressed with 20, 30, 40 and 50 wt % Al_2O_3 plus Si_3N_4 [13].

0022–2461/80/030601–10$03.00/0

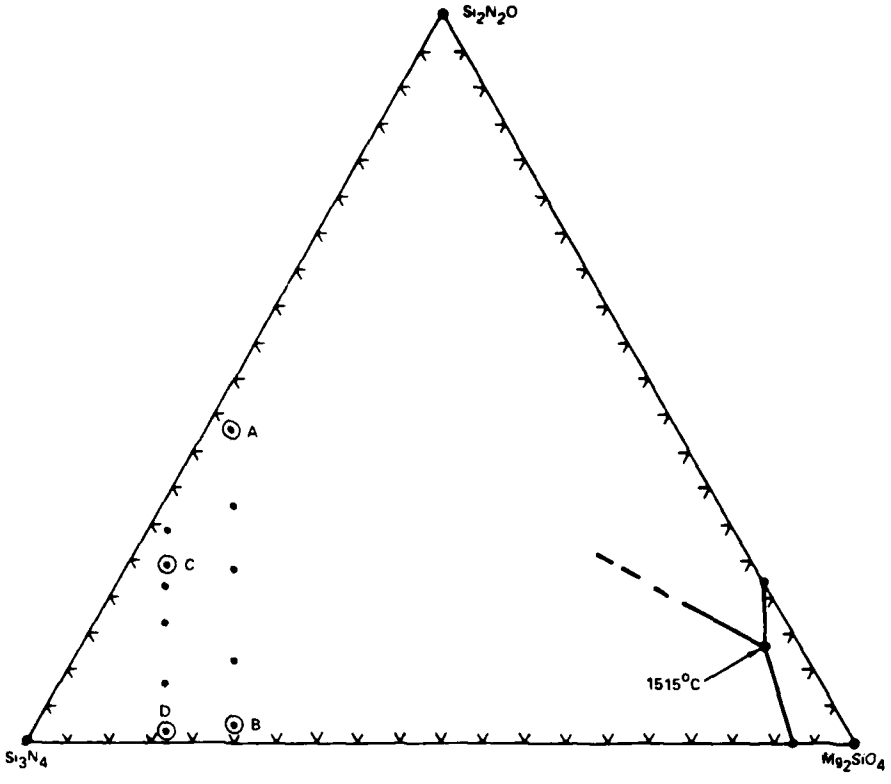

Figure 1 The Si_3N_4–Mg_2SiO_4–Si_2N_2O system illustrating compositions of materials used in this study in relation to eutectic composition.

behaviour of Si_3N_4 alloys, and a shift from one mechanism to another depends on composition.

The purpose of the present work was to characterize the creep behaviour of Si_3N_4 alloys as a function of composition in an attempt to classify the dominant creep mechanism in terms of the volume content of the glassy "grain-boundary phase". To accomplish this goal, well characterized alloy compositions were chosen from the Si_3N_4–Mg_2SiO_4–Si_2N_2O compatibility triangle of the Si–Mg–O–N system. Since eutectics in this compositional area are known, the relative volume fraction of the glassy phase for each composition could be estimated and related to the observed creep phenomena.

2. Experimental details

2.1. Materials

The compositions of the four materials (A, B, C, D) chosen for extensive study were part of two series of materials fabricated for a previous study concerning strength and oxidation [12]. Fig. 1 illustrates the compositions of these four materials (circled points), the compositions of the other materials within the two series, and the eutectic compositions and temperatures previously determined. All materials shown in Fig. 1 were prepared from high purity Si_3N_4 (e.g. 160 ppm Ca, 0.6 wt % O_2), SiO_2 and MgO powders, ball milled with WC media in plastic bottles, and hot-pressed at 1750° C for 2 h as reported elsewhere [12].

Phase identification was by X-ray diffraction. All materials contained β-Si_3N_4 and WC. Compositions A and C, contained Si_2N_2O in apparent proportion to that indicated by their position in the phase diagram; no Si_2N_2O was detected in B and D. The Mg_2SiO_4, expected to be present in all compositions, was not observed as a crystalline phase.

All materials were examined by transmission electron microscopy throughout this study. Dark-field imaging [14] revealed a glassy "grain-boundary phase" between all grains and at triple points as shown in Fig. 2. Extensive TEM work to

Figure 2 Dark-field image of the continuous glassy phase between Si_3N_4 grains.

quantify any difference in the volume content of the glassy phase in the four materials was not performed. Based on the above evidence (lack of a crystalline Mg_2SiO_4 phase and the presence of a glassy phase), the composition of the glassy phase was assumed to be the same as the ternary eutectic composition. Based on this assumption, the volume fraction of the glassy phase was estimated for each composition by using the lever rule to interpret the phase diagram and the appropriate molecular weights and densities.* Table I lists the estimated volume fractions of the glassy phase.

2.2. Creep experiments

Compressional creep testing was performed in air at 1400° C. Specimens (approximately 0.3 cm × 0.3 cm × 0.9 cm) were diamond cut and finished in a special jig so that parallelism of the two end surfaces was ensured. A high temperature extensiometer, described in the Appendix, was developed to measure strain. A dead weight, cantilevered (10:1) loading frame transmitted load to the specimen as shown in Fig. 10. The loading pads in contact with the specimen were made from either sintered or CVD SiC. Commercial grade, hot-pressed Si_3N_4 loading pads were observed to creep under the specimen and to result in unreliable strain measurements.

The apparent steady-state strain rates ($\dot{\epsilon}$) were analysed with respect to the empirical relation

$$\dot{\epsilon} = A\sigma^n \qquad (1)$$

in an applied stress (σ) range between 70 and 700 MPa. Load was applied after the temperature was stabilized at 1400° C for a period of 1 h. Throughout each experiment, temperature did not vary more than ± 2° C. Because oxidation affects the creep behaviour of these materials (as detailed in Part 3 [15]), a new specimen was used at each stress; steady-state creep rates were determined for periods ⩽ 20 h. The total strain for any experiment never exceeded 0.05.

2.3. Density determinations

Because cavities were expected to form during creep, their volume content was determined by precise density measurements as a function of creep strain at a compressive stress of 350 MPa for materials C and D. To avoid the possible closure of cavities during cooling, the compressive load was not removed until the specimen was cool. Cavitation was also examined as a function of applied stress (175 to 700 MPa) with the same materials at a strain of 0.03. Density measurements were also performed on materials A and B, but only at a creep strain of 0.03 at 350 MPa.

A sink-float technique was developed to measure the volume fraction of cavities produced during creep. Mixtures of diiodemethane (ρ = 3.3 g cm^{-3}) and neothane (ρ = 1.3 g cm^{-3}) were prepared until the specimen would neither sink or float. To minimize the effect of volatilization, the liquid plus specimen were transferred to a pychnometer with a volume previously determined over a temperature range of 15 to 30° C. The pycnometer containing the liquid and specimen was then either heated or cooled slowly until the specimen was suspended within the liquid. Liquid was either removed or added to the pycnometer to compensate its volume change before weighing. With this technique, the density of a specimen could be

TABLE I Composition and phase content of creep specimens

Specimens	Composition (mole fraction)			Phases identified	Vol. fraction of glassy phase
	Si_3N_4	Si_2N_2O	Mg_2SiO_4		
A	0.54	0.43	0.03	β-Si_3N_4, Si_2N_2O, WC	0.04
B	0.74	0.03	0.23	β-Si_3N_4, WC	0.17
C	0.71	0.24	0.05	β-Si_3N_4, Si_2N_2O, WC	0.05
D	0.83	0.01	0.16	β-Si_3N_4, WC	0.11

* The density of the glass was assumed to be 3 g cm^{-3}.

reproduced by using different starting fluid mixtures to ± 0.0003 g cm^{-3}. That is, the technique was capable of reproducing a density measurement to ± 0.01%.

The density of each specimen was determined before and after the creep experiment. The oxide scale and material to the depth of ~ 0.02 cm below the scale/bulk interface was removed by surface grinding prior to measuring the density of the crept specimens. Several crept specimens with end cracks were diced into 2 or 3 pieces to preclude the effect of the crack. It was observed that the cracks did not significantly affect density. To preclude density changes that might arise through oxidation, differential densities of a series of specimens from materials C and D were determined as a function of oxidation period at 1400° C.

3. Results

3.1. General behaviour

The strain–time response of all stressed specimens included a small elastic deformation upon loading, a primary period in which the strain rate decreased with time and an apparent steady-state period. A final tertiary period, where the strain rate increased with time, was observed at higher stresses for materials B and D. Some of these specimens contained a small crack which propagated parallel to the loading direction. Upon unloading, all materials exhibited a small elastic recovery followed by an anelastic strain recovery; this is detailed in Part 2 [16].

The steady-state creep rate had to be defined in a somewhat arbitrary manner since a true steady-state condition was never observed. For tests where tertiary creep did not develop, the creep rate was always observed to slowly decrease with time. This decrease in strain rate was most pronounced for those materials that exhibited the greatest rate of oxidation (B and D). When a specimen was crept at successive stresses, the "steady-state" creep rate at the higher stress could be lower than that observed at the initial, lower stress. When the stress was then decreased back to the initial value and sufficient time was allowed for the anelastic recovery, the new "steady-state" creep rate was significantly smaller than the original value for the unstressed specimen.

After many frustrating and apparently inconsistent test results of this nature, it was hypothesized the creep resistance was improved by oxidation. The experiments and results detailing this phenomenon are reported in Part 3 [15]. Thus, in order to classify the materials examined with Equation 1, the steady-state creep rate was calculated from data taken over the last 4 h period of a test that was terminated after ~ 20 h. In this manner, the apparent steady-state creep rate for a new specimen of the same material could be reproduced within ± 15%. Steady-state values were not used if the specimen exhibited tertiary creep.

3.2. Strain-rate/stress response

Equation 1 was used in examining the apparent strain-rate/stress response of the four materials. Fig. 3 illustrates this representation of the data with a log $\dot{\epsilon}$ versus log σ plot. As shown, composition strongly affects creep resistance. In

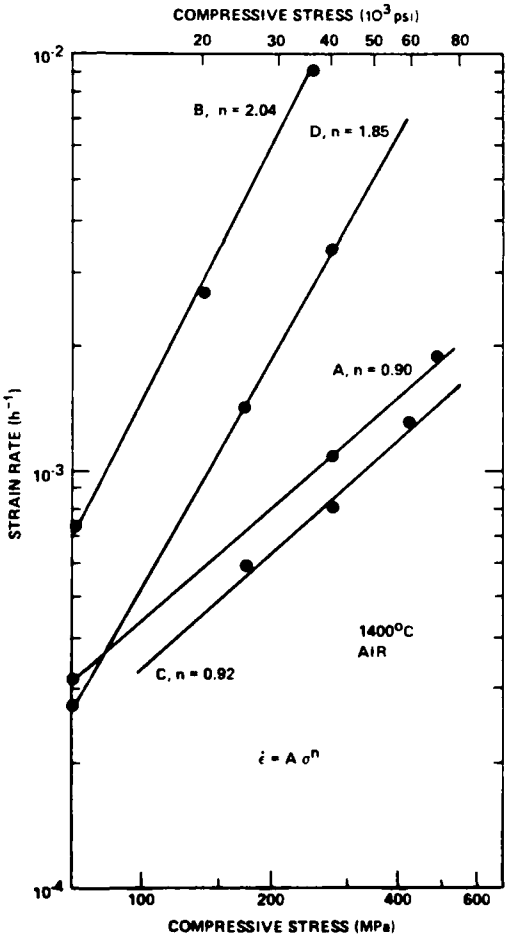

Figure 3 Apparent steady-state strain rate versus compressive stress of four materials examined; stress exponents (n) shown.

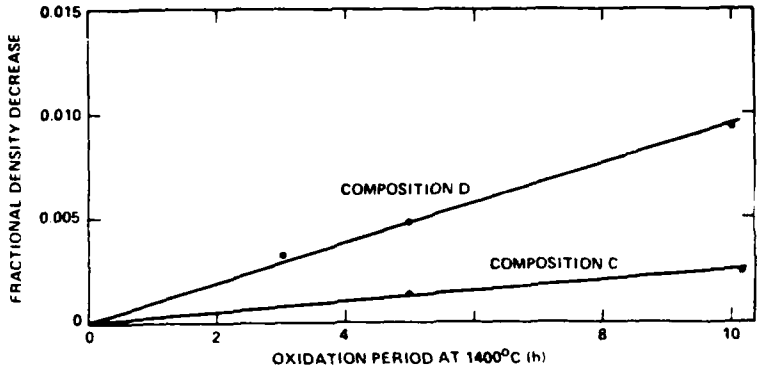

Figure 4 Fractional density change versus oxidation period at 1400° C for compositions C and D.

general, the material's resistance to creep can be ordered with respect to its estimated amount of glass phase (see Table I).

Strain-rate/stress exponents of materials closer to the ternary eutectic (B and D) are ~ 2, i.e. similar to values reported by others for commercial, hot-pressed material fabricated with MgO [2–5]. Stress exponents of materials furthermost from the ternary eutectic (A and C) are ~ 1. These data suggest that the principle mechanism responsibe for the creep behaviour strongly depends on composition.

3.3. Cavitation

Both cavitation and oxidation were found to affect density, therefore a control experiment was performed to determine the effect of oxidation alone on the change in density. The results for materials C and D are shown in Fig. 4. Compositional changes induced by oxidation are the cause of the observed decrease in density upon oxidation [17]; material D exhibited the greatest decrease because of its greater rate of oxidation.

The change in density (expressed as a void volume) observed for materials C and D as a function of creep strain is shown in Fig. 5. These data have been corrected for the density change induced by oxidation (Fig. 4). For material D, oxidation contributed between 20% and 30% of the total

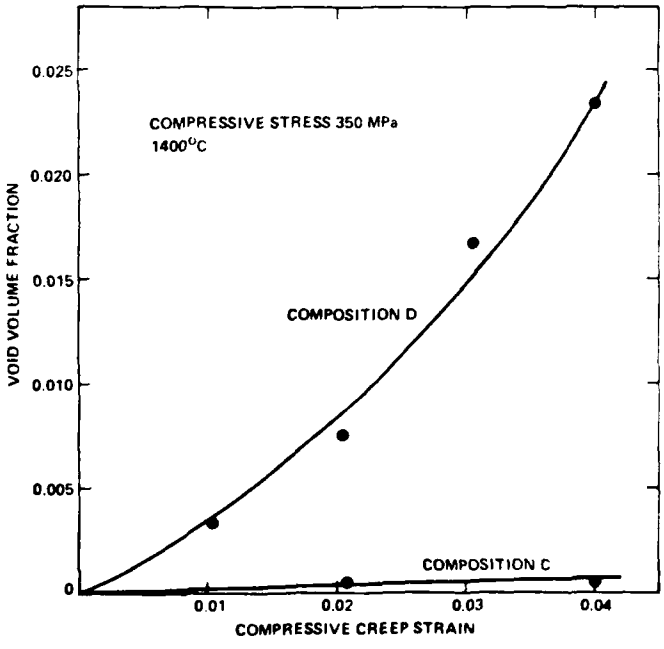

Figure 5 Fractional void volume versus creep strain under 350 Mpa compressive stress at 1400° C.

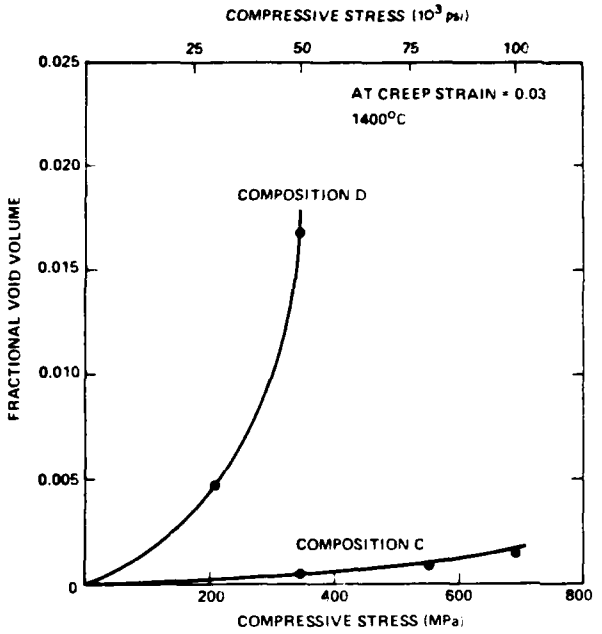

Figure 6 Fractional void volume versus compressive stress for strains = 0.03 at 1400 °C.

density change. The effect of stress on the void volume produced at a creep strain of 0.03 is shown in Fig. 6. Results of single experiments with the other two materials showed that material B exhibited extensive cavitation, whereas material A exhibited negligible cavitation. TEM studies of the crept materials qualitatively showed that materials B and D contained a higher density of cavities relative to materials A and C, consistent with data shown in Figs. 5 and 6.

Since it was recognized that cavities can be produced during ion-milling of specimens prepared for TEM studies, precaution was extended in identifying cavities that were most likely produced by creep. These precautions included observing both uncrept and crept specimens of the same material and comparing cavities observed in both thick and thin portions of ion-milled foils. Wedge-shaped cavities, typified by the example shown in Fig. 7, made up the largest proportion of cavities observed in crept specimens. These cavities were observed at triple-point grain junctions. Their morphology (i.e. rounded corners) and the apparent amorphous nature of the material around the cavity boundary strongly suggest that these cavities were vapour bubbles that grew within the glass phase during creep. Although less frequently observed, cavities were also observed to form between two grains which separated in a direction normal to their common boundary as shown in Fig. 8a. The fibrilous nature of the apparent glassy phase between the separating grains is shown at higher magnification in Fig. 8b. Such fibrils are commonly observed in the tacky separation of printers' ink and are caused by the growth and linking of many small vapour bubbles. Fig. 8a also illustrates a large number of wedge-shaped cavities; the density of cavities in this portion of the specimen was somewhat higher than observed in other portions of the same foil.

It should be noted that the grains were relatively free of dislocations, suggesting that dislocation

Figure 7 TEM micrograph of typical wedge-shaped cavity, C, produced during creep.

Figure 8 (a) Cavities produced by the separation of two grains perpendicular to their common boundary, (b) higher magnification of same grain pairs shows apparent glass fibrils, F.

motion is not a dominant mechanism of creep deformation in Si_3N_4 alloys up to temperatures of 1400° C. This same conclusion has also been reached by others [3, 4].

4. Discussion

The preceding experimental data clearly show that two concurrent mechanisms contribute to the creep behaviour of polyphase Si_3N_4 fabricated within the same compatibility triangle. Also, one mechanism can dominate the other depending on composition. The creep behaviour of compositions most remote from the ternary eutectic composition is dominated by an apparent diffusional mechanism which is indicated by both the linear stress dependence of the creep rate and the absence of cavitation. Cavitational creep is most pronounced in compositions closer to the ternary eutectic. For compositions in between those studied, it is presumed that the contribution of cavitation will decrease as the composition is shifted from one side of the compatibility triangle to the other. This hypothesis has been shown to occur, as detailed in a companion paper which discusses the effect of oxidation-induced compositional changes in creep behaviour [15].

The contribution of each of the two mechanisms to the general creep behaviour can be related to composition if it is assumed that both mechanisms are governed by the viscous, glassy phase and that the glassy phase has a composition close to that of the ternary eutectic composition. The latter assumption defines the volume fraction of glassy phase for any composition (see Section 2.1). The remainder of this section will relate the volume fraction of the viscous phase to the two mechanisms.

Diffusional creep in the context of the current Si_3N_4 alloys can be presumed to occur by the redistribution of matter through the viscous phase. Solution of Si_3N_4 and/or Si_2N_2O into the viscous phase and their reprecipitation elsewhere would be driven by differential chemical potentials that arise from localized stresses. The presence of localized stresses is documented in Part 2 which details the anelastic effect [16].

Stocker and Ashby [18] have modelled the diffusional creep of solid/liquid microstructures similar to that shown in Fig. 2. They assumed that the viscous grain-boundary phase "... enhanced creep by providing regions, or paths of high diffusive conductance" [18]. Differential chemical potentials that arise due to stress gradients provide the driving force for the diffusing species. Their analysis shows that the strain rate ($\dot{\epsilon}$) is related to the grain size (d), molar volume of the diffusing species (Ω), the molar fraction of the diffusing species (C) in the liquid, the volume fraction of the liquid phase (V_l),* the viscosity (η) of the liquid, and the applied stress (σ) as

$$\dot{\epsilon}_{diff} = \frac{8\Omega^{2/3}}{d^2\eta} C V_l \sigma. \qquad (2)$$

* Stocker and Ashby [18] assumed $V_l = S_0/d$, where S_0 is the thickness of the liquid phase between the grains. Lange [19] has shown that $V_l = 3S_0/d$; Equation 2 was thus modified by a factor of 3.

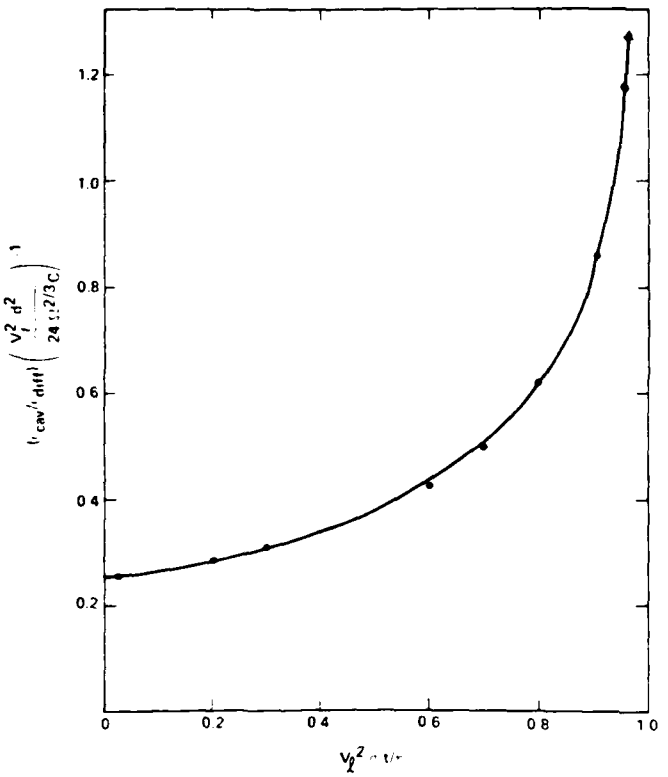

Figure 9 Comparison of strain produced by cavitation to strain produced by diffusion predicted for Equation 5.

Integrating this Equation assuming that the parameters on the RHS of Equation 2 are independent of time, results in

$$\epsilon_{diff} = \frac{8\Omega^{2/3} C V_1 \sigma t}{d^2 \eta}, \qquad (3)$$

indicating the creep strain is linearly dependent on V_1, σ and time (t).

With regard to cavitational creep, most investigators suggest that grain-boundary sliding is required for the growth of cavities. Lange [19] has pointed out that cavitation requires the separation of grains. He showed that grain separation and not sliding is the rate-controlling step in the growth of cavities. The results of his analysis,

$$\epsilon_{cav} = \left[\left(1 - \frac{V_1^2 \sigma t}{\eta}\right)^{-1/4} - 1\right] \frac{V_1}{3}, \qquad (4)$$

indicates a relatively complex dependence on V_1, σ, and t and no direct dependence on grain size. It should be noted that the strain rate for cavitational creep as indicated by Equation 4 cannot be expressed as a simple power law with respect to either time or stress.

Although the analysis resulting in Equations 3 and 4 may not be sufficiently explicit to quantitatively predict creep strains, the equations can be used to predict trends. A comparison of Equations 3 and 4 can be made by dividing one by the other; after rearranging:

$$\frac{\epsilon_{cav}}{\epsilon_{diff}} \left(\frac{V_1^2 d^2}{24\Omega^{2/3} C}\right)^{-1} = \frac{(1 - V_1^2 \sigma t/\eta)^{-1/4} - 1}{V_1^2 \sigma t/\eta}. \qquad (5)$$

The LHS of Equation 5 is plotted as a function of the dimensionless product $V_1^2 \sigma t/\eta$ in Fig. 9 in order to examine the conditions where one mechanism may be more dominant than the other. As shown in Fig. 9, the contribution of cavitational creep increases with increasing $V_1^2 \sigma t/h$, i.e. larger volume fractions of the liquid, higher stresses, longer times and lower viscosity. Because V_1 is squared, changes in V_1 will have a greater effect than changes in the other factors. With other factors held constant, the contribution of cavitational creep will increase with increasing grain size.

The trends predicted by Equations 3 to 5 are consistent with experimental data:

(1) materials with large V_1 cavitate, whereas

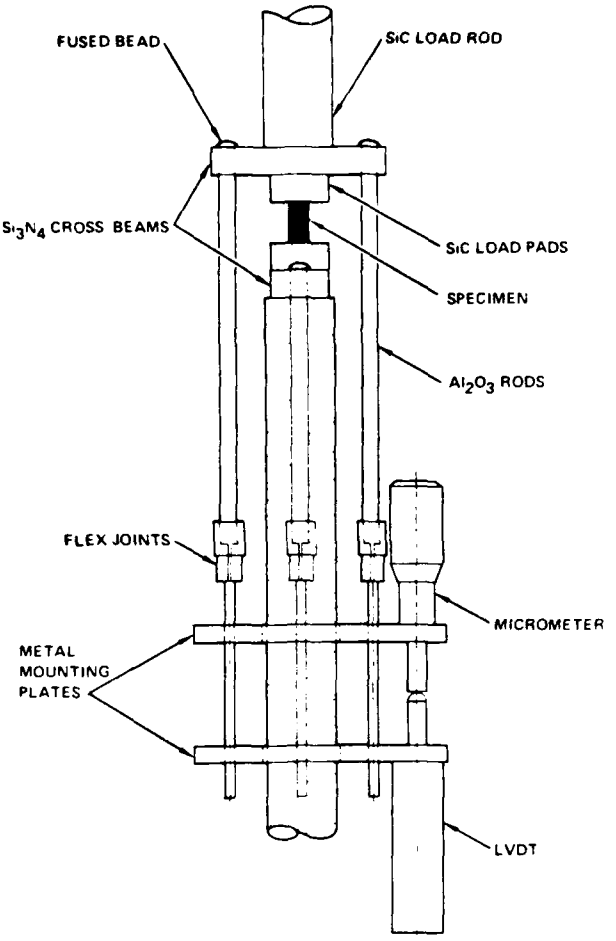

Figure 10 High-temperature extensometer developed for present study.

materials with smaller V_1 do not cavitate and appear to exhibit diffusional creep behaviour (Figs. 4 and 3, respectively) within the stress range examined;

(2) cavitation increases with increasing stress (Fig. 5); the stress dependence appears to mimic that expected for Equation 4;

(3) at lower stresses, the strain rates of all materials are more similar to one another relative to their large divergence at larger stresses, suggesting the dominance of diffusional creep at lower stresses in all materials relative to the dominance of cavitational creep in materials prone to cavitate (B and D) at higher stresses;

(4) tertiary creep behaviour is expected for those materials prone to cavitate as expressed by Equation 4.

It should be noted that at very high stresses, e.g. stress levels that exist at crack fronts, cavitational creep is expected to dominate. Cavitational creep at the crack front will cause sub-critical crack growth by the growth and linking of vapour bubbles [20]. Thus, it can be seen that the compositional dependence of the creep behaviour of Si_3N_4 alloys is of direct concern to their high-temperature fracture behaviour.

Appendix. High-temperature axial extensometer for compressive creep in air

The extensometer used in the high-temperature (1400° C) compressive creep tests is shown schematically in Fig. 10. The silicon carbide load rods are mounted in water-cooled holders outside the furnace. The ends which contact the extensometer are lapped flat and adjusted parallel. The two Si_3N_4 cross beams are identical and oriented at right angles to each other. Silicon carbide load

pads are used between the specimen and cross beams to minimize deformation of the pads and distribute the load into the cross beams. The alumina rods transmit the specimen deformation to the metal mounting plates located below the furnace. Each rod has a flex joint to assist in alignment of the parts. The linear variable differential transducer (LVDT) senses the motion of the mounting plates. The micrometer mounted in the upper metal plate is used to null the transducer output at the start of a creep test. It is also used to calibrate the output of the transducer signal.

Acknowledgement

This work was supported by the Air Force Office of Scientific Research, Contact No. F49620-77-C-0072.

References

1. N. J. OSBORNE, *Proc. Brit. Ceram. Soc.* **25**, *Mech. Prop. of Ceramics* (2) (1975) 263.
2. M. S. SELTZER, *Bull. Am. Ceram. Soc.* **56** (1977) 418.
3. R. KOSSOWSKY, D. G. MILLER and E. S. DIAZ, *J. Mater. Sci.* **10** (1925) 983.
4. S. V. DIN and P. S. NICHOLSON, *ibid.* (1975) 1375.
5. J. M. BIRCH and B. WILSHIRE, *ibid.* **13** (1978) 2627.
6. M. H. LEWIS, B. D. POWELL, P. DREW, R. J. LUMBY, B. NORTH and A. J. TAYLOR, *ibid.* **12** (1977) 61.
7. F. F. LANGE and C. A. ANDERSON, *Bull. Amer. Ceram. Soc.* (in press).
8. J. L. ISKOE, F. F. LANGE and E. S. DIAZ, *J. Mater. Sci.* **11** (1976) 908.
9. D. R. CLARKE and G. THOMAS, *J. Amer. Ceram. Soc.* **60** (1977) 491.
10. L. K. V. LOU, T. E. MITCHELL and A. H. HEUER, *ibid.* **61** (1978) 392.
11. F. F. LANGE, *J. Amer. Ceram. Soc.* (in press).
12. *Idem, ibid.* **64** (1978) 53.
13. *Idem*, Task I. Fabrication, Microstructure and Selected Properties of SiAlON Compositions, Final Rpt. Naval Air Systems Command, Cont. No. N00019-73-C-0208, 16 February (1974).
14. D. R. CLARKE, *Ultramicroscopy* **4** (1979) 33.
15. F. F. LANGE, B. I. DAVIS and D. R. CLARKE, *J. Mater. Sci.* **15** (1980) 616.
16. F. F. LANGE, D. R. CLARKE and B. I. DAVIS, *ibid.* **15** (1980) 611.
17. D. R. CLARKE and F. F. LANGE, (to be published).
18. R. L. STOCKER and M. F. ASHBY, *Rev. Geophys. Space Phys.* **11** (1973) 391.
19. F. F. LANGE, "Non-Elastic Deformation of Polycrystals with a Liquid Boundary Phase", in *Deformation of Ceramic Materials*, edited by R. C. Bradt and R. E. Tressler (Plenum, New York, 1976) pp. 361–81.
20. *Idem, J. Amer. Ceram. Soc.* **62** (1979) 222.

Received 5 July and accepted 28 August 1979

APPENDIX 7

COMPRESSION CREEP OF Si_3N_4/MgO ALLOYS
Part 4, ACTIVATION ENERGIES

F.F. Lange and B.I. Davis
Rockwell International Science Center
Thousand Oaks, California 91360

ABSTRACT

The activation energy of two Si_3N_4/MgO materials, fabricated in the Si_3N_4 -Si_2N_2O - Mg_2SiO_4 compatibility triangle of the Si-Mg-O-N system, was determined between 1300° and 1400°C under a compressive stress of 275 MPa. The activation energy of the material previously shown to exhibit pure diffusional creep was determined to be 660 KJ/mole, whereas the material shown to exhibit extensive cavitational creep had an activation energy of 1080 KJ/mole. These results are compared to results obtained by others for densification and slow crack growth.

INTRODUCTION

Previous articles[1-3] have reported the compressive creep behavior of four Si_3N_4 materials fabricated in the Si_3N_4-Si_2N_2O-Mg_2SiO_4 compatibility triangle of the Si-Mg-O-N system. Two pertinent results were: 1) Cavitation and diffusion are the two phenomena that concurrently contribute to creep strain. The creep behavior of compositions closer to the ternary eutectic (which are expected to contain a larger volume fraction of the continuous glassy phase) was dominated by cavitational creep, as determined by precise density measurements. Diffusional creep was dominant in those compositions closer to the Si_3N_4-Si_2N_2O tie line and furthest from the ternary eutectic; strain-rate/stress-exponents for these compositions were $n \simeq 1$. 2) A pre-oxidation treatment significantly improves the creep resistance. Within the temperature and stress-range examined, preoxidized materials exhibit diffusional creep (as determined by their stress exponent $n \simeq 1$) despite their behavior prior to the prolonged oxidation treatment. Other work[4] has shown that oxidation shifts the polyphase composition of Si_3N_4 toward the Si_3N_4-Si_2N_2O tie line and away from the ternary-eutectic composition, thus decreasing the volume fraction of the detrimental glassy phase. The purpose of the present article is to report the activation energies associated with materials that exhibit one of the two dominant mechanisms, viz, either cavitational creep or diffusional creep.

Creep activation energies (Q) have previously been reported for Si_3N_4 materials fabricated in the Si-Mg-O-N systems with the assumption that the creep strain rate ($\dot{\varepsilon}$) has a stress (σ) and temperature dependency as expressed by the empirical relation:

$$\dot{\varepsilon} = A\,\sigma^n \exp(-Q/RT) \quad . \tag{1}$$

Values of Q for commercial materials have been reported by Kossowsky et al,[5] (535 KJ/mole, tension), Seltzer[6] (703 KJ/mole, tension and compression), Din and Nicholson[7] (585 KJ/mole, bending) and Arons[8] (850 KJ/mole, tension).

Birsch and Wilshire[9] have reported a value of 650 KJ/mole for a variety of experimental Si_3N_4/MgO materials. The stress exponents (n) reported by these same investigators lie between 1.5 and 2.4, indicative of a cavitational dominated creep regime.[1] It should also be noted that "creep-hardening" due to oxidation was not a known phenomena in the experimental schemes mentioned above.

EXPERIMENTAL

Compressive creep experiments were performed on two materials in air as reported previously.[1] The specific composition of the two materials (denoted as A and B in Ref. 1), fabricated by hot-pressing, were (in mole fraction): A:0.755 Si_3N_4, 0.225 SiO_2, 0.020 MgO; B: 0.755 Si_3N_4, 0.090 SiO_2, 0.155 MgO. Both compositions lie within the Si_3N_4 - Si_2N_2O - Mg_2SiO_4 compatibility triangle of the Si-Mg-O-N system. Previous study[1] has shown that at 1400°C, the creep behavior of material A was dominated by diffusional processes (no density change, $n \simeq 1$) and material B was dominated by cavitational phenomena (density decreasing with increasing creep strain, $n \simeq 2$).*

Creep experiments were performed on both materials in air at 1300°, 1350° and 1400°C with a compressive stress of 275 MPa. An additional experiment was performed at 1300°C with material B at 450 MPa to determine if the material had the same creep behavior over the temperture range of interest. To minimize the effect of "creep-hardening" due to oxidation,[3] single specimens were used for each temperature and stress, and test periods were held to < 24 hrs. Activation energies were calculated from the data collected by using Eq. (1).

*As previously pointed out, $n = 2$ is not necessarily unique for cavitational processes. Theory indicates[1,10] that creep due to cavitation is not simply related to strain through a power law, i.e., if a power law is assumed, n will depend on the stress range of experiments.

RESULTS

For all cases, a short period of primary creep strain was followed by a longer period of apparent steady-state creep. Experiments were terminated prior to any development of tertiary creep. Table 1 reports the steady-state creep data for each of the two materials. An analysis of the creep behavior of material B at 1300°C resulted in a stress exponent of 1.91, consistent with a value of 2.05 previously reported for data obtained at 1400°C. An Arrhenius plot of these data is shown in Fig. 1, from which an activation energy of 660 KJ/mole is obtained for material A and 1080 KJ/mole is obtained for material B.

Table 1
Steady-State Creep Rates

	Temperature (°C)	Stress (MPa)	$\dot{\varepsilon}$ (hr^{-1})
Material A	1400	275	1.07×10^{-3}
	1350	275	2.82×10^{-4}
	1300	275	5.25×10^{-5}
Material B	1400	275	1.04×10^{-2}
	1350	275	8.04×10^{-4}
	1300	275	7.59×10^{-5}
	1300	450	1.56×10^{-4}

DISCUSSION

Results presented above for two different Si_3N_4/MgO materials fabricated within the same compatibility triangle indicate that the activation energy for pure diffusional creep is ~ 660 KJ/mole and ~ 1080 KJ/mole for creep dominated by cavitation. Speculations concerning the rate limiting processes that give rise to these results will not be discussed; instead,

these results will be compared to other high temperature processes reported for Si_3N_4/MgO material.

The first comparison will be made with densification processes which are known to occur by a solution-reprecipitation, i.e., diffusion through a liquid phase. It is not unreasonable to suspect that the diffusional processes that occur during the liquid-phase densification of Si_3N_4/MgO compositions are the same as those responsible for pure diffusional creep. Based on this premise, similar activation energies might be expected, even though the densification rates and creep rates may not be comparable. Activation energies for densification of Si_3N_4/MgO compositions have been reported by Bowen et al.[11] as ~ 690 KJ/mole in the temperature range of 1450° to 1550°C and by Lange and Terwilliger[12] as ~ 710 KJ/mole between 1500° and 1700°C. These values are very similar to ~ 660 KJ/mole determined here for diffusional creep, suggesting similar rate limiting steps for the two phenomena.

The second comparison will be made between the activation energies determined for creep dominated by cavitation and for slow crack growth observed in Si_3N_4/MgO materials at high temperature. Observations have shown that slow crack growth in dense Si_3N_4 materials occurs by a process that involves cavitation. Since cavitational creep will dominate over diffusional creep in the high stress regime of a propagating crack, slow crack growth in these materials is expected to occur by accelerated, cavitational creep. Thus, one might expect similar activation energies for slow crack growth and cavitational creep. Evans and Wiederhorn[13] obtained an activation energy of 920 KJ/mole for slow crack growth in commercial Si_3N_4 in the temperature range of 1300° to 1400°C. Although their value is in fair agreement with that reported here for cavitational creep (1080 KJ/mole), it should be noted that in a subsequent paper Evans et al.[14] reported a lower value (710 Kcal/mole) obtained in the range of 1150°C - 1350°C by a different method of analysis.

In conclusion, it should be noted in Fig. 1 that the creep rates for both materials examined here approach one another at 1300°C. It would be unreasonable to extrapolate these data to lower temperatures to predict that

material B would have a better creep resistance than material A. It would be more reasonable to expect that at lower temperatures, both materials will have similar creep behavior, i.e., diffusional creep will become more dominant at lower temperatures. This reasoning is consistent with the creep results of others. That is, when data is analyzed over a much wider temperature range, one would expect that the higher stress exponents observed in the high temperature regime (i.e., > 1300°C) would result in an average stress exponent > 1, but that the activation energy might be more indicative of the predominant data obtained at lower temperatures, i.e., an activation energy more similar to that of the diffusional processes.

ACKNOWLEDGEMENTS

This work was supported by the Air Force Office of Scientific Research under Contract No. F49620-77-C-0072.

REFERENCES

1. F.F. Lange, B.I. Davis and D.R. Clarke, "Compressive Creep of Si_3N_4/MgO Alloys, Part 1: Effect of Composition," J. Mat. Sci. 15, 601 (1980).

2. F.F. Lange, D.R. Clarke and B.I. Davis, "Part 2: Source of Viscoelastic Effect,": ibid 611 (1980).

3. F.F. Lange, B.I. Davis and D.R. Clarke, "Part 3: Effects of Oxidation Induced Compositional Change," 616 (1980).

4. D.R. Clarke and F.F. Lange, "Oxidation of Silicon Nitride Alloys: Relationship to Phase Equilibria in the Si_3N_4-SiO_2-MgO System," J. Am. Ceram. Soc. (in press).

5. R. Kossowsky, D.G. Miller and E.S. Diaz, "Tensile and Creep Strengths of Hot-Pressed Si_3N_4," J. Mat. Sci. 10, 983 (1975).

6. M.S. Seltzer "High Temperature Creep of Silicon-Base Compounds," Bul Am. Ceram. Soc. 56, 418 (1977).

7. S. Ud Din and P.S. Nicholson, "Creep of Hot-Pressed Silicon Nitride," J. Mat. Sci. 10, 1375 (1975).

8. R. Arons, Ph.D. Thesis, Columbia University (1978).

9. J.M. Birch and B. Wilshire, "Compressive Creep Behavior of Si_3N_4 Ceramics," J. Mat. Sci. 13, 2627 (1978).

10. F.F. Lange, "Non-Elastic Deformation of Polycrdystals with a Liquid Boundary Phase," Deformation of Ceramic Materials, Ed by R.C. Bradt and R.E. Tressler, p. 361, Plenum Press (1975).

11. L.J. Bowen, R.J. Weston, T.G. Carruthers and R.J. Brook, J. Mat. Sci. 13, 341 (1978).

12. G.R. Terwilliger and F.F. Lange, "Hot-Pressing Behavior of Si_3N_4," J. Am. Ceram. Soc. 57, 25 (1974).

13. A.G. Evans and S.M. Wiederhorn, "Crack Propagation and Failure Prediction in Silicon Nitride at Elevated Temperatures," J. Mat. Sci. 9, 270 (1974).

14. A.G. Evans, L.R. Russell and D.W. Richerson, "Slow Crack Growth in Ceramic Materials at Elevated Temperatures," Metal. Trans. 6, 707 (1975).

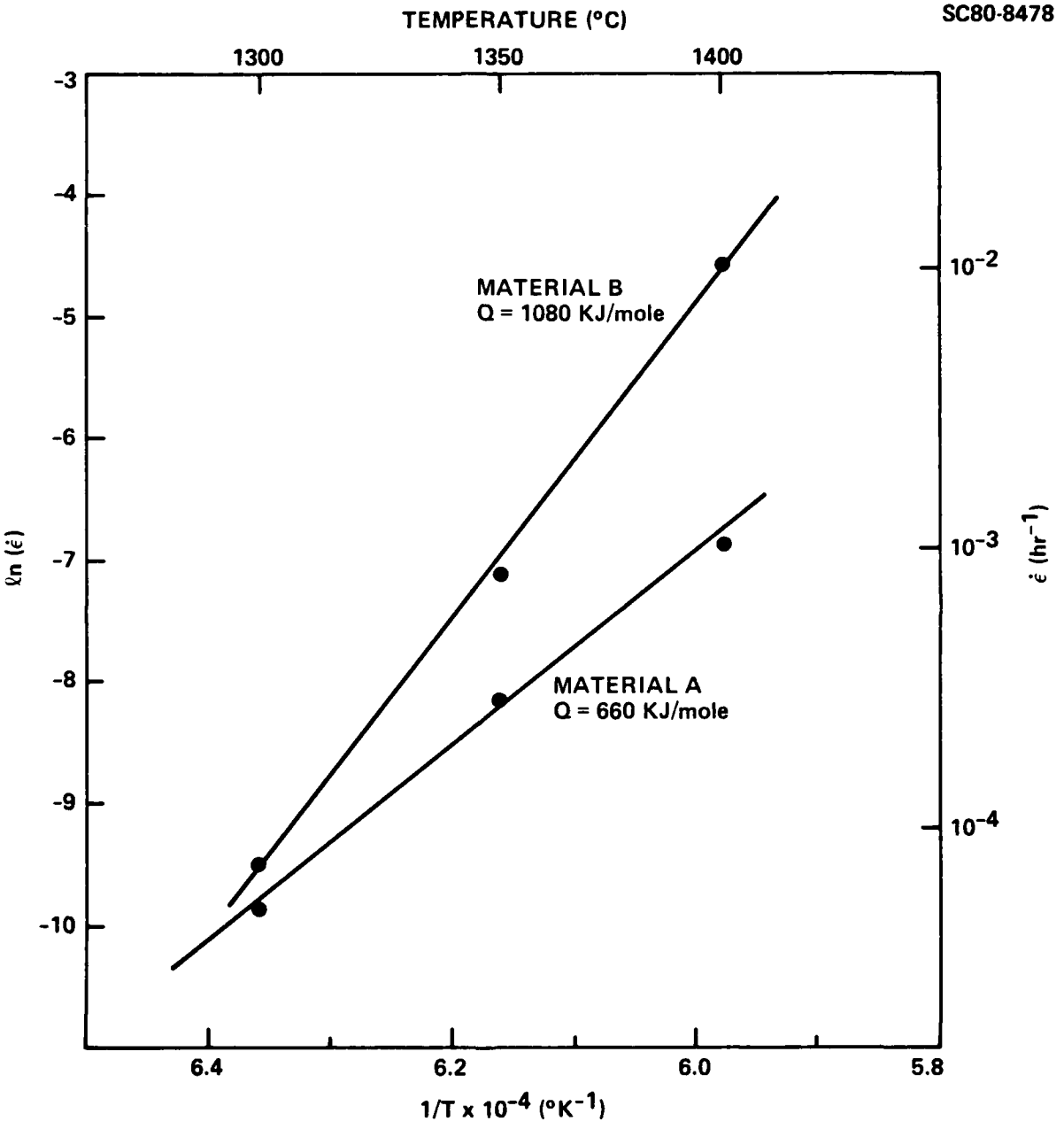

Fig. 1 Arrhenius plot of steady-state creep rates for materials A and B.

APPENDIX 8

JOURNAL OF MATERIALS SCIENCE 15 (1980) 611–615

Compressive creep of Si_3N_4/MgO alloys

Part 2 *Source of viscoelastic effect*

F. F. LANGE, D. R. CLARKE, B. I. DAVIS
Rockwell International Science Center, Thousand Oaks, California 91360, USA

Highly localized strain fields are observed at grain boundaries in crept specimens of Si_3N_4/MgO alloys which were frozen under stress. These fields disappear upon annealing. Unresolved asperities between the grain pairs appear to give rise to the strain field during deformation. Viscoelastic effects responsible for primary creep and strain recovery are explained in terms of grain-boundary sliding on the glassy interphase which is accommodated by the elastic strain arising at the asperities. Each boundary containing an asperity can be modelled as a simple Kelvin element. The spectrum of these boundaries within the bulk gives rise to a spectrum of relaxation times that is observed for the strain recovery effect. The highly stressed region at the asperity also gives rise to the higher chemical potential required to drive diffusional creep. Although the source of the asperities was not observed, the possibility of opposing ledges of either single or multiple interplanar height is discussed.

1. Introduction

Time-dependent creep strain recovery has been reported by Clews *et al.* [1] for porcelain and refractories, Morrell and Ashbee [2] for glass-ceramics, and, during the course of the present work, by Arons [3] for commercial grade, hot-pressed Si_3N_4. Each of these investigators has shown that the recoverable strain is linearly proportional to the stress imposed on the specimen prior to unloading, indicating that the recovery process is viscoelastic, a phenomenon commonly observed for glasses.

Viscoelasticity can be modelled with a Kelvin element, i.e. a spring in parallel with a dashpot, or an arrangement of such elements. The strain produced by stressing this element is exponentially dependent on time divided by a characteristic relaxation time. Upon unloading, the viscoelastic strain decays inversely to that observed upon loading. The process is analogous to the charging and discharging of a capacitor. Thus, if a viscoelastic recovery is observed upon unloading, a corresponding viscoelastic effect is produced upon initial loading. Within this frame of reference, Morrell and Ashbee [2] and Arons [3] each conducted an analysis based on the Boltzman superposition principle and both concluded that the primary creep observed in their respective materials was inversely related to the viscoelastic recovery phenomenon.

In the course of examining the creep behaviour of the Si_3N_4 alloys, detailed in Part 1 [4], a time-dependent strain recovery phenomenon was discovered independently of Arons [3]. This discovery was manifested by the following observations. First, during initial compressive creep experiments conducted with a load cell in a testing frame, unloaded, creep specimens were observed to produce a back stress that would build up as a function of time. This observation showed that the crept specimens contained residual stresses, which arose during creep, that produced a strain recovery upon unloading. Second, during initial tests in which a single specimen was examined at successive stresses, it was observed that when the stress was reduced, the initial strain rate at the lower load was negative for a period before increasing, after an extended period, to the strain rate expected for the applied stress. Third, direct observation of the complete strain behaviour after unloading showed a time-dependent strain recovery phenomenon. This strain recovery phenomenon was observed for

0022–2461/80/030611–5$02.50/0

all the materials examined in Part 1 [4]. Analysis of these recovery phenomena with respect to the viscoelastic model (plots involving log (recoverable strain) versus time) did not produce a single characteristic time but indicated a spectrum of relaxation times. Similar results were obtained by Clews *et al.* [1] for porcelain and refractories, Morrell and Ashbee [2] for glass-ceramic, and Arons [3] for hot-pressed Si_3N_4.

With the discovery in Arons [3] careful investigation, further work was concentrated on unusual features observed with TEM in crept specimens; as was uncovered, these were directly related to the viscoelastic phenomena.

2. Experimental details

Part 1 [4] described in more detail the two Si_3N_4 alloy compositions labelled (C and D) fabricated in the same compatibility triangle of the Si–Mg–O–N system, that were used in this study. In summary, composition C exhibited diffusional creep behaviour and did not cavitate, whereas cavitational creep appeared to dominate the behaviour of composition D. Although a continuous glassy grain-boundary phase was observed in both materials (Part 1, Fig. 2), composition C was furthest away from the ternary eutectic and thus was assumed to contain a smaller volume fraction of the glass. Both materials were observed to exhibit primary creep in which the strain rate decreased over a period to an apparent steady-state value, and both exhibited an apparent viscoelastic strain recovery.

Specimen foils were prepared for TEM studies from both materials in their as-fabricated, crept plus cooled under stress (1400° C, 350 MPa compression, 4% strain) and crept plus annealed* (1400° C, 1 h) states. Most strain is recovered after a 1 h anneal at 1400° C. Density measurements (Section 2.3, Part 1) were made for both the crept plus cooled under stress and crept plus annealed specimens.

3. Observations

The transmission electron micrograph in Fig. 1 illustrates the features, termed strain whorls, that were observed at the majority of grain pairs in foils prepared from the crept and cooled under load specimens. As indicated in Table I, the strain whorls were only seen in samples that had been

Figure 1 Examples of strain whorls observed at a majority of grain boundaries in crept specimens cooled under stress.

cooled under load. The strain whorls were located only along grain boundaries and, in general, appeared to be asymmetrical with respect to the boundary normal. In addition, the contours of the whorls appeared to originate from a single point, suggesting that the source might be one of a point contact between the grains. From both high-resolution bright- and dark-field imaging, it was determined that no inclusions or particles were present at the centre of the whorls. In addition, strain whorls were not seen at those locations (principally three grain junctions) where small inclusions could be found. Attempts to investigate the centres of the whorls by lattice fringe imaging were unsuccessful because of the abrupt changes in the deviation parameter (s) from the

TABLE I Occurrence of strain whorls

Material	C	D
As-fabricated	Absent	Absent
Crept and cooled under load	Present	Present
Crept, cooled under load and annealed (1 h, 1400 C)	Absent	Absent

* The crept specimens used for this study were diamond cut into several pieces for annealing and density measurements.

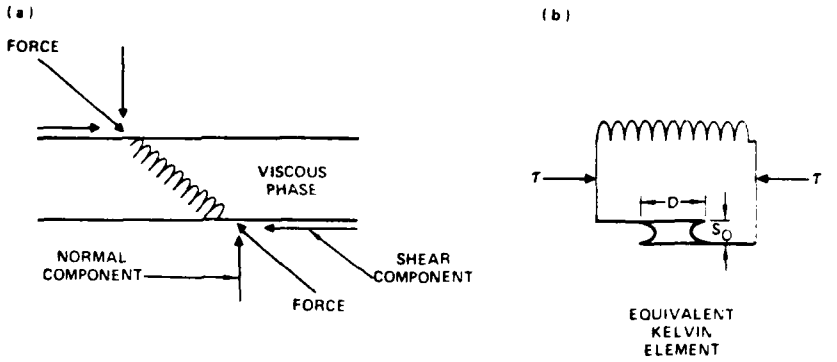

Figure 2 (a) Model of sliding grains separated by a glassy interphase and hindered from sliding by an asperity represented as a spring. (b) The Kelvin element representing (a).

exact Bragg condition in the vicinity of the whorls. That the whorls were, in effect, extinction contours resulting from a localized out-of-plane buckling of the electron microscope foil was determined from three experiments: (1) tilting the foil in the microscope caused the whorls to change shape and orientation; (2) at any foil orientation, each fringe or contour of the whorl could be made to appear bright in dark-field imaging by tilting the illumination, (equivalently, the diffraction pattern of the grains in the vicinity of the whorls was tilted with respect to that obtained from the same grains away from the whorls); (3) no two-beam diffraction conditions could be found for which a line of no contrast was formed, as is characteristic of strain centres produced by, for instance, misfitting precipitates [5].

These observations, when taken with the fact that the whorls were only seen to occur in those samples that have been cooled under load, confirm that the whorls are manifestations of a localized residual stress and are not artifacts produced in sample preparation.

An interesting observation on the occurrence of the whorls is illustrated by the micrograph of Fig. 8a in Part 1: the whorls are seen only on those grain boundaries whose plane lie approximately parallel to the direction of grain separation at L. This implies that the whorls form on those boundaries where the relative grain displacement includes a component of grain-boundary sliding.

Both density measurements and TEM observations of samples C and D indicated that the volume fraction of cavities remained unchanged after annealing.

4. Discussion

4.1. Viscoelastic effect

The presence of strain whorls in crept specimens cooled under load and their relaxation upon annealing illustrates that they depict (at least, in part) the stress fields responsible for the strain recovery. Their existence at grain boundaries and their general asymmetrical orientation* with respect to the grain boundary suggest that they arise and relax by grain-boundary sliding. Since a viscous phase separates each grain pair (Part 1, Fig. 2), the rate of grain-boundary sliding will be governed by the viscosity of the fluid between the grains and its thickness. Fig. 2a models this situation in terms of a spring fixed between two parallel plates which contain a viscous glass. The spring represents the asperity that gives rise to the strain whorl when the asymmetric force is applied across the plates.

Derivation of the time-dependent strain (ϵ_v) in relation to the areas of the asperity (A), the grain-boundary area (D^2), the thickness of the glassy interphase (S_0), the elastic modulus of the asperity (E), and the viscosity of the glass (η) is accomplished by summing the shear stress (τ) across the model:

$$\tau = E\frac{A}{D^2}\epsilon_v + \eta\frac{D}{S_0}\frac{d\epsilon_v}{dt}.$$

* The asymmetrical strain pattern indicates that the force couple at the origin is asymmetrical with respect to the grain boundary and that a shear component of this couple lie in the grain boundary. If their asymmetry were due to strongly anisotropic elastic properties in the two respective grains, one would not expect to see the commonly observed axis of symmetry within the strain whorls.

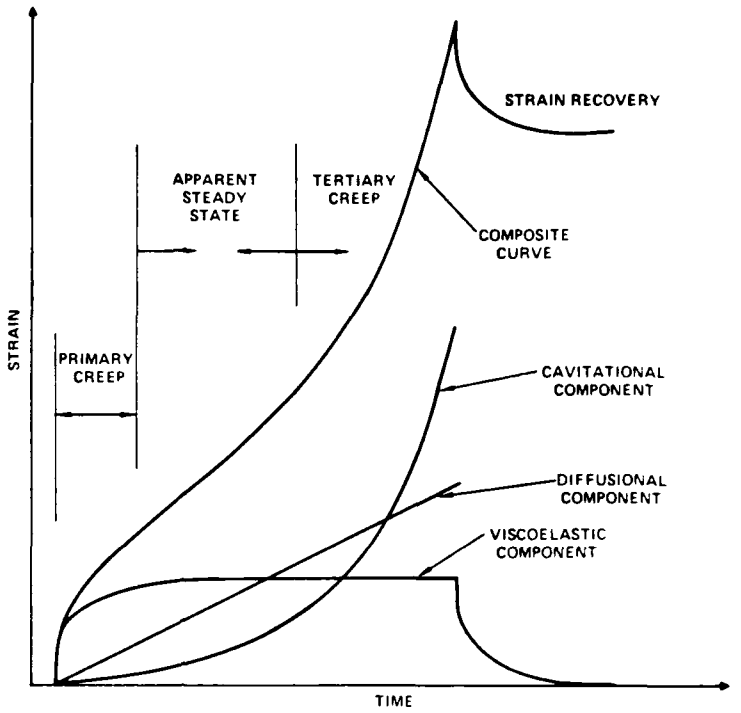

Figure 3 Functional forms of the three concurrent strain mechanisms that occur in Si_3N_4 alloys. The composite curve illustrates the experimental behaviour.

Upon integrating by parts:

$$\epsilon_v = \frac{\tau}{ER}\,1 - \exp\left(-\frac{tER\,V_1}{3\eta}\right).$$

where R is the ratio of the asperity area to the grain-boundary area ($R \equiv A/D^2$), and ($V_1 = 3S_0/D$). The relaxation time constant for the single element is thus $3\eta/ER\,V_1$.

This model is equivalent to a single Kelvin element shown in Fig. 2b, where the dashpot is represented by two sliding plates containing the viscous glass. Since the bulk of the material contains many of these Kelvin elements, each with its own characteristic relaxation time, the summation of these elements will produce a viscoelastic response with a spectrum of relaxation times. This view is consistent with our own observations and those of Arons [3] for Si_3N_4 alloys. It can thus be concluded that the viscoelastic response of Si_3N_4 alloys, which appears to be responsible for both the primary creep and strain relaxation transients, arises from both the viscoelastic response of the glassy grain-boundary phase itself and the sliding of grain boundaries which is accommodated by the elastic deformation of material adjacent to asperities between the grains.

It should be noted that the stress fields that arise at the asperities would also give rise to the differential chemical potentials required as the driving force from diffusional creep (Part 1, Section 4).

Combining the observations of Part 1 [4] with those of this study, three concurrent mechanisms may be cited as responsible for the general creep behaviour of polyphase Si_3N_4 alloys: viscoelastic, diffusional and cavitational creep mechanisms. The latter two are the persistent creep modes which account for the unrecoverable creep strain. The functional forms of these three mechanisms are shown in Fig. 3. When all three mechanisms contribute, the general creep behaviour will be equal to their sum. Thus, the three recognized stages of creep can be matched with a dominant mechanism as follows: (1) primary creep is dominated by viscoeleastic deformation due to grain-boundary sliding accommodated by elastic deformation at grain-boundary asperities and/or adjacent grains; this deformation is recoverable; (2) secondary creep

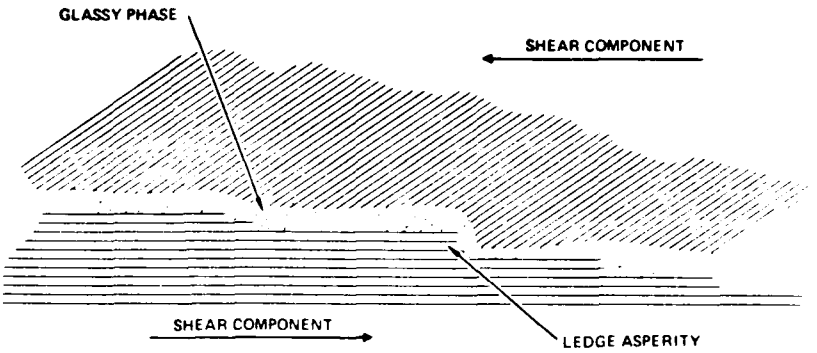

Figure 4 Model of ledge interference to form an asperity which give rise to strain whorls upon boundary sliding

may, for materials with a small amount of glass, be dominated by diffusional creep; (3) tertiary creep is dominated by cavitation and will be accentuated by the subcritical growth of pre-existing cracks. As will be shown in Part 3 [6], a fourth mechanism also exists which is related to oxidation-induced composition changes.

4.2. Asperities at grain boundaries

It is evident from the localization of the strain whorls, that some sort of asperity which hinders sliding, exists at the grain boundary. Within the resolution of current TEM studies, the source of the asperity was not evident. It is evident that the size of these asperities must be approximately equal to the thickness of the glassy phase between the grains (i.e. < 50 Å). Likely sources are thus crystalline second phases and ledges composed of one or more lattice planes.

Although secondary crystalline phases have not been observed within the glass phase between the grains, they are commonly observed at triple points. For the Si_3N_4 alloys studied here, tungsten-containing particles are commonly observed, but no strain whorls were seen in the Si_3N_4 grains adjacent to these particles. In addition, crystalline magnesium silicate phases were not observed in the present materials; if they were the asperities, they would be expected to quickly dissolve under stress.

Ledges of single and multiple interplanar height at grain boundaries have been observed in a number of different Si_3N_4 alloys [7–9]. It is likely that ledges of opposing sign which lock together as shown in Fig. 4 can act as asperities and give rise to the observed strain whorls. This is a possibility since the height of the grain-boundary ledges that have been observed is commensurate with the measured thickness (< 20 Å) of the intergranular phase. Because ledges are also expected to be present on all boundaries, except those formed by low index, crystalline planes, a sufficient number would exist to act as sources of strain. Dissolution of the grains during diffusional creep might also be expected to be more energetically favourable at grain-boundary ledges, particularly those that form stressed asperities. Dissolution would not eliminate the asperity since ledge contact would be maintained by grain-boundary sliding. Material at the opposing ledge interface would diffuse to other ledges of lower chemical potential. Thus, the hypothesis that opposing ledges can act to impede grain-boundary sliding opens up many interesting questions for further work.

Acknowledgement

This work was supported by the Air Force Office for Scientific Research, under Contract No. F49620-77-C-0072.

References

1. F. H. CLEWS, J. M. RICHARDSON and A. T. GREEN, *Trans. Brit. Ceram. Soc.* **45** (1956) 161.
2. R. MORRELL and K. H. G. ASHBEE, *J. Mater. Sci* **8** (1973) 1271.
3. R. M. ARONS, PhD Thesis, Columbia University, School of Engineering and Applied Science (1978).
4. F. F. LANGE, B. I. DAVIS and D. R. CLARKE, *J. Mater. Sci.* **15** (1980) 601.
5. M. F. ASHBY and L. M. BROWN, *Phil Mag* **8** (1963) 1083.
6. F. F. LANGE, B. I. DAVIS and D. R. CLARKE, *J. Mater. Sci.* **15** (1980) 616.
7. D. R. CLARKE and G. THOMAS, *J. Amer. Ceram. Soc.* **60** (1977) 491.
8. D. R. CLARKE, *ibid.* **62** (1979) 236.
9. D. R. CLARKE, to be published.

Received 5 July and accepted 28 August 1979.

APPENDIX 9

1817C$$$16 03-20-81 14-12-25

Journal
Sharon

A New Si_3N_4 Material: Phase Relations In The System Si-Sc-O-N and Preliminary Property Studies

P. E. D. MORGAN,* F. F. LANGE, D. R. CLARKE,* AND B. I. DAVIS

Structural Ceramics Group, Rockwell International Science Center, Thousand Oaks, California 91360

A new polyphase silicon nitride alloy has been developed using Sc_2O_3 as a densification aid. Subsolidus phase relations in the system Si-Sc-O-N are reported together with preliminary oxidation and compressive creep results of a representative composition in the Si_3N_4-Si_2N_2O-$Sc_2Si_2O_7$ phase field. Microstructural observations of the material are also presented.

PREVIOUS work on the densification of silicon nitride powders indicates that improved high-temperature mechanical properties may be obtained by the use of an oxide producing a more refractory-eutectic phase with SiO_2 (e.g. using Y_2O_3 in place of MgO).[1] However, problems[2] such as cracking caused by expansion on oxidation of the metal-silicon-oxynitrides (e.g. $Y_2Si_3O_3N_4$ etc.) suggest that the formation of such oxynitrides should be avoided. One approach is to select an oxide not likely to form quaternary metal-silicon-oxynitrides. Scandia is a possibility since Sc^{3+} has an ionic radius (0.088 nm) similar to Mg^{2+} and Zr^{4+}, both of which do not form mixed metal-silicon oxynitrides.[2] In other respects the silicate chemistry of Sc^{3+} is very similar to Y^{3+}; the Sc_2O_3-SiO_2 phase diagram is almost identical to the Y_2O_3-SiO_2 diagram.[3] For these reasons, an investigation was initiated to determine the subsolidus phase relations and properties of polyphase materials densified in the system Si_3N_4-Sc_2O_3-SiO_2.

To determine the phase relations' compositions formed with Si_3N_4,* Sc_2O_3 and SiO_2 were hot-pressed in graphite dies from 1600 to 1800°C. X-ray diffraction powder anaysis was used to identify the constituent phases and established the subsolidus phase relations. As shown in Fig. 1, no quaternary compounds were observed, and subsolidus tie lines only exist between Si_3N_4-Sc_2O_3, Si_3N_4-$Sc_2Si_2O_7$, and $Sc_2Si_2O_7$-Si_2N_2O. Sc_2SiO_5, previously reported,[4] was not observed in the present study.

For preliminary property study, a composition containing (in mole fraction) 0.74 Si_3N_4, 0.18 SiO_2, and 0.08 Sc_2O_3 near the Si_3N_4-$Sc_2Si_2O_7$ tie line in the Si_3N_4-$Sc_2Si_2O_7$-Si_2N_2O phase field was selected. The composition was chosen because the $Sc_2Si_2O_7$ phase is compatible with the oxidation product of Si_3N_4 (viz SiO_2) and because an equivalent composition with Y_2O_3 instead of Sc_2O_3 had previously been studied. The powders were milled in methanol with WC grinding media, dried, and then hot-pressed at 29 MPa in graphite dies. Table I lists the hot-pressing conditions, densities achieved, and the observed phases. As indicated, the theoretical density of 3.21 $g \cdot cm^{-3}$ could be achieved in 2 h at 1800°C, but a 4 h hold was required to nearly complete the $\alpha \rightarrow \beta$ phase transformation. The sluggish densification and transformation kinetics of this composition as evidenced by these results relative to other Si_3N_4 systems could be indicative of high eutectic temperatures within the system Si_3N_4-SiO_2-Sc_2O_3.

Specimens for preliminary oxidation and compressive creep experiments were diamond cut and ground from the billet hot-pressed at 1800°C for 4 h.

After 285 h of oxidation in air at 1400°C, the specimen had a slight patina and had gained 4.4×10^{-4} $kg \cdot m^{-2}$. Assuming that the oxidation followed parabolic kinetics (as do samples densified with MgO or Y_2O_3), the weight gain corresponds to a parabolic rate constant of $\approx 2 \times 10^{-11}$ $kg^2 \cdot m^{-4} \cdot s^{-1}$; a value ≈ 40 times lower than commercial HS130 Si_3N_4.[5] The oxidized surface had a glassy appearance and by EDAX was enriched in the elements Ca, Fe, and Al with a trace of Na.

The compressive creep measurements were conducted in air at 1400°C using the method described previously for the MgO densified Si_3N_4 alloys.[6] At all stresses, an apparent steady-state creep rate was observed after a short period of primary creep. The results using a single specimen which was deformed at successively increasing stresses (170 MPa to 550 MPa) are presented in Fig. 2. These data, plotted to determine the stress exponent (n) in the empirical relation $\dot{\varepsilon} = A\sigma^n$, suggest that $n \approx 1.2$ at stresses <275 MPa and $n = 3.3$ at larger stresses. Based on previous creep studies[5] with Si_3N_4/MgO and Si_3N_4/Y_2O_3 materials, these stress exponents suggest that the 1400°C, creep is dominated by diffusional processes at low stresses (<275 MPa) and by cavitational processes at higher stresses. The density of the specimen prior to and after the creep experiment was 3.2118 ± 0.0003 g cm^{-3} and 3.1397 ± 0.0003 g cm^{-3}, respectively. This decrease in density (2.3%) is approximately half of the total creep strain (3.97%) measured over the specimen's entire stress history and $\approx 75\%$ of the creep strain measured at stresses ≥ 278 MPa. Thus, as indicated by the high stress exponent (Fig. 2), it can be concluded that the creep strain is dominated by cavitational processes at stresses ≥ 275 MPa.

Further, it should be noted that the creep resistance of the present Si_3N_4/Sc_2O_3 material is 1 to 2 orders of magnitude superior to that of the Si_3N_4/MgO materials previously examined.[5]

The microstructure of the chosen Si_3N_4/Sc_2O_3 material was examined for the presence of an intergranular glass phase and any additional phases using the techniques of high-resolution electron microscopy and analytical electron microscopy. Figure 3 is a representative dark field transmission electron micrograph of the microstructure. The bright phase is crystalline $Sc_2Si_2O_7$ and the phase appearing dark is β-Si_3N_4. As with the microstructure of the Si_3N_4/Y_2O_3 alloys[7] the secondary phase ($Sc_2Si_2O_7$) appears to envelope and surround the silicon nitride grains. In addition to the highly prismatic morphology of the silicon nitride grains, this suggests that the silicon nitride recrystallized out of a liquid phase at high temperature. Observations by dark field and defocus imaging techniques[8] reveal the presence of an extremely thin (≈ 1 nm) and continuous intergranular phase at both the Si_3N_4/Si_3N_4 and $Si_3N_4/Sc_2Si_2O_7$ grain junctions, as illustrated by the dark field micrograph of Fig. 4. In addition, few large pockets of glass were seen, suggesting that the volume fraction of noncrystalline phase present was small.

In conclusion, a new and interesting polyphase Si_3N_4 material has been developed. Preliminary observations show that its oxidation and creep resistance are significantly better than other polyphase Si_3N_4 materials. As expected, densification is sluggish, presumably due to the refractory nature of this system (i.e. high eutectic or melting temperatures). In common with other polyphase Si_3N_4 materials, a continuous, intergranular glassy phase is present although there are indications that its volume fraction is significantly smaller. Further property improvements are expected from processing refinements.

Acknowledgment

It is a pleasure to thank E. H. Wright for his excellent work in support of this investigation.

References

[1] G. E. Gazza, "Hot-Pressed Si_3N_4," *J. Am. Ceram. Soc.*, **56** [12] 662 (1973).

[2] F. F. Lange, "Silicon Nitride Alloy Systems: Fabrication, Microstructure and Properties," *Int. Met. Rev.*, **247**, 1–20 (1980).

[3] Phase Diagrams for Ceramists, 1969 Supplement. Compiled by E. M. Levin, C. R. Robbins, and H. F. McMurdie. Edited by M. K. Reser. The American Ceramic Society, Inc., Columbus, Ohio, 1969.

[4] Toropov and Vinitera, *Russ. J. Inorg. Chem. (Engl. Transl.)* **7**, 1001 (1962).

[5] W. C. Tripp and H. C. Graham, "Oxidation of Si_3N_4 in the Range 1300° to 1500°C," *J. Am. Ceram. Soc.*, **59** [9–10] 399–403 (1976).

[6] F. F. Lange, D. R. Clarke, and B. I. Davis, "Compressive Creep of Si_3N_4/Magnesium Oxide Alloys Part I: Effect of Composition," *J. Mater. Sci.*, **15** [3] 601–610 (1980).

[7] D. R. Clarke, and G. Thomas, "Microstructure of Y_2O_3 Fluxed Hot-Pressed Silicon Nitride," *J. Am. Ceram. Soc.*, **61** [3–4] 114–18 (1978).

[8] D. R. Clarke, "On the Detection of Thin Intergranular Films by Electron Microscopy," *Ultramicroscopy*, **4** [1] 33–44 (1979).

CONTRIBUTING EDITOR—E. R. KREIDLER

Received November 24, 1980.

Supported in part by the Office of Naval Research under Contract No. N00014-79-C-0709, and by the Air Force Office of Scientific Research under Contract No. F49620-77-C-0072.

*Member, the American Ceramic Society.

*KBI high purity (85% α-Si_3N_4, 15% β-Si_3N_4).

Table I. Densification Results

Hot-pressing conditions	Density (g/cm³)	Phases
1750°C/2 h	2.62	α-Si_3N_4, β-Si_3N_4, $Sc_2Si_2O_7$, Si_2N_2O
1800°C/1 h	3.14	β-Si_3N_4, α-Si_3N_4, $Sc_2Si_2O_7$, Si_2N_2O
1800°C/2 h	3.21	β-Si_3N_4, $Sc_2Si_2O_7$, α-Si_3N_4, Si_2N_2O
1800°C/4 h	3.21	β-Si_3N_4, $Sc_2Si_2O_7$, α-Si_3N_4(Tr), Si_2N_2O

Fig. 1. Subsolidus phase relations observed in the Si-Sc-O-N system for samples hot-pressed in graphite dies at 1600° to 1800°C.

Fig. 2. Log-log plot of steady-state creep rate vs compressive stress for the $Si_3N_4/Sc_2Si_2O_7$ material.

Fig. 3. Dark-field transmission electron micrograph (using one of the $Sc_2Si_2O_7$ diffraction spots) illustrating the morphology of the crystalline $Sc_2Si_2O_7$ phase (bright) and the β-Si_3N_4 phase (dark).

Fig. 4. Dark-field transmission electron micrograph revealing the presence of a continuous glass phase at the Si_3N_4/Si_3N_4 grain junctions, *A*, and surrounding the $Sc_2Si_2O_7$ grain, *B*. Less apparent but also observable is the glass phase around the $Sc_2Si_2O_7$ grain, *C*.

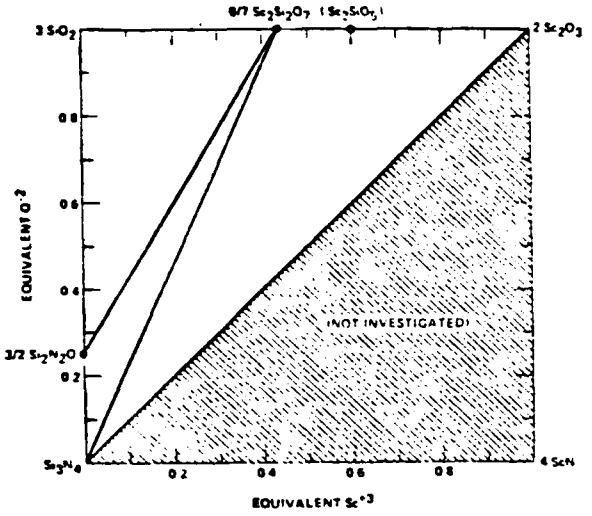

Fig. 1 Subsolidus phase relations observed in the Si-Sc-O-N system for samples hot-pressed in graphite dies at 1600° to 1800°C.

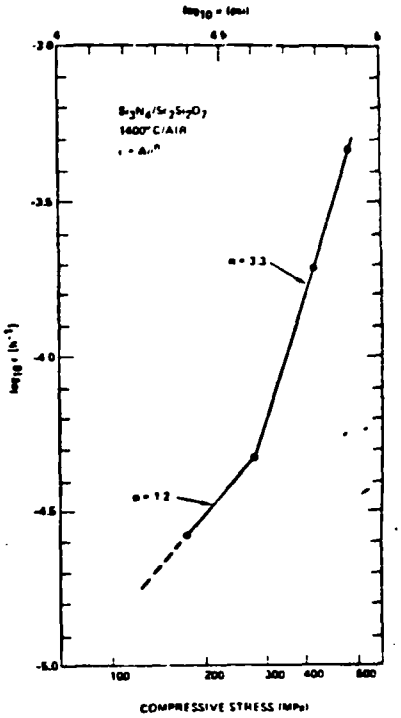

Fig. 2. Log-log plot of steady-state creep rate as compressive stress for the $Si_3N_4/Sc_2Si_2O_7$ material.

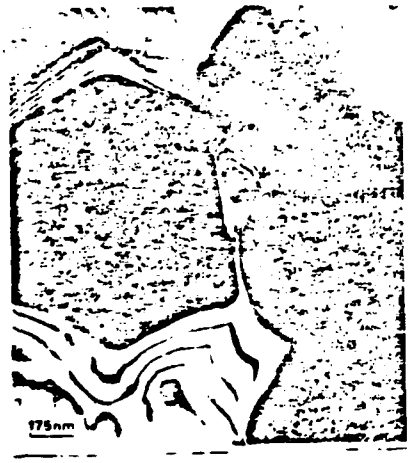

Fig. 3. Dark-field transmission electron micrograph (using one of the $Sc_2Si_2O_7$ diffraction spots) illustrating the morphology of the crystalline $Sc_2Si_2O_7$ phase (bright) and the β-Si_3N_4 phase (dark).

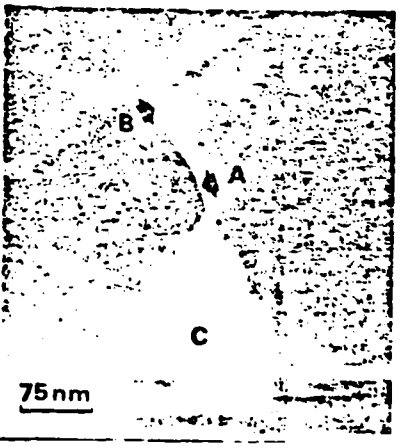

Fig. 4. Dark-field transmission electron micrograph revealing the presence of a continuous glass phase at the Si_3N_4/Si_3N_4 grain junctions, *A*, and surrounding the $Sc_2Si_2O_7$ grain, *B*. Less apparent but also observable is the glass phase around the $Sc_2Si_2O_7$ grain, *C*.

APPENDIX 10

COMPRESSIVE CREEP AND OXIDATION RESISTANCE OF A Si_3N_4 MATERIAL FABRICATED IN THE Si_3N_4-Si_2N_2O-$Y_2Si_2O_7$ SYSTEM

F.F. Lange and B.I. Davis
Structural Ceramics Group
Rockwell International Science Center
Thousand Oaks, California 91360

and

H.C. Graham
Air Force Materials Laboratory
Wright-Patterson AFB, Ohio 45433

ABSTRACT

The compressive creep behavior and oxidation resistance of a Si_3N_4/$Y_2Si_2O_7$ material with a composition 0.85 Si_3N_4 + 0.10 SiO_2 + 0.05 Y_2O_3 was determined at 1400°C. Diffusional creep was dominant for compressive stresses < 310 MPa; cavitational creep dominated above this stress. A pre-oxidation treatment (1600°C/120 hrs) significantly increased the creep resistance. A parabolic rate constant of 4.2×10^{-11} $Kgm^2 \cdot m^{-4} \cdot s^{-1}$ indicates excellent oxidation resistance. These results are discussed relative to previous work.

1.0 INTRODUCTION

Polyphase Si_3N_4 densified with the aid of Y_2O_3 can contain unmwanted crystalline phases, viz. $Y_2Si_3O_3N_4$, $YSiO_2N$ and/or $Y_5(SiO_{3.67}N_{.33})O$, which readily oxidize at low temperatures; this increases their occupied volume and causes surface stress to develop which can eventually lead to cracking and general material degradation.[1,2] Within the Si-Y-O-N system, this problem can be averted by fabricating compositions in the Si_3N_4-Si_2N_2O-$Y_2Si_2O_7$ compatibility triangle which avoids the unwanted phases.[3]

Previous property measurements of materials with compositions within this desired compatibility triangle show significant improvements relative to commercial material and polyphase materials fabricated in other systems. Andersson has reported flextural strengths in the range of 480-550 MPa at 1400°C.[4] Preliminary results have indicated that the oxidation resistance of these materials are in the range observed for CVD Si_3N_4.[1] Oxidation does not produce strength degrading surface pits in these materials as found for commerical Si_3N_4/MgO materials.[5] Based on these interesting results, high temperature compressive creep and oxidation measurements were conducted so that the properties of these new Si_3N_4 materials could be better understood.

2.0 EXPERIMENTAL

The composition chosen for study lies on the sub-solidus Si_3N_4-$Y_2Si_2O_7$ tie line and has a composition of 0.85 Si_3N_4, 0.10 SiO_2 and 0.05 Y_2O_3. Composite powders were milled with WC media and methanol in a plastic bottle. The powder was hot-pressed at 1780°C, 28 MPa for 2 hrs. XRD showed that the dense material contained β-Si_3N_4 and α-$Y_2Si_2O_7$.

Creep experiments were performed in air at 1400°C in the same manner described previously.[6] The creep behavior was examined for the material in both "as-cut" and oxidized (1600°C/100 hr) states.

Thermal gravimetric analysis was performed at 1400° in 150 torr of oxygen, using a pre-mixed O_2/Ar gas at a flow rate of ~ 75 cm^3/min previously dried by passing through activated alumina and magnesium perchlorate. The polished, rectangular specimen was hung in the furnace with an Al_2O_3 fiber.

3.0 RESULTS

3.1 Creep

The strain-time behavior of all specimens was indicative of a short primary stage followed by an apparent steady-state stage; a tertiary stage was not observed within the stress/time regime of the experiments. Observations at 1400°C indicated that the material was not as susceptible to the oxidation-induced creep-hardening effects previously observed for Si_3N_4/MgO materials. Namely, steady-state creep rates were observed for periods up to 24 hrs and, once sufficient time had elapsed for anelastic recovery, the same creep rate was obtained at a previously examined lower stress after an extensive period at a higher stress. For this reason, the pre-oxidation treatment was performed at 1600°C.

Figure 1 summarizes the compressive creep behavior of the as-cut and pre-oxidized (1600/120 hrs) material, determined over the stress range of 140 MPa to 550 MPa using the empirical relation

$$\dot{\varepsilon} = A\sigma^n \quad . \tag{1}$$

Data for both as-cut and pre-oxidized materials resulted in a stress exponent $n \simeq 1$ at stresses < 310 MPa and $n \simeq 2$ at stress > 310 MPa. The pre-oxidation treatment at 1600°C was found to improve the creep resistance.

3.2 Oxidation

Figure 2 summarizes the weight gain vs time data observed at 150 torr O_2 at 1400°C plotted for assumed parabolic rate law. A measurable weight

change was not recorded in the initial 10 hr period. After this initial period, the oxidation behavior was slightly greater than expected for a parabolic rate law. A slight reaction with the Al_2O_3 fiber was noted by the glassy appearance of the surface adjacent to the hole in the specimen. This may have adversely contributed to the oxidation results. Assuming a parabolic rate law, the parabolic rate constant was calculated to be 4.2×10^{-11} $Kg^2 \cdot m^{-4} \cdot s^{-1}$.

An examination of the oxidized surface by XDA showed that the nearly transparent oxide scale consisted of highly textured β-$Y_2Si_2O_7$ (ASTM 22-1103) and α-crystoblite. Observation of the β-Si_3N_4 substrate as a major phase in the diffraction pattern was indicative of the very thin oxide scale. The concentration of the $Y_2Si_2O_7$ in the scale was greater than that observed within the bulk material, suggesting the diffusion of Y to the surface during oxidation. Observations of the oxide scale in the SEM revealed prismatic crystals on the surface which contained high concentrations of Y; these crystals were presumably $Y_2Si_2O_7$.

4.0 DISCUSSION

4.1 Creep

The creep resistance of this new material is certainly better than the Si_3N_4/MgO materials previously examined.[6] The further improvement after an oxidation treatment suggests that compositional changes are occurring close to the surface which decrease the volume fraction of the glassy phase as previously observed for the Si_3N_4/MgO materials.[7,8]

At the lower stress regime, the stress exponent of $n \simeq 1$ suggests that diffusional creep is dominant, whereas at higher stresses, the higher stress exponent ($n > 2$) is indicative of cavitational creep. Transition from creep dominated by diffusion to cavitation appears to occur at ~ 310 MPa. This transition has been predicted;[6] although diffusion and cavitation are concurrent phenomena, theory indicates that cavitation will be more pronounced at high stresses. The observation that the transition stress is not significantly

affected by the oxidation treatment might be related to the fact that the apparent compositional change which results in improved creep resistance only occurs near the surface and that the bulk of the material exhibits little or no compositional change during oxidation.

4.2 Oxidation

The parabolic rate constant of 4.2×10^{-1} Kg^2 $m^{-4} \cdot s^{-1}$ is 20 times lower than that previously reported for commerical HS130* at 1400°C.[9] It is also lower than values measured for other polyphase Si_3N_4 materials determined at 1400°C.

Clarke and Lange[8] have shown that the parabolic rate law exhibited by Si_3N_4/MgO materials is due to a compositional change that takes place in the bulk just below the oxide scale. This compositional change is due to the diffusion of Mg and impurities from the bulk into the oxide scale. Cation diffusion to the scale is caused by the attempt of the glassy phase to equilibriate with the SiO_2 formed on the surface through the oxidation of Si_3N_4. The effect of the compositional change is to decrease the volume fraction of the glassy phase which is the path for fast diffusion of oxygen and oxide products (viz N_2). Similar phenomena are expected for other polyphase Si_3N_4 materials.

Enrichment of the oxide scale with yttrium, as observed by the higher concentration of $Y_2Si_2O_7$ in the scale relative to the bulk, is proof that yttrium diffuses to the surface during oxidation. Since the $Y_2Si_2O_7$ crystalline phase in the bulk is compatible with SiO_2, there is no driving force for the Y in the $Y_2Si_2O_7$ crystalline phase to diffuse to the surface. On the other hand, the composition of the glassy phase, expected to lie in the Si_3N_4-Si_2N_2O-$Y_2Si_2O_7$ compatibility triangle, is not in equilibrium with SiO_2. Thus there is a driving force for the Y in the glassy phase to diffuse to the

*Norton Co., Worchester, Mass.

surface. The improved oxidation resistance of the Si_3N_4/Y_2O_3 material examined here is believed to be due to the lower amount of glassy phase relative to other materials, as indicated by the crystalline $Y_2Si_2O_7$ observed within the bulk, and the higher viscosity of the glassy phase, as indicated by the higher eutectic temperature ($\sim$ 1560°C)[10] for the compatibility triangle in which the material is fabricated.

Despite the improved oxidation resistance of the current material relative to other polyphase Si_3N_4 materials, it should be noted that the parabolic rate constant for CVD Si_3N_4 is $\sim 10^{-13}$ $Kg^2 \cdot m^{-4} \cdot s^{-1}$ at 1400°C. This indicates that significant improvements can still be sought.

ACKNOWLEDGEMENTS

This work was performed for the Air Force Office of Scientific Research under contract F49670-77-C-0072.

REFERENCES

1. F.F. Lange, S.C. Singhal and R.C. Kuznicki, "Phase Relations and Stability Studies in the Si_3N_4-SiO_2-Y_2O_3 Pseudoternary System," J. Am. Ceram. Soc. 60, 249 (1977).

2. F.F. Lange "Silicon Nitride Alloy Sysems: Fabrication, Microstructure and Properties," Met. Rev. Inter. (in press).

3. F.F. Lange and S.C. Singhal, "Silicon Nitride Compositions in the Si_3N_4-Y_2O_3-SiO_2 System," U.S. Patent 4,102,698.

4. C.A. Andersson "Proc. DoE Workshop in Ceramics for Advanced Heat Engines," ed. by F.C. Moore, Jan. 1977.

5. F.F. Lange "Reaction of Iron with Si_3N_4 Materials to Produce Surface Pitting," J. Am. Ceram. Soc. 61, [5-6] 270 (1978).

6. F.F. Lange, B.I. Davis and D.R. Clarke, "Compressive Creep of Si_3N_4/MgO Alloys Part 1 Effect of Composition," J. Mat. Sci. 15, 601-610 (1980).

7. ibid "Part III Effects of Oxidation Induced Compositional Change," 616-618.

8. D.R. Clarke and F.F. Lange, "Oxidation of Si_3N_4 Alloys Relationship to Phase Equilibria in the Si_3N_4-SiO_2-MgO System," J. Am. Ceram. Soc. (in press).

9. W.C. Tripp and H.C. Graham, "Oxidation of Si_3N_4 in the Range 1300°C to 1500°C," J. Am. Ceram. Soc. 58, 399 (1976).

10. D.R. Clarke, "Densification of Si_3N_4 Alloys Using a Eutectic Liquid: An Experimental Test," Sintering Processes. Ed. by G.C. Kuczynski, pp. 303-310, Plenum (1980).

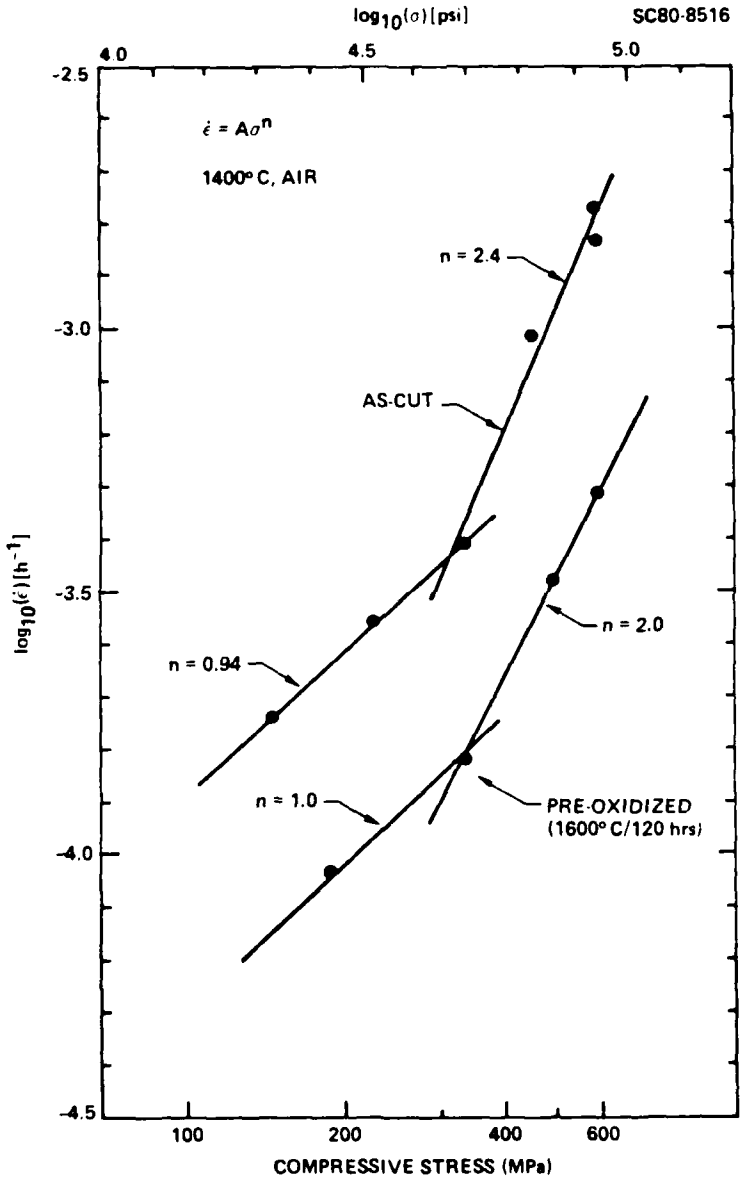

Fig. 1 Steady-State creep behavior as a function of applied compressive stress at 1400°C in air for an as-cut and pre-oxidized (1600°C/120 hrs) material with the composition: 0.85 Si_3N_4, 0.10 SiO_2, 0.05 Y_2O_3.

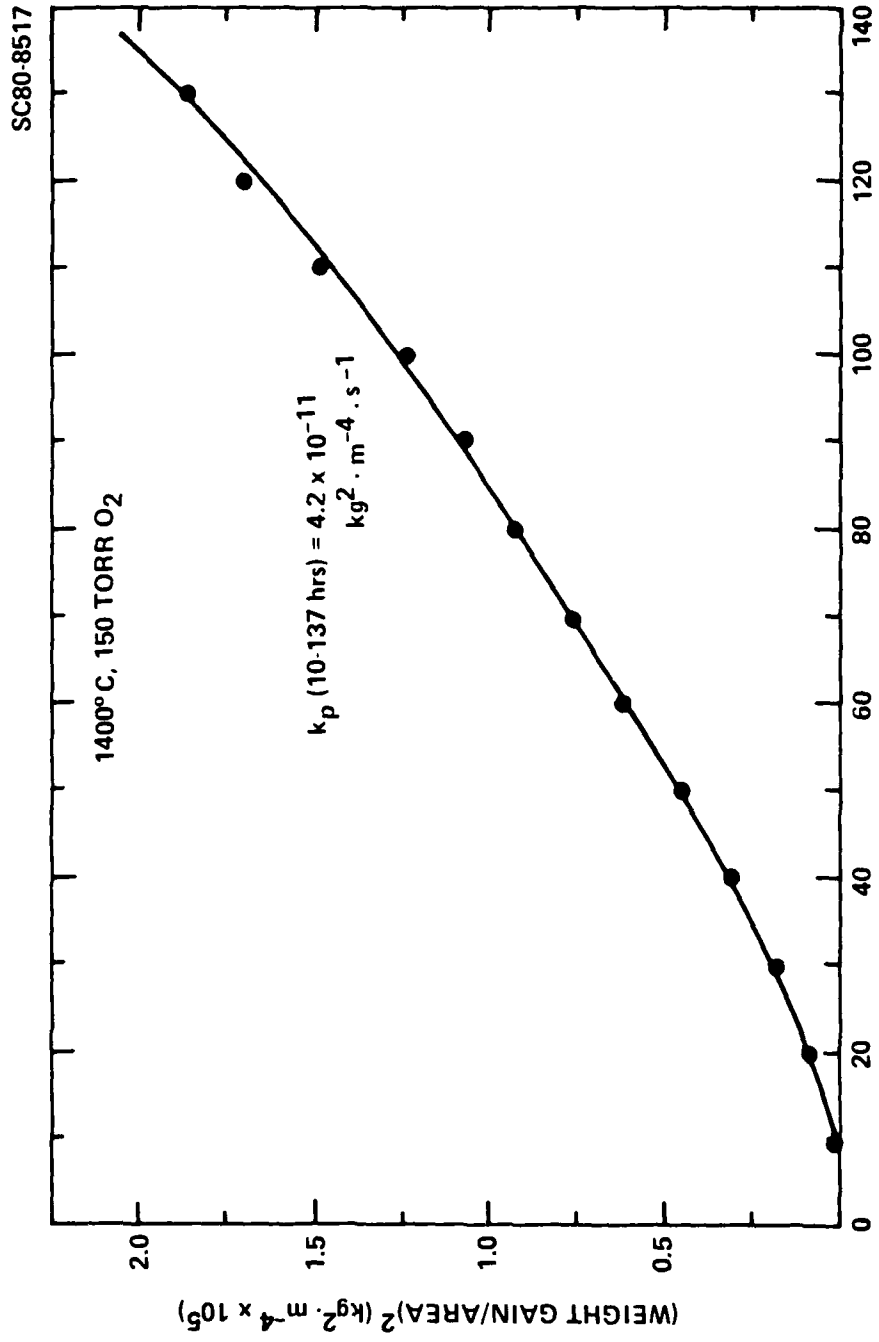

Fig. 2 Oxidation behavior at 1400°C in 150 torr of dry oxygen.

APPENDIX 11

JOURNAL OF MATERIALS SCIENCE 15 (1980) 616–618

Compressive creep of Si_3N_4/MgO alloys

Part 3 *Effects of oxidation induced compositional change*

F. F. LANGE, B. I. DAVIS, D. R. CLARKE
Rockwell International Science Center, Thousand Oaks, California 91360, USA

A comparison of "creep" resistance in as-fabricated and pre-oxidized specimens of different Si_3N_4/MgO alloys shows that pre-oxidation not only significantly reduces the apparent steady-state creep rate, but can also change the stress dependence from a non-linear to a linear behaviour. This phenomenon is discussed in terms of compositional changes induced by oxidation.

1. Introduction

During the course of this investigation of the compressive creep behaviour of four Si_3N_4/MgO alloys, it became apparent that oxidation was significantly affecting results (see Part 1, Section 3.1) [1], i.e. oxidation appeared to produce a form of strengthening. Results of an independent investigation of the oxidation behaviour of the same alloys showed that oxidation produces a compositional change because of the diffusion of oxygen into the bulk and of nitrogen, magnesium and impurities out of the bulk [2]. Since the creep behaviour of the Si_3N_4/MgO alloys was found to be significantly affected by composition [1], it was suspected that the apparent hardening effect was being produced by oxidation-induced compositional changes. Experiments were therefore planned to illustrate this effect.

2. Experimental details

Specimens (approximately 0.3 cm × 0.3 cm × 0.9 cm) were diamond cut from Si_3N_4/MgO alloy compositions A, B and D (see Part 1, Fig. 1). The series of specimens for this investigation were pre-oxidized at 1400° C for 100 h prior to the creep experiments. For comparative purposes, one specimen was diamond ground after oxidation so that material was removed to a depth of 0.1 cm from all surfaces. The oxide surface layer was not removed from the other specimens. Sectioning after testing showed that the thickness of the oxide surface scale was dependent on composition, but was never $> 50\,\mu m$. Because the oxide scale is partially liquid at 1400° C [2], it is not expected to support load. Inclusion of the oxide scale thickness in the specimen dimensions used in calculating the applied stress, thus resulted in a small error (~ 3%) for the assumed applied, compressive stress.

Compressive creep testing was performed at 1400° C in air as outlined in Part 1, Section 2. After testing, representative specimens were sectioned so their gross compositional change could be determined by using X-ray diffraction.

Unlike the unoxidized specimens (Part 1, Section 3), the pre-oxidized specimens exhibited an extensive period of steady-state creep. Within the time frame of each experiment (~ 25 h at each stress)* the strain rate was constant over the last ~ 80% of the period before the specimen was unloaded. Periods of primary creep and strain recovery were also observed for each composition. Tertiary creep was not observed.

The empirical equation relating the steady-state creep rate ($\dot{\epsilon}$) to the applied compressive stress (σ)

$$\dot{\epsilon} = A\sigma^n,$$

was used in analysing the data. The log–log plots of these data are shown in Fig. 1 along with the data for the unoxidized specimens previously presented in Part 1 of this series [1]. As shown, the pre-oxidation treatment significantly improved

* The test period was designed to be shorter than the pre-oxidation period so that significant changes in the material, due to an added period of oxidation during testing, could be prevented.

0022–2461/80/030616–3$02.30/0

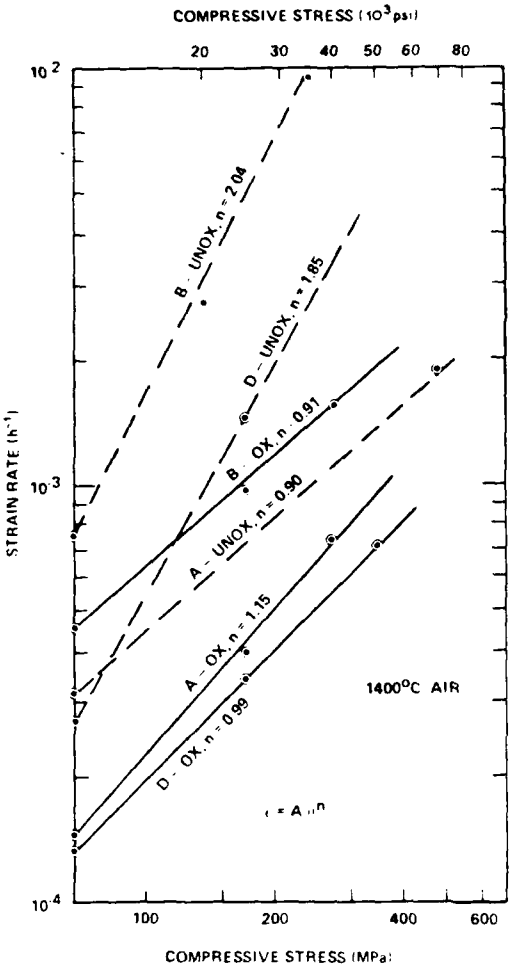

Figure 1 Log–log plot of apparent steady-state creep rate versus compressive stress for Si_3N_4/MgO alloy compositions A, B and D in the as-fabricated states (broken lines) and their pre-oxidized states (1400° C, 100 h); n is the stress exponent for creep rate.

the creep resistance of all alloys. Greatest improvement was achieved for compositions B and D. The strain rate for all the pre-oxidized compositions was linearly related to stress, indicating the dominance of diffusional creep as the persistent mode of deformation [1]. Data for the pre-oxidized specimen which was surface ground to remove the oxide scale was similar to the data for specimens in which the scale was not removed. This observation indicated, as expected, that the surface scale was not responsible for the improved creep resistance.

X-ray diffraction data of sectioned, pre-oxidized specimens revealed the presence of Si_2N_2O in materials B and D that was not present in the as-fabricated compositions (Part I, Table I). This observation showed that the pre-oxidation treatment shifted the bulk composition toward the Si_2N_2O end member of the Si_3N_4–Si_2N_2O–Mg_2SiO_4 compatibility triangle in which the initial materials were fabricated.

4. Discussion

Conclusive evidence is presented which shows that a pre-oxidation treatment can significantly improve the creep resistance of Si_3N_4/MgO alloys as suspected by earlier work in this investigation [1]. The effect of oxidation on composition changes and the effect of compositional change on creep behaviour will be the subject of discussion.

An independent study of the oxidation behaviour of the complete compositional series from which the materials reported here were taken, has resulted in the following conclusions [2] with respect to the current study:

(1) oxidation not only results in the formation of a relatively thin, friable surface scale, but also results in a compositional gradient that can penetrate deep into the bulk;

(2) the compositional gradient is a result of the diffusion of oxygen into the bulk and of nitrogen, magnesium, and impurities out of the bulk; diffusion is presumed to occur within the glassy interphase. The Mg and impurities (Ca and Fe) concentrate in the surface scale; the bulk is depleted of these same impurities;

(3) for materials studied here, Si_2N_2O is the major phase at the scale/bulk interface and its concentration decreases as the centre of the bulk is approached.

These results show that oxidation causes compositions initially on the Si_3N_4–Mg_2SiO_4 side of the compatibility triangle to shift toward the Si_3N_4–Si_2N_2O side; the shift is greatest as the scale/bulk interface. Depending on the specimen thickness and the oxidation kinetics (time and temperature) the compositional shift can be significant at the specimen centre. Interpreted in another manner, oxidation causes the initial composition to shift away from the ternary eutectic, i.e. the glass interphase acts as a fugitive phase during oxidation.

When these results are applied to the present study, it is evident that a pre-oxidation treatment

of 100 h at 1400° C for the specimen size used in the study was sufficient to cause a significant shift to compositions that exhibit predominantly diffusional creep. This is demonstrated by materials B and D. In their as-fabricated state, cavitational creep was dominant [1]; in their pre-oxidized state, diffusional creep was dominant. This shift in creep behaviour is consistent with the shift in their integrated composition and the observed compositional effect on creep behaviour as detailed in Part 1 [1]. The unchanged deformation behaviour (with regard to mechanism and not creep resistance) of composition A is also consistent with this view. Details of the effect of the compositional gradient produced by oxidation on the mechanics of creep deformation have not been explored in the present study. Study of this effect will be important not only for defining the explicit creep hardening function, but also for using this phenomenon to improve the creep resistance of poorer quality materials.

Acknowledgement

This work was supported by the Air Force Office of Scientific Research under Contract No. F49620-77-C-0072.

References

1. F. F. LANGE, B. I. DAVIS and D. R. CLARKE, *J. Mater. Sci.* **15** (1980) 601.
2. D. R. CLARKE and F. F. LANGE, to be published

Received 5 July and accepted 28 August 1979.

APPENDIX 12

Development of Surface Stresses During the Oxidation of Several Si_3N_4/CeO_2 Materials

F. F. LANGE* and B. I. DAVIS

IT HAS been demonstrated that compressive stresses can arise on the surfaces of Si_3N_4 materials because of the molar volume increase that accompanies the oxidation of a secondary phase.[1] When the oxidation conditions are optimum, the compressive surface stresses can be used to increase the apparent strength of the material.[1] On the other hand, over-optimum conditions can lead to surface spalling and general material degradation, which can be devastating.[2]

Silicon nitride alloys densified with CeO_2 can contain a secondary phase with an apatite crystal structure and an apparent formula of $Ce_4(SiO_{3.67}N_{0.33})_3O$ (or $Ce_5(SiO_4)_3N$). At <1000 C, this phase oxidizes to CeO_2 and SiO_2 with a volume change of 8.4%. Initial experiments indicated that oxidation did not result in material degradation at 1000 C.[3] Further experiments were conducted to determine if degradation might occur at lower temperatures.

Two Si_3N_4/CeO_2 materials fabricated with 15 and 20 wt% CeO_2 were subjected to various periods of oxidation in air at 400° to 900° C. The Ce-apatite phase was identified in both materials; the 15 wt% CeO_2 composition contained the smaller amount of the Ce-apatite. An indentation technique* was used in determining the apparent critical stress intensity factor (K_a) of the material.[4] As detailed elsewhere,[1] residual surface stresses that develop during oxidation are reflected in the K_a measurement, viz. compressive surface stress increased K_a. Specimens were indented prior to oxidation and after each oxidation period. New specimens were used at every temperature.

Oxidation of the Ce-apatite was monitored at the surface by X-ray diffraction. Intensities of the (121) Ce-apatite ($I_{Ce\text{-}A}$, $d = 2.89$ Å) and the (101) β-Si_3N_4 (I_β, $d = 2.66$ Å) diffraction peaks were determined before oxidation and after each oxidation period.

The results for oxidation at 400°, 500°, and 600° C are shown in Fig. 1. At all temperatures, the oxidation of the Ce-apatite was more rapid for the 20 than for the 15 wt% composition, as indicated by the change in the $I_{Ce\text{-}A}/I_\beta$ intensity ratio vs oxidation period. Likewise, the buildup of compressive stresses at the surface, as indicated by the increase in K_a vs oxidation period, was also more rapid in the 20 wt% composition. If it is assumed that oxidation occurs by diffusion through the Ce-apatite and/or its oxidation products, this difference can be explained by the larger area fraction of the continuous Ce-apatite phase in the 20 wt% composition.

Material degradation was first noted when the initially flat, polished surface developed an "orange-peel" texture suggestive of surface spalling observed for oxidized Si_3N_4-ZrO_2 materials.[2] Once this observation was made, further oxidation would lead to the development of large through cracks. At 400 C, degradation was not noted for either composition within the experimental period (40 h). At 500° C, the orange-peel surface texture developed on the 20

Received July 2, 1979; revised copy received July 23, 1979.
Supported by the Air Force Office of Scientific Research under Contract No. F49620-77-C-0072.
The writers are with the Rockwell International Science Center, Thousand Oaks, California 91360.
*Member, the American Ceramic Society.

*An indentation load of 20 kg was used. Specimens were polished before the oxidation treatment; oxidation did not hinder the subsequent measurements of the crack lengths associated with the indentation.

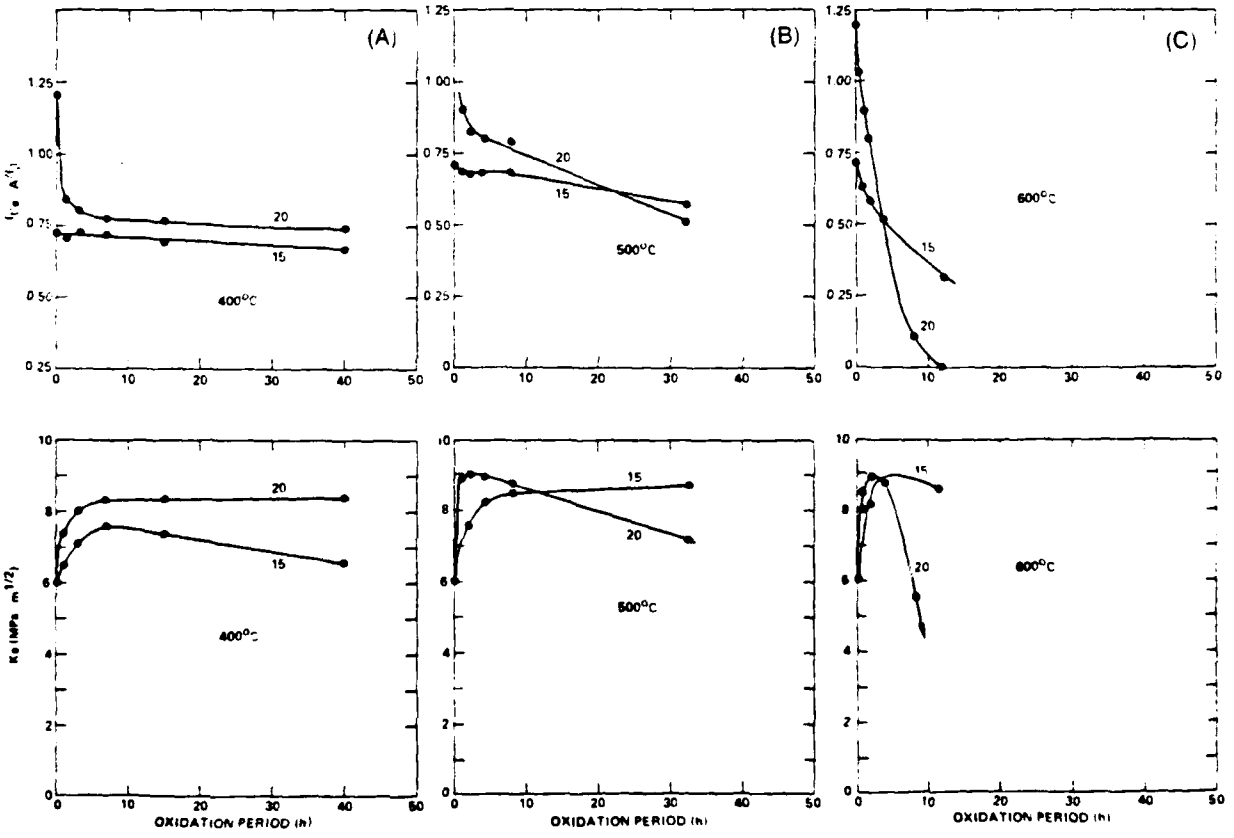

Fig. 1. Intensity ratio of the (121) Ce-apatite ($I_{Ce\text{-}A}$) and (101) β-Si_3N_4 (I_β) diffraction peaks and the apparent stress circuitry factor measured at the surface vs oxidation period at (*A*) 400°, (*B*) 500°, and (*C*) 600°C.

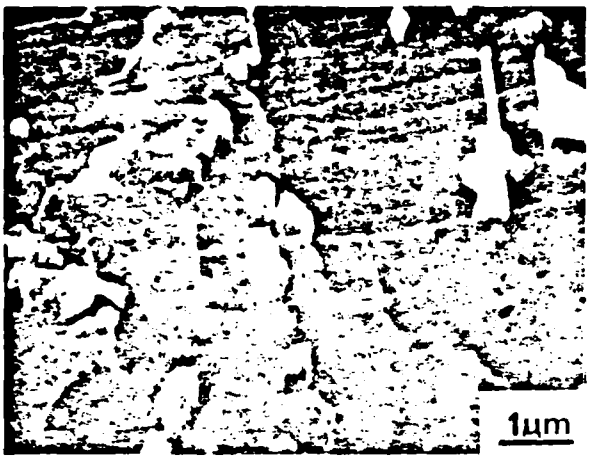

Fig. 2. Protrusion of Ce-rich oxidation products on the surface of a 20 wt% CeO_2/Si_3N_4 alloy oxidized in air at 900 C for ≈5 min. Note uplifted Si_3N_4 grains as indicated by displaced grinding scratches.

wt% composition after 8-h exposure. At 600 C, the 20 wt% composition contained many through cracks after 8 h, and the 15 wt% composition had an orange-peel surface. Cracks developed (≈1 h) in both materials at 700 C.

In general, the orange-peel texture developed when K_{ii} was ≈9 MPa m$^{1/2}$ consistent with similar observations for oxidized Si_3N_4/ZrO_2 materials.[3] Thus the observed decrease in K_{ii} after achieving a value of ≈9 MPa m$^{1/2}$ is believed to be due to the release of surface stresses by spalling.

Scanning electron microscopy (SEM) was used to examine the unoxidized and oxidized specimens. Surfaces with the orange-peel appearance were confirmed to contain cracks nearly parallel to the surface. At 900 C, protrusions were observed to develop on the initially flat surface after short periods (5 min) of oxidation. As shown in Fig. 2, these protrusions appeared to decorate grain boundaries and triple points, viz. locations where the Ce-apatite phase was identified* on unoxidized specimens. The protrusions were Ce-rich, as determined with a nondispersive X-ray analysis in the SEM. Note also in Fig. 2 that some Si_3N_4 grains appear uplifted, as indicated by the displaced grinding scratches. Individual protrusions were no longer distinguishable for longer periods (≈1 h) of oxidation at 900 C as a general Ce-rich surface scale developed. No protrusions were noted at lower temperatures.

These observations show that the preferential oxidation of the Ce-apatite secondary phase results in the development of compressive stresses at the surface. Prolonged oxidation at ≈900 C results in surface spalling and cracking. At higher temperatures, these stresses appear to be somewhat relieved by the extrusion of the oxide product from the interior to the surface, consistent with the fact that degradation is not observed for prolonged oxidation periods at 1000 C.

It must be concluded that the Si_3N_4/CeO_2 materials investigated here would not be useful high-temperature structural materials when placed in an oxidizing temperature gradient which includes the critical temperature range of 400 to 900 C. Extension of the extrusion phenomenon to much lower temperatures would be necessary for this problem to be overcome.

*The large difference in atomic number between Ce and Si made possible the phase contrast in the SEM which was confirmed by EDAX.

[1] F. F. Lange, "Compressive Surface Stresses Developed in Ceramics by an Oxidation Induced Phase Change," to be published in the *Journal of the American Ceramic Society*.

[2] F. F. Lange, S. C. Singhal, and R. C. Kuznicki, "Phase Relations and Stability Studies in the Si_3N_4-SiO_2-Y_2O_3 Pseudoternary System," *J. Am. Ceram. Soc.* **60** [5–6] 249–52 (1977).

[3] F. F. Lange, "Si_3N_4-ZrO_2-SiO_2 Materials: Phase Relations and Strength," to be published in the *American Ceramic Society Bulletin*.

[4] A. G. Evans and E. A. Charles, "Fracture Toughness Determinations by Indentation," *J. Am. Ceram. Soc.* **59** [7–8] 371–72 (1976).

A Review of the *T* Phase

S. L. SARKAR and J. W. JEFFERY

A NEW single phase devoid of any solid solution and termed the *T* phase was reported by Gutt.[1] He suggested a molar composition of $5.6(2CaOSiO_2)$-$4.4(3CaOMgO2SiO_2)$ for this phase in the system $2CaOSiO_2$-$3CaOMgO2SiO_2$. Sharp *et al*.[2] also detected a new phase in basic arc-furnace slag, very similar to that of Gutt. The strongest lines of Sharp *et al*.'s phase were in accordance with Gutt's *T* phase. Schlaudt and Roy,[3] who repeated Gutt's work, confirmed his findings.

Midgley[4] determined the cell parameters of the *T* phase as $a = 10.72 \times 10^{-10}$, $b = 18.41 \times 10^{-10}$, $c = 6.64 \times 10^{-10}$ m, space group *Pmcn*. The sample prepared by Gutt[1] was reinvestigated by the present writers by X-ray powder photography using a focusing camera.* A microddensitometer trace of the photograph is given in Fig. 1, together with the indices obtained, starting with Midgley's cell but using iterative refinement (Table I). The refined orthorhombic lattice dimensions are $a = (10.795 \pm 0.028) \times 10^{-10}$, $b = (18.838 \pm 0.048) \times 10^{-10}$, $c = (6.803 \pm 0.018) \times 10^{-10}$ m.

Biggar,[5] who suggested a composition $Ca_6MgSi_4O_{12}$ (C_3MS_2) for bredigite, claims that the *T* phase of Gutt[1] and the phase reported by Sharp *et al*.[2] are identical with bredigite. Gutt,[6,7] from his studies on the binary system C_2S (dicalcium silicate, Ca_2SiO_4)-C_3MS_3 (merwinite, $Ca_3MgSi_2O_8$), demonstrated a finite field for the *T* phase, which he claims coexists in adjacent fields with an α' form of dicalcium silicate and merwinite.

Bredig[8] considered merwinite to be an Mg-substituted calcium orthosilicate, probably the α' polymorph of C_2S. The crystal structure of merwinite was determined by Yamaguchi and Suzuki[9] and Moore and Araki[10]; they showed, on structural grounds, that merwinite cannot be regarded as a polymorph of C_2S stabilized by Mg. On the grounds of crystallochemical evidence, i.e. the similarity of space groups and cell parameters, Midgley[4] stated that the name bredigite should not be confined to the composition C_3MS_2, but should be regarded as the name given to a room-temperature minor-ion stabilized form of α_L'-C_2S. Gutt and Nurse,[11] however, are of the opinion that it would be undesirable to use the name bredigite for both C_3MS_2 and α_L'-C_2S, even though it seems likely that they form a solid solution series.

Since only enough material was available for an X-ray powder photograph, electron microprobe or X-ray fluorescence analysis could not be conducted on this controversial phase to determine its elemental composition. Therefore, no definite conclusions can presently be drawn. Several questions still remain, (*a*) the signifi-

Received July 23, 1979.

At the time this work was done, the writers were with the Department of Crystallography, Birkbeck College, London WC1E 7HX, United Kingdom. S. L. Sarkar is now with the Marine Technology Center, Imperial College, Department of Metallurgy and Materials Science, London SW7 2BP, United Kingdom.

*Nonius Guinier camera, Enraf Nonius, Delft, The Netherlands.

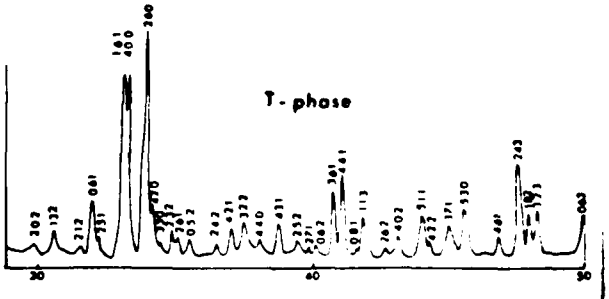

Fig. 1. Microdensitometer trace of the *T* phase


DA
FILM